

**UNDERSTANDING THE ROLE TOPOGRAPHICAL FEATURES  
PLAY IN STIMULATING THE ENDOGENOUS PERIPHERAL  
NERVE REGENERATION ACROSS CRITICALLY SIZED NERVE  
GAPS**

A Dissertation  
Presented to  
The Academic Faculty

by

Vivek Mukhatyar

In Partial Fulfillment  
of the Requirements for the Degree  
Doctor of Philosophy in the  
Wallace H. Coulter Department of Biomedical Engineering

Georgia Institute of Technology  
December 2011

**UNDERSTANDING THE ROLE TOPOGRAPHICAL FEATURES  
PLAY IN STIMULATING THE ENDOGENOUS PERIPHERAL  
NERVE REGENERATION ACROSS CRITICALLY SIZED NERVE  
GAPS**

Approved by:

Dr. Ravi V. Bellamkonda, Advisor  
School of Biomedical Engineering  
*Georgia Institute of Technology*

Dr. Robert E. Guldberg  
School of Mechanical Engineering  
*Georgia Institute of Technology*

Dr. Thomas H. Barker  
Department of Biomedical Engineering  
*Georgia Institute of Technology*

Dr. Philip Santangelo  
Department of Biomedical Engineering  
*Georgia Institute of Technology*

Dr. Arthur English  
Department of Cell Biology School of  
Medicine  
*Emory University*

Date Approved: [Month dd, yyyy]

*To my parents Geeta and Jayesh Mukhatyar*

*Matru Devo Bhava,  
Pitru Devo Bhava,  
Guru Devo Bhava*

(From Upanishad)

.

*We should have the same gratitude for our parents and teachers (guru) as we have for God.*

## ACKNOWLEDGEMENTS

My past six years in Atlanta pursuing my PhD has been an exciting journey filled with some amazing memories. I have been lucky to meet so many great people who have helped me immensely in my pursuit of my PhD degree. The constant support of my family, friends, work colleagues and my mentors have helped me cross this finish line and I will be always be grateful to them for it. I am grateful to have this opportunity to thank them for the part they have played in my journey.

First and foremost, I would like to express my sincere gratitude to my advisor, Dr. Ravi Bellamkonda for giving me an opportunity to join his lab and for being a great mentor over the years. I am extremely grateful to him for giving me countless opportunities to grow as a good scientist by exposing me to grant writing, sending me to several domestic and international conferences and providing me constant guidance throughout my graduate studies. I will always be thankful to him for his patience and encouragement he has given me as well as pushing me time to time to tackle my weaknesses. His excellent support has helped me develop into the scientist that I am now. His positivity has always encouraged me to be a better scientist and after every one on one meeting with him, I felt that I could conquer the world. I am enormously thankful to him for making me part of his lab family and all that I have learnt from him will undoubtedly help me with every future endeavor. Thank you for everything you have done for me Dr. Bellamkonda and you truly have been an inspiration over the last five years.

I would also like to thank my committee members, Dr. Tom Barker, Dr. Art. English, Dr. Robert Guldberg and Dr. Philip Santangelo for their continual support and

input on my thesis. They have all provided me with invaluable guidance that has driven my project and significantly improved the quality of the science that I have done. I have had the privilege to work with each of them at different aspects of the project and I have learnt significantly from each of them. First I would like to thank Dr. Tom Barker for his collaboration on the fibronectin study. I thank him for all the guidance and insights he provided me as well as his critical review of my paper which led to a very smooth acceptance process. I would like to thank Dr. Art English for all the help he has given me with the understanding fundamentals of peripheral nerve regeneration. I have enjoyed our conversations and I have learnt a lot from him over the years. I am also thankful to him for taking time out of his schedule to teach me how to extract muscle tissue from the animals. I would like to thank Dr. Robert Guldberg for teaching me the fundamentals of animal work. When I started my research project, I had a fear of doing animal work, but after taking his class on live animal modeling, I was a lot more comfortable with it and it has become one of my favorite things to do in lab. Finally, I would like to thank Dr. Santangelo for his insightful comments on my project as well as the conversations I have had with him. His suggestions has given me a different perspective and provided me with several ideas for continuation of my work in future. All my committee members have always been very approachable and I am extremely thankful to have had the pleasure to have them as mentor for my project.

I would also like to thank our collaborators who have played an important role in my project. I would like to thank Dr. Anders Garcia and Dr. Manuel Solmeron Sanchez with their help with my fibronectin study. Their guidance and input helped drive the study and helped with the smooth acceptance of the manuscript. I would like to

especially thank Dr. Sanchez for teaching me Atomic Force Microscopy and teaching me about Spain during his sabbatical visit at Georgia Tech. It was a pleasure to work with him and I thank him for giving me a new skillset that will help me immensely in the future. I also want to thank Dr. Satish Kumar for teaching me the basics of electrospinning and allowing us to use his facilities for fabricating scaffolds.

In addition, I would like to acknowledge several people in the IBB and BME whose technical guidance has influenced my project and taught me several skills that has helped me immensely during the course of my PhD. I would first like to thank Dr. Laura O'Farrell for imparting her knowledge regarding animal work and her assistance in the *in vivo* aspects of my project. She has always taken time to explain the smallest details and has had the patience to teach me the ropes around the PRL which has led me to become a decent surgeon and become passionate about animal work. I would also like to thank Kim Benjamin and the rest of the PRL staff for helping me at every stage of my animal studies and I believe that without their help we would not have been able to finish the animal studies as efficiently as we did. I would also like to thank Aqua from the histology lab for her mentorship and teaching me tissue sectioning as well as staining. I have picked up some really useful techniques from her and it has allowed me to add another whole dimension to my research. I would also like to express my sincere gratitude to the BME administrative department for their guidance and keeping me on track with reminders to important deadlines. I would like to specially thank Sally Gerrish, Beth Bullock and Shannon Sullivan for their help throughout my PhD.

I would like to express my gratitude to everyone in Bellamkonda lab over the last six years who have taught me a lot and without their help this thesis would not have been

possible. I would like to specially acknowledge my undergrads who have worked really hard to help me make deadlines and mentoring them has been one of the most rewarding experiences of my life. I would also like to thank my friends and my family who have given me continuous support and made this journey more enjoyable.

## Table of Contents

	Page
ACKNOWLEDGEMENTS	iv
LIST OF TABLES	xiv
LIST OF FIGURES	xv
SUMMARY	xviii
CHAPTER 1	1
1.1 Specific Aims	1
1.1.1 Specific Aim I	2
1.1.2 Specific Aim II	3
CHAPTER 2	4
2. Literature Review	4
2.1. Injuries to the Peripheral Nervous System	4
2.1.1 Introduction	4
2.1.2 Current strategies to address peripheral nerve injuries and their limitations	4
2.2 The regenerative sequence	6
2.2.1 Endogenous Sequence for nerve regeneration	6
2.2.2 Influencing the regenerative sequence	9
2.3 Tissue engineering strategies to enhance nerve regeneration	13
2.3.1 Tubular scaffolds to guide nerve growth: Natural Materials	13
2.3.2 Tubular scaffolds to guide nerve growth: Synthetic Materials	13
2.3.3 Tubular scaffolds to guide nerve growth: Design Specifications	16
2.3.4 Limitations of tubular scaffolds	18



2.4 Exogenous factors to enhance regeneration	18
2.4.1 Growth Factors to promote cellular phenotype	18
2.4.2 ECM molecules	20
2.4.3. Cell transplantation	22
2.4.3.1. Schwann cell Transplantation	22
2.4.3.2. Genetically Modified Cells	24
2.4.3.3. Stem Cells	24
2.4.4. Electrical Stimulation	26
2.5. Topographical cues to understand mechanisms in vitro	27
2.5.1. Micro/Nanopatterning in vitro to better understand axon guidance	27
2.5.2. Microfabrication to create patterns to observe the effects of topographical cues	27
2.5.3 Observing axonal interaction with ECM proteins using dip-pen nanolithography	28
2.6. Fiber Based Topographical cues	29
2.6.1 Self assembling peptide nanofibers	29
2.6.2. Silk fibers to enhance nerve regeneration	30
2.6.3 Magnetically aligned nanofibers for cell alignment	31
2.6.4 Biosynthetic and synthetic fibers	31
2.6.4.1 Fabrication through electrospinning	34
2.6.4.2 Synthetic electrospun fibers for neural tissue engineering	34
2.6.4.3 Biosynthetic fibers with conductive properties	35
2.6.4.4 Biosynthetic fibers to aid in Schwann cell migration	35

2.6.4.5 Topography for controlled migration of Schwann cells	36
2.7. Topographical filler materials to augment peripheral nerve regeneration	36
2.8 Conclusion	40
CHAPTER 3	41
3. Role of Fibronectin in topographical guidance of neurite extension on electrospun fibers	41
3.1. Introduction	41
3.2. Material and Methods	43
3.2.1 Fabrication of polymer films with aligned and smooth topographies	43
3.2.2 Harvesting of Schwann cells and dorsal root ganglia (DRG)	43
3.2.3 Neurite outgrowth and Schwann cell migration assay	44
3.2.4 Fibronectin adsorption assay	45
3.2.5 Fibronectin depletion and competition assays	46
3.2.6 Atomic force microscopy	47
3.2.7 Fibronectin organization by Schwann cells	47
3.2.8 Statistical analysis	48
3.3 Results	49
3.3.1 Schwann cell migration and neurite outgrowth from DRG	49
3.3.2 FN Adsorption from serum	49
3.3.3 Effects of FN depletion from serum on DRG behavior	50
3.3.4 Influence of competitive binding of Cyclo-GRDGS on FN mediated response	55
3.3.5 Inhibition of integrin binding motif of fibronectin	55

3.3.6 Influence of topography on fibronectin organization and production	56
3.4. Discussion	61
CHAPTER 4	68
4. Effects of topography on the endogenous regenerative sequence in long peripheral nerve gap	68
4.1. Introduction	68
4.2. Material and Methods	71
4.2.1 Fabrication of thin-film based scaffolds	71
4.2.1.1 Fabrication of Aligned, Random and Smooth thin-films	71
4.2.1.2 Assembly for tubes for implantation	71
4.2.2 <i>In vivo</i> Implantation	72
4.2.3 Evaluation of nerve bridging	75
4.2.3.1 Experimental groups	75
4.2.3.2 Electrophysiology	75
4.2.3.3 Nerve Conduction Velocity	76
4.2.3.4 Relative Gastrocnemius Muscle Weight Measurement	76
4.2.3.5 Muscle Atrophy	77
4.2.3.6 Immunohistochemical analysis	77
4.2.3.7 Trichrome Staining	79
4.2.3.8 Myelin thickness, axonal diameter and myelinated axon count	80
4.2.4 Molecular analysis of explanted nerve	81
4.2.4.1 Tissue Collection for molecular analysis	81
4.2.4.2 Cytokine array for 5 day samples	81

4.2.4.3 qRT-PCR for 3 week samples	82
4.2.5 Fiber Permeability	83
4.2.6 Statistical Analysis	83
4.3. Results	84
4.3.1 Histological analysis of regenerated axons and Schwann cell migration	84
4.3.1.1 Axonal growth and Schwann cell migration 3 weeks post implantation	84
4.3.1.2 Axonal growth and Schwann cell migration 22 weeks post implantation	89
4.3.2 Number of myelinated axons	97
4.3.3 Myelinated sheath thickness and axonal diameter	97
4.3.4 Muscle weight and muscle fiber diameter	100
4.3.5 Compound action potential velocity	102
4.3.6. Fibrin organization 5 days post injury	102
4.3.7. ECM Organization at 3 weeks and 22 weeks post injury	102
4.3.8 Macrophage response to topography in a long gap	107
4.3.9 Cytokine array	107
4.3.10 qRT-PCR	111
4.3.11 Scaffold permeability	115
4.4. Discussion	116
CHAPTER 5	127
5. Conclusions and Future Directions	127
APPENDIX A: OpTIMIZATION of Fiber Diameter	136
APPENDIX C: Fabrication of LONG Lipidmicrotubes for sustained delivery of biomolecules	141

APPENDIX D: NT-3 For Promoting Schwann cell function across long peripheral nerve gaps	154
APPENDIX E: Protocol for staining Fibrin	174
References	176

## LIST OF TABLES

Table 1-1: Strategies to stimulate different steps of peripheral nerve regeneration	11
Table 1-2: Tissue engineering strategies to augment nerve regeneration in a critical length gap	12
Table 4-1: List of animals studies and outcome measures	74

## LIST OF FIGURES

Figure 1-1. Regenerative sequence of events in a non-critical length gap through a conduit.	8
Figure 1-2. Electrospinning Setup.	33
Figure. 3-1: Characterization of electrospun fibers and smooth films.	51
Figure. 3-2: DRG growth on aligned and smooth thin films.	52
Figure. 3-3: Fibronectin adsorption on aligned and smooth film topographies.	53
Figure 3-4: Quantitative analysis of Schwann cell migration in fibronectin depleted serum.	54
Figure. 3.5. Schwann cell migration and neurite outgrowth analysis in GRGDSP inhibited media.	57
Figure. 3.6. DRG Schwann cell migration and neurite outgrowth in HFN7.1 antibody inhibited fibers.	58
Figure. 3.7. Atomic force microscopy images of PAN-MA polymer topography.	59
Figure. 3.8. ECM organization	60
Figure 4-1: Schematic diagram of film-based scaffolds used to bridge long peripheral nerve gaps.	74
Figure 4-2: Schwann cell cable formation at 3 weeks in the proximal section of the film-based scaffolds.	85
Figure 4-3: Schwann cell cable formation at 3 weeks in the middle section of the film-based scaffolds.	86
Figure 4-5: Quantification Schwann cells migration and neurite outgrowth at 3 weeks.	88

Figure 4-6: Regenerating cable formation at 22 weeks in the proximal section of the film-based scaffolds.	91
Figure 4-7: Schwann cell cable formation at 3 weeks in the middle section of the film-based scaffolds	92
Figure 4-8: Schwann cell cable formation at 3 weeks in the distal section of the film-based scaffolds.	93
Figure 4-9: Quantificaiton of Schwann cell area at 22 weeks.	95
Figure 4-10: Percentage of Schwann are in the total regenerated cable at 22 weeks.	95
Figure 4-11. Quantificaiton of Axonal area at 22 weeks.	96
Figure 4-12: Percentage of Axonal area in the total regenerated cable at 22 weeks.	96
Figure 4-13: Axonal myelination.	98
Figure 4-14: Quantification of myelin thickness and axonal width.	99
Figure 4-15: Cross section analysis of gastrocnemius muscle.	101
Figure 4-16: Compound action potential velocity.	101
Figure 4-17: Fibrinogen staining 5 days post-surgery near the proximal end of the conduit.	103
Figure 4-18: Fibroblast and Lamin localization in a mature regenerated cable.	105
Figure 4-19: Trichrome staining to evaluate the localization of Collagen within the nerve conduit.	106
Figure 4-20: Macrophage localization at diffenent location and timpoints.	109
Figure 4-21: Cytokine array analysis five days after injury.	110
Figure 4-22: Gene expression analysis using real-time PCR analysis from the proximal half of the 15 mm conduit at 3 weeks.	113



Figure 4-23: Gene expression analysis using real-time PCR analysis from the distal half of the 15 mm conduit at 3 weeks.	114
Figure 4-23: Fiber permeability study.	115
Figure A-1. Aligned electrospun fibers fabricated using polymeric solutions of different concentrations.	136
Figure A-2: DRG study in response to fiber diameter.	137
Figure B-1: Fabrication of PLLA fibers.	138
Figure B-2: A. Schwann cells on TCPS and aligned PLLA films.	139
Figure B-3. PCL nerve guidance channel fabricated using dip coating technique.	140
Figure C-1: Average Lipid Microtubule Length at two Cooling Rates.	146
Figure C-2: Images of Microtubules at Two Cooling Rates.	147
Figure C-3: Average Lipid Microtubule Length After Altering Solution Ratio.	148
Figure C-5: Average Microtubule Length after Passage through Needles.	149
Figure C-6: Average BSA release from lipid microtubules over two weeks.	150
Figure D-1: Scratch Wound Assay.	166
Figure D-2: DRG Growth on Aligned Fibers After 1 Week.	167
Figure D-3: Effects of NT-3 after 16 Days In Vivo.	170
Figure D-4: Quantitative 20 Week Nerve Morphology.	171
Figure D-5: Compound Action Potential Conduction Velocity at 20 Weeks.	172
Figure D-6: Gastrocnemius Muscle at 20 Weeks.	173
Figure E-1: Picro-mallory fibrin staining.	175

## SUMMARY

Severe traumatic injuries and surgical procedures like tumor resection often create peripheral nerve gaps, accounting for over 250,000 injuries in the US annually. The clinical “gold standard” for bridging peripheral nerve gaps is autografts, with which 40-50% of patients regain useful function. However, issues including their limited availability and collateral damage at the donor site limit the effectiveness and use of autografts. Therefore, it is critical to develop alternative bioengineered approaches that match or exceed autograft performance.

With the use of guidance channels, the endogenous regeneration process spontaneously occurs when successful bridging of short gaps (< 10mm) occurs, but fails to occur in the bridging of longer gaps ( $\geq 15$ mm). Several bioengineered strategies are currently being explored to bridge these critical size nerve gaps. Other labs and ours have shown how filler materials that provide topographical cues within the nerve guides are able to enhance nerve growth and bridge critical length gaps in rats. However, the mechanism by which intra-luminal fillers enhance nerve regeneration has not been explored. The main goal of this dissertation was to explore the interplay between intra-luminal scaffolds and orchestrated events of provisional fibrin matrix formation, glial cell infiltration, ECM deposition and remodeling, and axonal infiltration - a sequence we term the ‘regenerative’ sequence. We hypothesized that the mechanism by which thin films with topographical cues enhance regeneration is by serving as physical ‘organizing templates’ for Schwann cell infiltration, Schwann cell orientation, extra-cellular matrix deposition/organization and axon infiltration.

We demonstrate that aligned topographical cues mediate their effects to the neuronal cells through optimizing fibronectin adsorption *in vitro*. We also demonstrate that aligned electrospun thin films are able to enhance bridging of a critical length nerve gap *in vivo* by stabilizing the provisional matrix, creating a pro-inflammatory environment and influencing the maturation of the regenerating cable leading to faster functional recovery compared to smooth films and random fibers. This research will advance our understanding of the mechanisms of peripheral nerve regeneration, and help develop technologies that are likely to improve clinical outcomes after peripheral nerve injury.

# CHAPTER 1

## 1.1 Specific Aims

Peripheral nerve injuries present a serious clinical challenge. Greater than 250,000-300,000 peripheral nerve trauma cases are reported every year in the United States. After nerve trauma, the standard clinical operating procedure is to appose the two nerve ends and suture them together without generating tension where possible. If the gap is large so that tensionless apposition is not possible, a nerve autograft - typically the patient's own sural nerve - is used as a bridge. While autografts are the best clinical bridging option available today, there are many drawbacks to this procedure, including the need for a secondary surgery, loss of donor site function, limited availability, modality mismatch (arising from a sensory nerve being used to repair a motor or mixed nerve), and neuroma formation at the donor or graft site. Therefore there is a clear and urgent, unmet clinical need to find an alternative approach to the use of autografts. Driven by this need, several bioengineering strategies are being pursued. Commercially, polymeric hollow 'guidance channels such as the collagen nerve guidance channel (NeuroGen®, Integra Life Sciences) are available and are typically used to bridge gaps less than 10mm. In the research phase bioengineers are exploring various intra-luminal scaffolds to further enhance the function of the hollow, saline filled nerve guidance channels including the use of intra-luminal hydrogel based scaffolds. [1] Unfortunately, regeneration across such constructs is limited because of the lack of understanding of how regeneration takes place across them.

Previous research in the lab shows the use of polymer fiber-based topographical/structural cues to stimulate endogenous nerve repair across long gaps that

previously could not be bridged using other bioengineered strategies. These findings are consistent with other reports of fibrillar structures presenting topographical cues strongly influencing axon guidance in development and in regeneration due to aligned fibers presenting an anisotropic guidance cues to axons. But the effects of topography on peripheral nerve regeneration are still under studied.

Thus rational design of intra-luminal scaffolds requires us to understand the mechanistic interplay between polymer fiber-based topography and endogenous regenerative sequence of peripheral nerves. This regenerative sequence spontaneously occurs when successful bridging of short gaps ( $< 10\text{mm}$ ) occurs, but fails to occur in the bridging of longer gaps ( $\geq 15\text{mm}$ ). The regenerative sequence involves a fibrin cable formation, extracellular matrix deposition/remodeling (laminin and fibronectin), glial/support cell (fibroblasts and Schwann cells) infiltration into the gap, and regenerating axons that follow.

Our central hypothesis is that thin polymer films with aligned topographical cues augment, organize or replace endogenous fibrin/ECM cable formation between the two severed ends, facilitating ECM remodeling and efficient Schwann cell and nerve fiber migration, resulting in successful regeneration across critically sized nerve gaps ( $\geq 15\text{mm}$  in rats). Our specific aims are as follows:

### 1.1.1 Specific Aim I

**Examine the effects of fiber topography on Schwann cells to understand their role in the nerve regeneration process in vitro.**

*Our working hypothesis* was that Schwann cells are key to the nerve regeneration process and aligned topographical features enhance their migration and their ability to

stimulate nerve growth. The objectives of this aim were to fabricate scaffolds with different topographical cues, and investigate their interactions with neuronal cell to elucidate the mechanism by which oriented cues augment their function. In order to test this, we fabricated aligned, random and smooth topographies of PAN-MA polymer. Next we compared the adsorption of fibronectin on these scaffolds. Finally, we investigated the mechanistic relation between adsorbed fibronectin on oriented films and the migration of Schwann cells and axons *in vitro*. The outcomes of this Aim are discussed in Chapter 3.

#### 1.1.2 Specific Aim II

**Determine the interplay between polymer fiber-based thin film topography and fibrin cable/ECM organization and glial cell migration during repair of critically sized nerve gaps**

Our working hypothesis was that thin polymer films with oriented fibers promote endogenous fibrin/ECM organization and aids in effective Schwann cell migration. This in turn will result in successful nerve regeneration across long gaps. We fabricated electrospun aligned and random fibers as well as smooth film-based scaffolds. The oriented fiber scaffolds were tested with other topographies to investigate their ability to influence the regenerative sequence *in vivo* in a sciatic nerve gap model. Scaffold were explanted after five days, three weeks and 22 weeks to evaluate the effects of different topographies on the different steps of regeneration. The results of this Aim are discussed in Chapter 4.

## CHAPTER 2

### 2. LITERATURE REVIEW

#### 2.1. Injuries to the Peripheral Nervous System

##### 2.1.1 Introduction

Peripheral nerve injuries present a significant clinical challenge, as more than 250,000-300,000 peripheral nerve trauma cases are reported every year in the United States.[2] Injuries to the peripheral nervous system (PNS) are common and are a major source of disability, impairing the ability to move muscles and/or feel normal sensations, or resulting in painful neuropathies. Traumatic nerve injuries resulting from collisions, motor vehicle accidents, gunshot wounds, fractures, lacerations, and other forms of penetrating trauma, affected more than 250,000 US patients in 2002. Due to the difficulties in treating such injuries, more than 200,000 patients are left without any benefit of medical intervention. Even among the patients who receive treatment for traumatic peripheral nerve injuries, more than 50% show no measurable signs of recovery, or else suffer from drastically reduced muscle strength.[3] Due to poor recovery, a majority of patients are required to return for follow-up care to address the continued functional deficits. Surgical injuries result from surgical procedures such as prostatectomy (to remove prostate tumors). Prostatectomy procedures most often require sacrificing one or both of the cavernosal nerves while removing the tumor, adversely affecting erectile function and bladder control. In 2002, more than 260,000 US patients suffered major injuries to cavernosal nerves due to prostatectomies.

##### 2.1.2 Current strategies to address peripheral nerve injuries and their limitations

The advent of the operating microscope and advanced microsurgical techniques have improved clinical results and popularized nerve autograft surgeries after injury.[4] After nerve trauma, the standard clinical operating procedure is to appose the two nerve ends and suture them together without generating tension where possible. If the gap is large such that tensionless apposition is not possible, a nerve autograft - typically the patient's own sural nerve - is used as a bridge. While autografts are the best clinical bridges available today, there are many drawbacks to this procedure, including the need for a secondary surgery, loss of donor site function, limited availability, modality mismatch (arising from a sensory nerve being used to repair a motor or mixed nerve), and neuroma formation at the donor or graft site. Therefore, there is a clear and urgent, unmet clinical need to find an alternative approach that matches or exceeds the performance of autografts. Autografts possess several advantages in that, they are biocompatible, non-toxic, and provide a support structure to promote axonal adhesion and extension. However, a serious drawback to the use of autografts is that the availability of disposable nerve segments is limited, and multiple lengths of nerve graft are often needed to bridge the gap between the injured nerve stumps.[5] Moreover, only 40-50% of patients regain useful function when receiving autografts.[3] In addition, autografts contain inhibitory chondroitin sulfate proteoglycans (CSPGs), which may reduce their performance as bridges.[6, 7] Another drawback of autografts is that there may be a dependence on the type of autograft used for the modality of nerve regenerated. Using sural nerve grafts (which are the most commonly used autograft in humans) may exclude regenerating motor nerves.[8] Therefore there is a need for alternative strategies to bridge nerve gaps. Driven by this need, several bioengineering strategies are being pursued, primarily

involving the use of hollow polymeric ‘guidance channels’ such as the collagen tube (NeuroGen®, Integra Life Sciences) alone, or using guidance channels as carriers for hydrogel based scaffolds for nerve repair.[1] However, these have attained limited success, and present an opportunity for regenerative medicine and tissue engineering approaches.

## **2.2 The regenerative sequence**

### 2.2.1 Endogenous Sequence for nerve regeneration

Wallerian degeneration occurs at the distal axonal stump within the first 24hr after axotomy. The consequent production of myelin debris causes influx of macrophages followed by Schwann cell proliferation in the basal laminae as the bands of Büngner.[9-12] The basic sequence of events leading to successful nerve regeneration (when gaps are shorter) through guidance tubes has been characterized and schematically shown here (Fig 1.).[13, 14] Within a day of the initial injury, the tube fills with plasma exudate, and precursor molecules from within this fluid gradually coalesce into an oriented fibrin matrix that physically bridges the nerve gap. Cell types including fibroblasts and Schwann cells migrate from both nerve stumps through the aligned fibrin matrix and begin to multiply and differentiate, enriching and transforming the surrounding matrix.[14, 15] The Schwann cells migrating from the proximal nerve stump advance along with regenerating axons, which grow through the enriched matrix through the developing cellular regeneration cable that spans the nerve gap. Subsequently, regenerating axons and more migratory Schwann cells follow along this fibrin/extracellular matrix (ECM)/glial cell bridge, and the regenerating axons follow, entering the distal nerve stump and eventually making connections to the end organ.



Although scrambled, these re-formed neuromuscular junctions (NMJ's) significantly improve function, as suggested by surgical experience.

The formation of a continuous fibrin cable/matrix across the severed axonal ends is a critical step in the regenerative sequence, as the initial influx of Schwann cells involved in regeneration is dependent upon the physical support and guidance that the oriented matrix provides.[14, 16] In cases where this fibrin cable fails to form, for example across longer gaps, the cause is often attributed to improper or incomplete fibrin matrix formation.[13, 14] Furthermore, the structure of the fibrin matrix determines the organization, alignment, and distribution of the infiltrating glial cells (largely Schwann cells and fibroblasts to a lesser degree), and thus influences the morphology of the developing regeneration cable.[14, 16-18] A properly formed and located fibrin cable in the initial stages of regeneration, thus sets into motion the sequence of events culminating in Schwann cell stimulated peripheral nerve regeneration.[19]

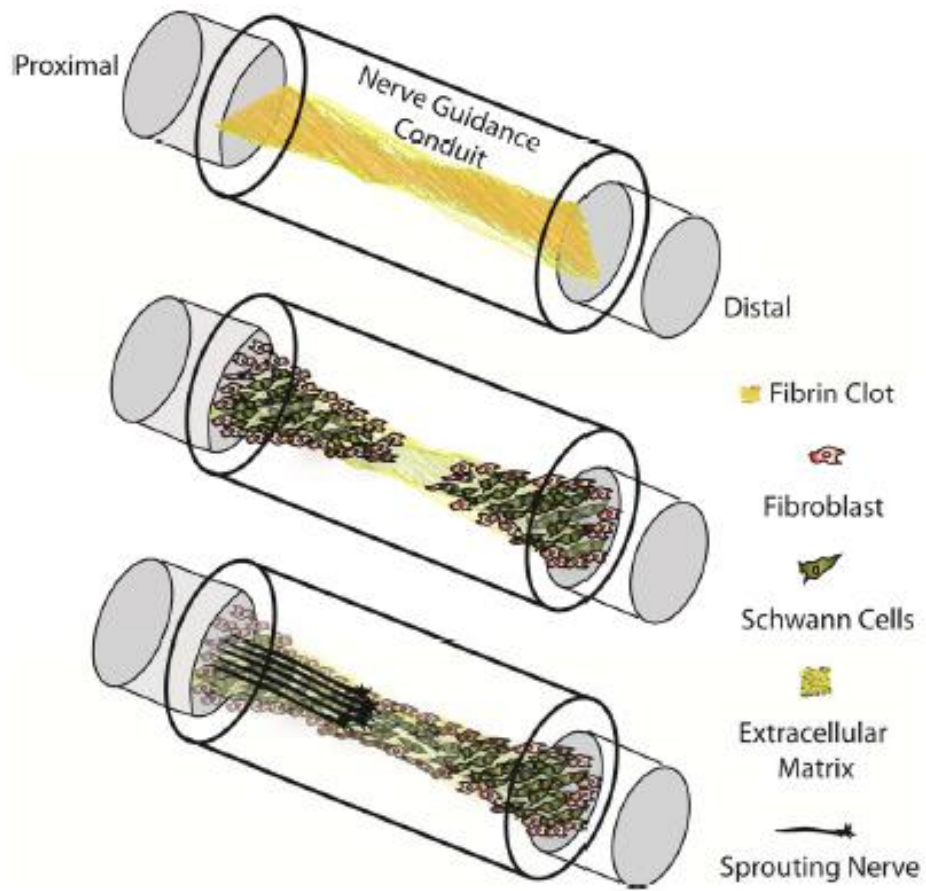


**Figure 1-1. Regenerative sequence of events in a non-critical length gap through a conduit.**

### 2.2.2 Influencing the regenerative sequence

The formation of the nerve cable can be influenced by a variety of factors, including guidance tube composition [20] and dimensions,[18] the addition of exogenous factors such as fibrin precursors,[14] and the incorporation of scaffolding material within the tube [21, 22] or the incorporation of cells with polymer guidance channels.[23, 24]

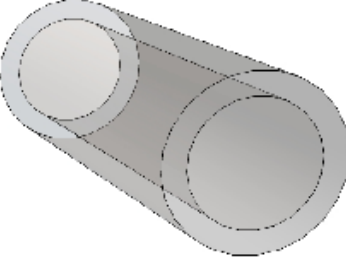
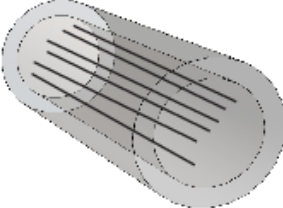
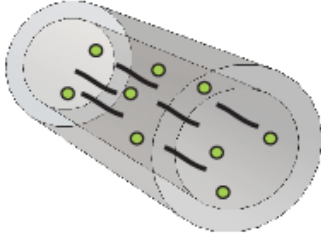
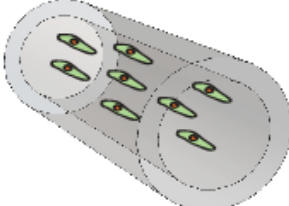
Various tissue engineering strategies have been used to influence different aspects of the regenerative process (Table 1-1) with hope for functional recovery. Initially, natural and synthetic guidance channels alone were used to ‘guide’ nerve regeneration from the proximal to the distal stump. They helped confine the growth cones to the lumen of the channel and directed nerve regeneration towards the distal nerve stump. While these tubular scaffolds were able to bridge small gaps (>10 mm) they typically failed to enable regeneration across larger gaps, perhaps because they are unable to sustain a contiguous fibrin cable over longer gaps. Therefore in order to augment or replace the function of the endogenous fibrin cable, ECM organization and glial cell migration into the lumen, tubular conduits have been filled with natural and synthetic scaffolding materials. These materials provide the necessary topographical cues that influence cell migration and its growth specific phenotypes. Additionally, by adding growth factors and ECM molecules to these scaffolds, nerve growth as well as supporting cell migration and behavior has been promoted in critical length gaps in various animal models. Finally, cell transplantation into tubular scaffolds has helped promote various aspects of the regenerative sequence by releasing neurotrophins and growth factors to promote nerve growth as well as creating the ECM to direct the regenerating nerve to its distal target.

The subsequent sections discuss how these strategies have been used to influence the regenerative sequence to promote peripheral nerve repair across nerve gaps (Table 1-2).

**Table 1.1.Strategies to stimulate different steps of peripheral nerve regeneration**

<b>Regenerative Sequence</b>	<b>Methods</b>
<b>Formation/Organization of Fibrin Cable</b>	Aligned fiber based film scaffolds Microfilaments
<b>Infiltration of Schwann cells and other supporting cells</b>	Tubular conduits Aligned fiber based film scaffolds Cell transplantation Chemotactic and growth factors Neurotrophins
<b>Formation/Remodeling of Extracellular Matrix</b>	Aligned fiber based film scaffolds ECM molecule delivery
<b>Axonal Regeneration</b>	Growth factor delivery

Table 1.2 Tissue engineering strategies to augment nerve regeneration in a critical length gap

Scaffold Design	Commonly used materials
<b>Tubular Constructs</b> 	<i>Natural</i> <ul style="list-style-type: none"> <li>• Artery</li> <li>• Veins</li> <li>• Collagen</li> </ul> <i>Synthetic</i> <ul style="list-style-type: none"> <li>• Silicon</li> <li>• poly(vinylidene fluoride-trifluoroethylene)</li> <li>• PLLA</li> <li>• PGA</li> <li>• PCL</li> <li>• PHB</li> </ul>
<b>Material Tube Fillers</b> 	<i>Synthetic</i> <ul style="list-style-type: none"> <li>• Microfilament</li> <li>• Poly(L-lactide-co-glycolide) (PLGA) fibers</li> <li>• Poly acrylonitrile-methacrylate electrospun aligned fibers</li> </ul> <i>Natural</i> <ul style="list-style-type: none"> <li>• Collagen Fibers</li> </ul>
<b>Biochemical Tube Fillers</b> 	<i>Growth Factors</i> <ul style="list-style-type: none"> <li>• NGF</li> <li>• BDNF</li> <li>• FGF</li> <li>• CNTF</li> <li>• NT-3</li> <li>• Gelectin-1</li> </ul> <i>ECM Molecules</i> <ul style="list-style-type: none"> <li>• Laminin</li> <li>• Fibronectin</li> </ul>
<b>Cell Transplantation</b> 	<ul style="list-style-type: none"> <li>• Schwann Cells</li> <li>• Genetically Modified Cells</li> </ul> <i>Stem Cells</i> <ul style="list-style-type: none"> <li>• Mesenchymal Stem Cells</li> <li>• Bone marrow Stromal cells</li> </ul>

## **2.3 Tissue engineering strategies to enhance nerve regeneration**

### 2.3.1 Tubular scaffolds to guide nerve growth: Natural Materials

Early attempts at enabling nerve regeneration included the use of nerve grafts obtained from donor nerves. These procedures revolved around a central thesis that functional sacrifices resulting from donor nerve grafts is necessary in order to rehabilitate critical higher order function.[25-27] Employing the use of non-nerve tissue to facilitate nerve regeneration for the first time, Paul Weiss showed that a narrow piece of tubular arterial cuff could be used to bridge nerve gaps, while successfully preventing neuromas and unwanted plasticity.[28] Venous and arterial grafts are biocompatible, and provide confinement of neurotrophic factors released from the distal stump, thereby driving nerve regeneration.[29-31] Among natural tubular scaffolds, autogenous venous nerve grafts have been the most successful in achieving functional recovery across 10 mm nerve gaps.[29, 32] Venous grafts remain intact throughout the process of nerve regeneration and are easier to extract compared to arterial grafts.[29] These natural tubular scaffolds promote nerve regeneration by influencing the different steps of the regenerative process, help confine cell migration and also provide the substrate which aids in fibrin cable and ECM formation. While natural materials have good biocompatibility, they often collapse when used in longer nerve gaps. Additionally, issues related to the limited availability of these explants as well as autograft triggered immune response are a few among many other reasons that prompted exploration of alternative materials to direct nerve growth.[33]

### 2.3.2 Tubular scaffolds to guide nerve growth: Synthetic Materials

Synthetic tubular scaffolds have similar advantages to natural scaffolds but additionally provide mechanical and structural control.[34] In the recent past, several guidance techniques using artificial nerve conduits have been developed to guide nerve regeneration towards the distal stump.[35, 36] The isolated environment provided by guidance channels helps confine and concentrate neurotrophic factors that are released by supporting cells while protecting the axons against collapse and invasion from immune cells.[29] The use of guidance channels eliminates functional loss at the donor site, a condition that is commonly associated with the use of autografts. Initial studies employing the use of short impermeable silicone tubes showed promising nerve regeneration across 3 mm gaps,[37] although, significant fibrosis and nerve compression was subsequently associated with the use of these tubes.[38-40]

With the advent of biodegradable materials and changes in tube design,[20, 36] tubular scaffolds carry the promise of being used increasingly to entubulate nerve ends, while facilitating isolated and directed growth across the nerve gap. These scaffolds provide more control over length and diameter and are more readily available when compared to autografts.[34] Tubular scaffolds can be modified to support cell growth, allow for exchange of nutrients and degrade at a rate slower than the rate of regeneration.[20] These favorable features have inspired the development of biodegradable nerve guidance channels as viable alternatives to autografts.

Biodegradable polymers such as poly(L-lactic acid) (PLLA), polyglycolic acid (PGA) and poly(lactic-co-glycolic) acid (PLGA) were originally the materials of choice for synthesizing conduits, due to their relative abundance and applicability.[41-43] Traditionally, a modified dip-molding method with particulate leaching has been used to



fabricate biodegradable polymer conduits to support nerve regeneration.[44] Conduits made from these polymeric biomaterials were shown to successfully facilitate nerve regeneration across 8-10mm gaps.[45-49] Axon density in PLLA biodegradable porous nerve conduits was similar to that of autografts in a 10 mm sciatic nerve defect.[42] Although synthetic materials provide more control over the overall design specifications of the conduit, their continued use is restricted due to a number of disadvantages: a) their surface chemistry and hydrophobic nature are incompatible with regenerating cells and tissue;[50] b) their elastic properties do not match that of soft tissue; c) they are difficult to derivatize and immobilize, and hence often hard to work with; [51] d) acid by-products of the degrading scaffolds create a toxic environment for cells, and have been speculated to inhibit axonal growth; [52] e) rapid break down of larger polymer masses following initial degradation drastically reduces the overall life of the implant.[51] More recently, newer polymers based on natural materials such as poly(3-hydroxybutyrate) (PHB), and biocompatible synthetic co-polymers such as poly(L-lactide-co- $\mu$ -caprolactone) (PCL) have shown promising results in similar applications.[49, 53, 54] PHB is a naturally occurring linear polyester of bacterial origin that is biochemically synthesized for use in biomedical applications. This polymer has a very high Young's modulus of approximately 4 GPa [55] and has only recently been used in nerve conduits.[56, 57] PCL is a semi-crystalline synthetic co-polymer currently being favored for the fabrication of nerve conduits. Like other synthetic biopolymers, it is degraded by acid-hydrolysis of the ester bond, releasing acidic monomers. Compared to other synthetic co-polymers however, its crystalline structure, large molecular weight and hydrophobic properties make it less susceptible to degradation. The slow degradation rates of PCL scaffolds

results in reduced accumulation of toxic byproducts, thereby facilitating cell proliferation and tissue synthesis *in vitro* and *in vivo*. [58, 59] Degradation products are effectively eliminated via renal clearance. For applications where faster degradation of PCL is required, chemical modifications to the PCL diol can be made to result in a macromer susceptible to faster degradation. [60]

### 2.3.3 Tubular scaffolds to guide nerve growth: Design Specifications

The design criteria for fabrication of scaffolds should address various factors including but not limited to- elastic modulus, permeability, topography, swelling ratio, degradation rate, size of degradation products and clearance. [51] The elastic modulus of the scaffold should be at least 1200 kPa in order to be used in bridging peripheral nerve gaps. [61] These scaffolds can resist compressive and tensile forces, both during the surgery as well as from surrounding tissue post implantation. Early studies on the effects of porosity on nerve regeneration suggest the need for semi-permeable conduits in order to promote regeneration of myelinated and unmyelinated axons. [62] In the recent past, Improvements in conduit design have led to greater control over dimension, porosity and topography. By controlling the flow rates of polymer solutions, semipermeable hollow fiber membrane (HFM) guidance channels can be created. These conduits act as a molecular sieve, facilitating the diffusion of various trophic factors while limiting the infiltration of inhibitory molecules. The fabrication process can also be controlled to create an aligned texture on the inner walls of the conduit, thereby making it more amenable to axonal growth. [63] The extent of permeability however should be limited to the range of 50,000-100,000 daltons, as nerves regenerating in extremely porous environments display the presence of connective tissue and unwanted neural

plasticity.[64] Scaffolds made up of electrospun micro- and nanofibers are structurally similar to fibers present in the ECM, and hence do not have the disadvantages presented by rigid scaffolds. PLGA microsphere based spiral scaffolds as well as aligned nanofiber scaffolds incorporating blended materials such as PCL/gelatin, PLGA/PCL, PCL/chitosan and PCL/collagen claim to achieve superior cell attachment and proliferation when compared to traditional materials.[65-69] Materials that are susceptible to rapid degradation display larger mesh sizes, reduced elastic modulus and increased swelling. Hence, a low degree of swelling is necessary to maintain the integrity of the conduit and to prevent nerve compression. Degradation products released as a result of conduit hydrolysis can render the environment toxic if not cleared promptly. In order for the degradation products to be effectively cleared via renal clearance, they should be soluble in the blood stream and be <50 kDa in size.[70]

Fibrous protein scaffolds using collagen, fibronectin and laminin facilitate attachment of support cells during neovascularization, and provide guidance cues for regenerating axons.[71] Collagen has been a favored biomaterial due to its ability to self-assemble into biodegradable fibrils of significant strength.[72, 73] Collagen tubes made up of type-1 bovine collagen are flexible, can be co-infused with other ECM proteins such as laminin, and are strong enough to be sutured.[74] They have been shown to match autograft performance over short gaps (4 mm) in rodents and primates, and can support regeneration over longer 15 mm gaps.[74, 75] These conduits also enabled enhanced revascularization, Schwann cell association and axonal regeneration compared to silicone tubes, across 5 mm and 10 mm sciatic nerve gaps.[76] Comparing fibrin glue and PHB conduits, Kalbermatten et al.[77] reported superior nerve regeneration and Schwann cell

migration in fibrin glue conduits than PHB conduits. The use of electrospinning techniques to make aligned nanofibrous scaffolds makes proteins like collagen attractive targets for the production of biodegradable fibrous scaffolds. However, the process may significantly alter the biological properties of collagen when electrospun out of fluoroalcohols, and should hence be avoided.[78]

#### 2.3.4 Limitations of tubular scaffolds

Both natural and synthetic tubular scaffolds promote endogenous repair mechanisms of nerve regeneration by stimulating cell migration and guiding axonal growth. They also serve as excellent model systems to understand the cellular and functional aspects of peripheral nerve regeneration. While these conduits provide the necessary guide for the nerve and the supporting cells, they have failed to bridge gaps longer than 10 mm in rats without the addition of exogenous factors. They fail to maintain a stable fibrin cable which is essential to guide Schwann cell migration and stimulate the rest of the cellular events necessary for successful nerve regeneration.[34] In order to provide a stable substrate for fibrin matrix organization and Schwann cell proliferation, structural support inside the tubular scaffolds may need to be introduced to enable bridging of longer nerve gaps.

### **2.4 Exogenous factors to enhance regeneration**

#### 2.4.1 Growth Factors to promote cellular phenotype

Previous strategies to bridge nerve gaps have typically not been successful when trying to bridge gaps greater than the critical gap (15 mm in rats) length. These techniques have failed because they are not able to sustain fibrin cable formation, stimulate Schwann cell migration, or provide a substrate upon which ECM can organize

and support neurite outgrowth. In order to create scaffolds that can match or exceed the performance of autografts, these limitations have to be addressed. These approaches focus on including biochemical elements (with or without structural elements) to enhance cell migration, aid cell adhesion, and provide other trophic factors to enhance the function of cells involved in the nerve regeneration process.

Even though, different topographies from natural filaments to polymeric fiber films have been used to augment cell migration, their effects can be enhanced by the conjugative delivery of biomolecules to further stimulate cell behavior. Cao et al.[79] used nerve growth factor (NGF) gradients to direct neurite extension *in vitro*. These factors can be directly incorporated into the conduit to enhance nerve regeneration.[80] NGF has also been integrated into biodegradable electrospun fibers for long term release.[81] While NGF has been used to directly affect neurite outgrowth, other growth factors have been explored to indirectly improve nerve regeneration. Since axons are attracted to chemotactic factors, most strategies designed to induce neurite outgrowth focus on contact guidance and diffusible factors. Biodegradable poly(phosphoester) polymer microspheres have been used for sustained release of NGF to promote nerve regeneration.[82] While soluble factors provide short term trophic support, delivery vehicles like nanoparticles and lipid microtubules have been used for sustained delivery of growth factors and other biomolecules.[1, 83]

Brain-derived neurotrophic factor (BDNF), fibroblast growth factor (FGF) and ciliary neurotrophic factor (CNTF),[84] have also been used to elicit growth promoting behavior in neuronal and glial cells. BDNF in particular, has been shown to improve the myelination phenotype of Schwann cells *in vitro*.[85] BDNF encapsulated in calcium

alginate allowed for its prolonged and continuous release, and consequently increased axonal regeneration.[86] The joint use of BDNF and collagen tubulization resulted in better regrowth than in treatments without BDNF. Furthermore, animals given this joint treatment had axons with larger diameters.[87] The incorporation of FGF into the inner layer of a double layered nerve guide allowed for continuous release. Its presence resulted in enhanced Schwann cell proliferation.[82] The integration of FGF into collagen films using a layer-by-layer assembly technique increased the bioactivity of the substrate while maintaining the integrity of the growth factor.[88]

While neurotrophins have been primarily studied to stimulate nerves, recent studies have shown that they may have important effects on glial cells such as Schwann cells. Neurotrophin-3 (NT-3) has been suggested as a potent stimulator of Schwann cell migration based on *in vitro* results.[85, 89, 90] Galectin-1 has also shown to improve Schwann cell migration after peripheral nerve injury. Administration of galectin-1 in acellular grafts induced Schwann cell migration from both the proximal and distal side.[91] By encouraging cell migration, the subsequent steps of nerve regeneration can be indirectly stimulated through the use of neurotrophins and growth factors.

#### 2.4.2 ECM molecules

ECM molecules such as laminin and fibronectin have been used to provide adhesion sites and stimulate neurite extension *in vitro* and nerve regeneration *in vivo*. While endogenous ECM production by support cells has been promoted by topographical cues, tissue engineered scaffolds can also be fabricated to stimulate enhanced regeneration by providing exogenous ECM molecules.

ECM molecules have been incorporated into guidance channels to encourage peripheral nerve regeneration. Microlithography substrates that were patterned with laminin were able to direct Schwann cell orientation.[92] Previous work with scaffolds presenting laminin and NGF in 10 mm nerve gaps were comparable to autografts in terms of gastrocnemius muscle weight and sciatic functional index. Since scaffolds with just laminin or NGF were not able to successfully bridge the nerve, the study suggested that the presence of both ECM molecules and growth factors is necessary for peripheral nerve repair.[93] Anisotropic scaffolds with gradients of laminin and NGF embedded in hydrogels have shown to be comparable to those of nerve autografts in a challenging 20 mm nerve gap in rat; however, this was not true of isotropic scaffolds. The use of laminin gradients in anisotropic scaffolds matched autograft performance in terms of number of myelinated axons and axon density.[1]

Fibronectin is another widely used ECM molecule with adhesion motifs that have been shown to guide nerve growth. Fibronectin patterned surfaces were able to spatially control neurite outgrowth *in vitro*. [94] Fibronectin mats and cables were used as ECM based scaffolds to guide neurite outgrowth in small gaps.[95] These surfaces were able to provide biochemical support as well as directional cues to the regenerating nerve and supporting cells. Hydrogels made up of a combination of ECM molecules consisting of collagen-1, fibronectin, laminin and hyaluronic acid have been used to study neurite outgrowth.[96] These hybrid gels were rich in ligand presentation for adhesion and migration while promoting nerve regeneration.[96, 97] Other self-assembly polymeric hydrogels with specific cell adhesion motifs have also been fabricated for neural tissue engineering purposes.[98] Overall, growth factors and ECM molecules can enhance cell

phenotypes; their use in *in vivo* studies has steadily been increasing, due to their long term availability and bioactivity. Thus the ability of ECM molecules to stimulate neurite outgrowth growth can be used simultaneously with other strategies to enhance endogenous repair mechanisms of peripheral nerves.

### 2.4.3. Cell transplantation

Many delivery systems have been used to deliver growth factors, ECM molecules, and other biomolecules to augment nerve regeneration. But a major drawback of the delivery system is that they are not capable of sustaining active release of these molecules over the complete course of the peripheral nerve regeneration process. In 25 mm gap rat models, electrophysiological recovery was observed after 50 days, resulting in a growth rate of 0.5 mm/day.[99] However, regeneration across such a large gap was only possible due to the addition of neurotrophic factors to the conduit, which can only be delivered once. As a result, techniques to stimulate resident populations of Schwann cells to continually express these supportive factors have been developed. These modified Schwann cells are then loaded into nerve bridging conduits to aid in the progression of myelination and influence other steps of the regenerative sequence as described below.

#### *2.4.3.1. Schwann cell Transplantation*

Besides promoting the migration of Schwann cells using topographical and biochemical cues, some methods have directly introduced Schwann cells into the nerve gap. Though, initially, the transplantation of Schwann cells was implemented in an effort to overcome the challenge posed by long gaps that prevented regeneration. Schwann cells were implanted in L-lactide and  $\epsilon$ -caprolactone conduits to bridge 12 mm gaps. In these copolymer guides, regeneration represented by axonal extension was present midway



through the defect.[24] Additionally, large concentrations of Schwann cells (greater than  $5 \times 10^5$ ) were seeded in conduits to support a longer nerve defect (18mm). The results of this setup showed a correlation between the number of Schwann cells implanted and the number of myelinated axons that were present at the distal end. It was also noted that Schwann cells imparted the majority of their beneficial effects during the early stages of regeneration.[23]

Schwann cell transplantation has been used along with other techniques described above to ameliorate the process of nerve regeneration. Collagen conduits filled with Schwann cell-implanted filaments and Matrigel incorporated with Schwann cells were used to bridge a 24 mm gap. The Schwann cell conduits resulted in larger axonal densities and diameters than the controls without Schwann cells.[100] To attempt to achieve results comparable to those produced by autografts, small intestinal submucosa (SIS) conduits filled with Schwann cells were implanted. These conduits were more effective than conduits without Schwann cells. With sciatic function indexes and extensor postural thrust testing, the loaded conduits came close to the numbers generated by the use of an autograft.[88, 101] Similarly, Schwann cells have been grown on SIS and implanted in SIS sponges, where they have been shown to effectively aid in regeneration. On these surfaces, they are able to adhere, migrate, and express growth factors.[88] To determine the effects of allogeneic versus syngeneic Schwann cells, both were loaded into PHB conduits. Even though allogeneic cells underperformed in comparison to syngeneic cells, their availability makes them a more attractive option, especially when time is crucial to the effectiveness of the regenerative process.[102] Co-encapsulation of fibrin matrix and Schwann cells in biodegradable polymeric tubes also promoted

Schwann cell migration compared to empty tubes with the same polymer.[77] Using a novel cell culture system comprised of a thermoresponsive micropatterned surface, Tsuda et al. demonstrate the ability to grow endothelial cells, and harvest cell sheets by utilizing the thermoresponsive properties of the polymer, poly(N-isopropylacrylamide) (PIPAAm).[103] This technique could potentially be used to culture and harvest viable glial cell sheets for subsequent implantation into scaffolds. Thus, combining cell transplantation with other techniques can be utilized to affect several steps of the regenerative sequence.

#### *2.4.3.2. Genetically Modified Cells*

To further improve the performance of Schwann cells, they have been genetically engineered to positively affect their inherent release mechanisms and factor expression capabilities. Schwann cells have been modified to overexpress low and high molecular weight FGF-2 isoforms through somatic gene transfer. The low molecular weight isoform was found to have an inhibitory effect on regeneration which was evident in the low rate of myelination, while the high molecular weight isoform was observed to encourage myelination, especially in the distal region.[104] Schwann cells have also been transfected to produce glial cell line-derived neurotrophic factor (GDNF). These genetically modified cells were then injected into a conduit in order to bridge a 10 mm defect. After 16 weeks, the conduits with the GDNF expressing Schwann cells produced a greater number of myelinated nerves with higher nerve conduction velocities.[86]

#### *2.4.3.3. Stem Cells*

Alternative methods have also been investigated with the approach of using stem cells and their inherent potential to differentiate into cells that exhibit the Schwann-cell

phenotype. Skin derived stem cells have been employed in conduits to bridge 16 mm gaps. Their enhancement effect shows that these stem cells may also be a source of supportive factors that are utilized in repair.[105] Additionally, ectomesenchymal stem cells (EMSCs) were treated for 6 days in forskolin and bovine pituitary extract in order to induce Schwann cell-like behaviors. The EMSCs were combined with collagen and then injected into PLGA conduits made for 10 mm gaps. The conduits with EMSCs produced sciatic functional index values that were statistically comparable to those found in the autograft group.[106] In a comparison between the performance of mesenchymal stem cells and Schwann cells, mesenchymal stem cells were able to mimic Schwann cells but were unable to match their myelination capabilities.[107] In another study, nerve regeneration distance in 14 mm nerve conduits in rats were significantly better with mesenchymal stem cell encapsulation in fibrin matrix compared to empty tubes.[77] Similarly, bone marrow stromal cells have been transplanted into the nerve injury site where they were observed to have differentiated into Schwann cells. This process takes advantage of bone marrow stromal cells, which are easily acquired and prepared for injection.[94] In a 12 mm rat sciatic nerve model, bone marrow stem cell derived Schwann cells significantly increased the number of regenerated axons compared to control group without cell transplantation.[108] Induced pluripotent stem cells (iPS) were first induced from mouse embryonic stem (ES) cells and adult fibroblast cells by the introduction of four transcription factors.[109] Since then, the possible use of iPS cells in nerve regeneration has garnered significant interest. Dimos et al. [110] showed for the first time that iPS cells isolated from a patient diagnosed with a familial form of amyotrophic lateral sclerosis (ALS) can be directed to differentiate into motor neurons.

Cell viability is of particular interest for stem cell transplantation in an artificial conduit. Therefore, to boost cell viability collagen immobilized nanofibers have been used to culture cortical neural stem cells and could be used for peripheral nerve scaffolds.[78] Thus, when cell transplantation techniques are combined with other previously discussed strategies, the endogenous mechanisms of nerve regeneration can be significantly enhanced.

#### 2.4.4. Electrical Stimulation

A major challenge to a successfully regenerating is to avoid muscle atrophy due to the length of time it requires to bridge the nerve gap and innervate the target muscle. To this end, we have discussed several strategies to promote nerve regeneration throughout the chapter. Electrical stimulation is another technique that has been used to promote nerve regeneration. Electrical stimulation is known to positively influence nerve regeneration both *in vitro* and *in vivo*. [64] Previous work has shown that electrical stimulation to the soleus nerve of rabbits after a crush injury promoted twitch force, tetanic tension and muscle action potential in soleus muscle indicating enhanced axonal growth [111]. To elucidate how electrical stimulation accelerated nerve growth, other groups evaluated its effects on production of growth factors as well as other cellular responses. Stimulating motoneurons at 20 Hz for 1 hr accelerated sprouting of axons after nerve injury [112, 113]. After electrical stimulation, BDNF and trkB receptor expression was unregulated in motoneurons [113]. Similar observations were observed by another group where they observed increased neurotrophin production after electrical stimulation following nerve repair using a nerve allograft [114]. Electroconductive piezoelectric poly(vinylidene fluoride-trifluoroethylene) conduits showed enhanced nerve regeneration when compared to unpoled tubes.[115] More recently, polypyrrole (PPy) conduits functionalized to carry neuronal growth factor (NGF), stimulated the growth and

differentiation of PC12 cells, similar to cells growing in NGF-containing media *in vitro*. [116] Other recent advances include the potential use of electrically active and functionalized carbon nanotube (CNT) scaffolds as suitable substrates for the growth and attachment of neurons. [117-119]

Thus, future strategies can use electrical stimulation in conjunction with other scaffolds discussed throughout this chapter to accelerate successful nerve repair following a peripheral nerve injury.

## **2.5. Topographical cues to understand mechanisms in vitro**

### 2.5.1. Micro/Nanopatterning in vitro to better understand axon guidance

Multitudes of physical and biochemical signals are required for optimal regeneration of the central (CNS) and the peripheral nervous systems (PNS). Understanding the rules governing axonal guidance could inform strategies to design regenerative therapies such that optimal topographical and biochemical cues can be presented to regenerating axons. Micro/nanopatterning on two dimensional substrates provides us with the degree of spatial control necessary to probe axonal response to well-controlled topographical and biochemical cues [120, 121]. Some of the nanotechnology based efforts described in this section are invaluable in informing the next generation of tissue engineering strategies aimed at repairing or regenerating the nervous system.

### 2.5.2. Microfabrication to create patterns to observe the effects of topographical cues

Neural tissue engineering scaffolds are often designed with specific topographical guidance cues which aid in the adhesion and migration of neuronal cells. Microfabrication techniques developed for use in the microelectronics industry have been adapted to achieve micro- and nanoscale patterning on experimental substrates. For

instance, using photolithography, lanes with depths ranging from 50 nm – 6  $\mu\text{m}$  can be etched and different chemistries laid on the fused-silica slide substrate, in order to understand the effects of hierarchical interactions on cellular behavior [122]. For instance, lanes patterned with alternating hydrophobic methylsilane and laminin can be applied to evaluate neurite orientation in response to patterning and surface chemistry simultaneously. These studies point to the conclusion that neurites preferentially adhere to adhesive laminin substrates and also respond to topographical gratings of differing depths. The neurites become highly aligned when the groove depths exceed 1  $\mu\text{m}$ . Other fabrication techniques such as electron beam lithography also allow us to fabricate substrates with features down to a few nanometers [123, 124], potentially allowing multiple cues to be sampled by the same axon or growth cones. This level of control enables further study into how information might be processed or integrated by single axons or growth cones. Thus, nanoscale patterning technologies provide an important tool in promoting our understanding of growth cone function with regard to their ability to detect and process topographical and biochemical cues.

### 2.5.3 Observing axonal interaction with ECM proteins using dip-pen nanolithography

Dip-pen nanolithography (DPN) is another technique which has been applied to study how axons interact with their extracellular environment. DPN has been used to print collagen and collagen like structures with line widths of 30-50 nm [125]. This technique provides a robust means of organizing collagen into its hierarchical structure, while maintaining its bioactivity. Briefly, lyophilized rat tail collagen can be thiolated in an acidic environment to maintain its bioactivity. Atomic force microscopy is then used to perform the DPN, by dipping the AFM tip in the aqueous peptide solution and

patterning in tapping mode, while changing the angle to achieve collagen like structures. This technology has vast potential in nanopatterning because it can be used to fabricate a variety of polymers at size scales similar to their natural states. In terms of neural tissue engineering, this technology can be very useful in understanding neuronal responses to different topographical cues and peptide epitopes, as well as in designing scaffolds with nanoscale features to enhance cellular behavior.

Proteins, synthetic amino acids, and small peptides can be patterned on different substrates with extraordinary spatial control to modulate axonal growth. Nanopatterning can thus provide higher resolution to differentially provide chemoattractants and repellants at specific sites within the vicinity of a single growth cone for the purpose of probing basic cell behavior [121] and improving the design of constructs used in neural tissue engineering.

## **2.6. Fiber Based Topographical cues**

Natural fibers can be formed from materials such as amphiphilic molecules, silk, and collagen. The inherent properties of fiber based materials make them highly biocompatible, given their permeability and compliant nature. In particular, permeability allows for the diffusion of needed nutrients that enhance the adhesion and migration of cells. However, these same properties make the production of such fibers complex, and fiber orientation to guide cell migration is hard to control [126].

### 2.6.1 Self assembling peptide nanofibers

Natural fibers can be formed through the fabrication of peptide-based amphiphilic molecules. These molecules exist in solution and then self assemble when introduced to

suspensions of cells such as neural progenitor cells [98]. Forces from ionic bonding, hydrogen bonding, van der Waals interactions, and hydrophobic responses drive the formation of the peptide self assembly process and generate a gel-like solid [98]. The hydrophilic heads of the amphiphilic molecules can be designed to include specific epitopes. For example, the incorporation of the sequence isoleucine-lysine-valine-alanine-valine (IKVAV) can help promote neurite growth [127]. Nanofibers with IKVAV built in are 5-8 nm in diameter and range from hundreds of nanometers to a couple of micrometers in length [98]. When compared to laminin and poly(D-lysine) substrates, cells cultured on IKVAV nanofibers differentiated more quickly. Additionally, these nanofibers performed better than coatings of IKVAV soluble peptides because the nanofibers provide higher density of epitopes [98]. Thus, these fibers with the incorporation of specific epitopes into nanofibers are shown to aid in neuronal differentiation.

Peptide-amphiphile nanofibers can also be produced through soft lithography. In this process, a stamp of the fiber orientation is created and then pressed upon a solution of peptide-amphiphilic molecules [128]. This arrangement is then evaporated, sonicated, and dried to produce aligned nanofibers. The dimensions of the fibers depend on the percent weight of peptide amphiphiles. For 5 wt % peptide solution, the fibers produced had a width of 200-300 nm with a height of about 55.1 nm while the 1 percent solution produced widths of 150 nm and a height of 23.1 nm [128]. However, they have only been shown to be compatible with media and further studies need to be done with cell cultures to better determine their effects.

#### 2.6.2. Silk fibers to enhance nerve regeneration



Silk fibroin fibers represent another class of natural fibers that has been used to promote nerve regeneration. After the removal of sericin, which causes adverse immunological responses, the silk fibroin was extracted to produce fibers that were 15 micrometers in diameter. Their effects on DRGs and Schwann cells showed their biocompatibility and ability to promote cell growth [129]. Silk fibers from spiders have also been utilized to produce conduits. Extracted from the glands of spiders, these fibers are 10 micrometers in diameter and allow for better adhesion than polydioxanone monofilaments. In addition to adhesion, they are able to support cell migration and are biocompatible and biodegradable; however, their tedious extraction method is a major limitation [130].

### 2.6.3 Magnetically aligned nanofibers for cell alignment

Collagen is commonly used since it is a natural component of the ECM, providing structural strength through fibrous networks. Collagen can also be magnetically treated to produce a gel rod of aligned collagen fibrils. In strong magnetic fields a high degree of collagen alignment is produced. This was shown through a comparison of collagen gel produced in a magnetic field of 4.7T and 9.4T [131]. As a result, when seeded with dorsal root ganglia (DRGs), this alignment facilitated oriented neurite extension. When combined with Schwann cells, directed migration occurred and was further enhanced in the presence of 10% fetal bovine serum [131]. This data suggests that aligned collagen fibers are promising candidates as substrates for guided nerve regeneration.

### 2.6.4 Biosynthetic and synthetic fibers

Biosynthetic and synthetic fibers can be created through a variety of process include extrusion and electrospinning. While naturally derived polymers including

collagen, elastin, and gelatin would be useful starting materials for fabrication of oriented substrates for nerve regeneration, they present technical challenges from a fabrication perspective. One solution may be to mix natural materials with synthetic polymer solutions.

To 'electrospin' a fiber, a difference in voltage is used to propel polymer fibers to a target (Figure 1.2). Oriented fibers can be fabricated by having the target spin at high speeds. Electrospun fibers can have functional groups that can be exploited to aid in cell adhesion [126]. Furthermore, these aligned fibers guide glial alignment and promote directed growth (Figure 1.2.C). Like natural fibers, most biosynthetic materials are hard to fabricate due to their inherent properties, while synthetic fibers are the least problematic to produce .

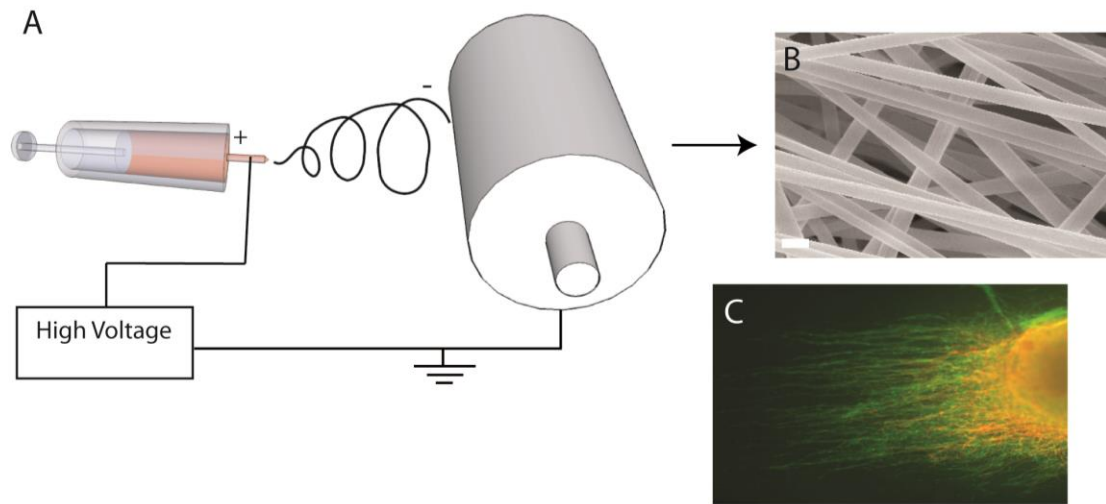


**Figure 1-2. Electropinning Setup.** A) Electropinning setup to fabricate aligned fibers. B) Scanning electron micrograph of thin film of aligned electrospun fibers. C) Dorsal root ganglion seeded on aligned electrospun film.

#### *2.6.4.1 Fabrication through electrospinning*

Relative to extrusion and other techniques, electrospinning is a facile method of producing nanofibers. Fabrication starts with a polymer solution or melt that is pumped from a syringe. The polymer stream travels from a charged syringe to an oppositely charged collector. Before anchoring to the collector, electrostatic repulsion between the strands results in “splaying” which produces extra-fine fibers [126]. To enhance the alignment of the fibers, collectors such as rotating drums or discs can be used. Electrospinning can be tailored to match the size of nerve fibers *in vivo* or to match mechanical properties of the nerve. These properties can be tailored through the manipulation of several factors, including the flow rate, voltage, distance between the syringe and the collector, design of the collector, and viscosity of the polymer solution or melt. The rotational speed of the collector can also be altered to change the orientation of the fibers. Nevertheless, the speed can only be increased as long as the collected polymer jet is still continuous. Examples of electrospun fibers for neural tissue engineering are given below.

#### *2.6.4.2 Synthetic electrospun fibers for neural tissue engineering*

The most widespread synthetic polymers in neural tissue engineering are poly(alpha-hydroxy esters) which include poly(glycolic acid) (PGA), poly(lactic acid) (PLA), and a co-polymer of the two poly(lactic-co-glycolic acid) (PGLA). These synthetic polymers are frequently used due to their advantageous biodegradable properties and their ease of electrospinning [132, 133]. Another member, polycaprolactone (PCL), is also used when a slower rate of degradation is desired especially in some drug delivery applications.

#### *2.6.4.3 Biosynthetic fibers with conductive properties*

Since natural materials are difficult to spin, they can be co-spun with synthetic polymers. For instance, a conductive polymer, polyaniline (PANi) can be combined with gelatin and then electrospun [134]. Several polymer solutions with varying amounts of PANi were produced and their fibers ranged from 924 nm to 48 nm in size [132]. The solutions with higher concentrations of PANi produced thinner fibers. Additionally, the proportion of gelatin in the solution should not be less than 5% due to the possibility of beads forming on the fibers. These fibers were then seeded with H9c2 rat cardiac myoblasts, and the cells were shown to proliferate [135]. Interestingly, when the width of the fiber was greater than 500nm, cell alignment was induced. These properties of biocompatibility and conductivity show promise for future implementation in nanofiber scaffolds.

#### *2.6.4.4 Biosynthetic fibers to aid in Schwann cell migration*

To improve axonal regeneration, one study compared aligned poly-caprolactone (PCL) and a combination of PCL and collagen fibers. The mixed solution consisted of 25% collagen and 75% PCL constrained by the fact that increasing the proportion of collagen also increases the difficulty of spinning aligned fibers [136]. In this study, the PCL fibers were 889-259 nm in diameter while the collagen and PCL fibers were 705-377 nm in diameter [136]. After DRGs were seeded on the fibers, the collagen and PCL fibers were observed to produce more directed neurite outgrowth. With the seeding of Schwann cells, the mixed fibers were shown to have better adhesion and faster migration [136]. These effects are probably due to the presence of collagen which is naturally found

in the ECM. Therefore, the incorporation of collagen into nanofibers can aid in Schwann cell migration and axonal regeneration.

#### *2.6.4.5 Topography for controlled migration of Schwann cells*

Topographies are generated to mimic the existing physiological structures of the ECM in the hopes that similar cues will promote cellular growth, adhesion, and differentiation. Schwann cells play a significant role in neurite extension and migration since they myelinate axons. They also secrete ECM molecules like laminin and produce numerous neurotrophic factors such as NGF, BDNF, and NT-3, which aid in the nerve regeneration process. Utilizing micropatterned filaments allows Schwann cells to be properly aligned to form bands of Bungner, a critical phase in axonal regeneration. This alignment is what directs neurite outgrowth. These microstructured filaments can then be inserted into a conduit to enhance regeneration in rat nerve gaps. Conduits incorporated with oriented nanofiber scaffolds have also been able to recreate the bands of Bungner. These nanofiber scaffolds promote Schwann cell migration after peripheral nerve injuries and have shown functional outcomes comparable to autografts.

### **2.7. Topographical filler materials to augment peripheral nerve regeneration**

In longer gaps (>10 mm in rats) regeneration is limited by the lack of a stable fibrin cable formation. This results in no Schwann cell infiltration into the nerve conduit along the fibrin cable/bridge. Schwann cells along with other supporting neuroglia are critical for successful peripheral nerve regeneration because they produce the necessary trophic factors and ECM molecules to guide axonal growth and enhance regeneration.[137-139] Several strategies have been developed to stimulate Schwann cell migration and align axonal growth. These strategies focus on alignment and movement of

supporting cells because their directed development is essential for nerve growth. By providing substrates that facilitate efficient migration of Schwann cells into the nerve gap, and enhancing their ability to provide trophic support, endogenous cellular mechanisms can be optimized to stimulate nerve regeneration.

Theoretically, internal scaffolding (internal to the tube which now acts as a carrier of the scaffolding) can enhance regeneration by some combination of (1) bolstering the fibrin matrix by contributing to its formation and maintenance; and (2) replacing its function, by providing an alternative source of aligned substrate, thereby being able to support and direct the migration of supporting glial cells such as Schwann cells. Topography also has been shown to influence both cellular phenotype and ECM organization. Recent stem cell literature has stressed how different topographies have influenced stem cell fate towards a specific cell type. Similar observations have also been made in the field of biomaterials. Materials with microscale topographies have been shown to influence cell alignment [140, 141] and ECM organization [142, 143] in different cell types including neural cells.[134]

Several materials have been introduced to the nerve gap using conduits as carriers to stimulate the different steps of regeneration. These materials range from natural ones to synthetic ones. Since it is a naturally occurring component of the ECM, collagen has been used in applications for nerve regeneration. Its compatibility and structural strength make it an attractive candidate for substrates.[144, 145] Magnetically aligned collagen fibers have been used to adequately bridge 6 mm nerve gaps in mice.[146] In longer gaps in rats, collagen filaments supported a higher number of myelinated axons compared to collagen tubes [145] and were able to match autograft performance in the number of

myelinated axons.[145, 147] While small gaps (< 10 mm in rats and < 30 mm in humans) can be bridged using tubulization methods, providing aligned collagen fibers helps traverse longer gaps by supporting Schwann cell migration and directing neurite outgrowth. The use of nanometer-sized cell/ECM multilayer films can be used to facilitate attachment of a second layer of cells.[148] The technique involves the use of a layer-by-layer fabrication process to deposit ECM components on top of a layer of cells, and can potentially be used to support schwann cell migration and neurite outgrowth. Even though these substrates created from ECM components provide the surface ligands that stimulate adhesion and migration of cells, control over their structural features is hard to achieve since they are difficult to fabricate and handle for use in nerve regeneration.

Processing techniques to manipulate polymers at micro- and nano- scales such as micro lithography, microcontact printing and electrospinning have been used to fabricate synthetic scaffolds with structural features similar to naturally occurring matrix with relative ease. Features such as micro- and nano- topographies and mechanical properties can be modulated using these methods. Aligned microfilament scaffolding, fabricated using the wet spinning process, for example, has been shown to enhance migration of Schwann cells,[149] thus preventing premature dissolution of the fibrin cable.[21, 140, 150] Early experiments involving scaffolding of aligned filaments with diameters on the scale of tens to hundreds of microns were first conducted by the Williams lab.[13, 14] The aligned filaments were theorized to promote regeneration primarily by stabilizing the formation of the fibrin matrix by providing physical anchoring. In both cases, the scaffolding ultimately aids – whether directly or indirectly – in facilitating the proper



migration of support cells such as Schwann cells and thus helps to guide the formation of the initial regeneration cable.

Grooved patterns created by microcontact printing have also been shown to align Schwann cells and elicit expression of their neurotrophic factors *in vitro*. [138] Compared to smooth conduits, these micropatterned channels enhanced the number of myelinated axons in damaged sciatic nerves in rats. [151] Electrospun poly(L-lactide-co-glycolide) (PLGA) fibers have been used to create tubular scaffolds with guidance cues. [152] These scaffolds were able to grow nerves without eliciting an inflammatory response. In another study, the same polymer was used to create microbraided conduits which showed the presence of a fibrin cable one week after implantation. [152] Even though these scaffolds have increased roughness compared to normal tubular scaffolds, they were not completely able to sustain nerve growth in critical length gaps. Electrospun fiber films have been loaded into a semipermeable scaffold to promote nerve regeneration. Poly acrylonitrile-methacrylate (PAN-MA) electrospun aligned fibers have been loaded into a polysulfone tube to stimulate endogenous Schwann cell migration in 17 mm nerve gaps in rats. [33] Compared to empty tubes and randomly oriented fibers, aligned fiber based conduits were able to elicit nerve growth and improved functional recovery. These scaffolds have been shown to align glial cells and encourage organized ECM formation (Fig 2.). Even though the function of aligned fibers has not been elucidated, it has been hypothesized that they stimulate endogenous repair by either sustaining, augmenting or replacing the fibrin cable. More recently, naturally occurring fibers such as silk fibers have been evaluated as new materials for guiding nerve growth in tubes. [88] These fibers have been shown to sustain Schwann cell growth. Overall, substrates with

anisotropic topographical cues may enable efficient migration of Schwann cells into the nerve gap either by stabilizing or augmenting the stable fibrin cable, and thus facilitate nerve regeneration from the proximal to the distal end of the gap. Thus it is clear that both the organization of the fibrin matrix, its stability and the ability of glial cells to migrate into the nerve gap may all be influenced by appropriate material substrates providing topographical cues within a tubular prosthesis.

## **2.8 Conclusion**

From a design perspective, there are two critical parameters that govern the success of a regenerative medicine approach – a) is the design criteria for the scaffold/transplant appropriate from a biological perspective; and b) is the engineering minimalist and amenable to convenient regulatory and manufacturing translation. If one were to apply the above ‘design template’ to the problem of peripheral nerve regeneration, the design criteria for the scaffold needs to be governed by an understanding of the molecular sequence of events and the mechanisms that are involved in the regeneration process. Therefore the objective of this thesis was to understand the interplay between the topographical cues presented by thin-film scaffolds and the endogenous sequence of regeneration.

## CHAPTER 3

### 3. ROLE OF FIBRONECTIN IN TOPOGRAPHICAL GUIDANCE OF NEURITE EXTENSION ON ELECTROSPUN FIBERS

#### 3.1. Introduction

Functional recovery after peripheral nerve injury is critically dependent on both the rate as well as degree of regeneration and reinnervation of target tissues [153]. Each year, approximately 100,000 patients undergo peripheral nerve surgeries in United States and Europe [154]. Even though microsurgery techniques are adequate for short nerve lesions, no satisfactory methods are available to bridge long peripheral nerve gaps, and the “gold standard” of using autografts has several drawbacks that limit its use. Besides falling short on the extent of regeneration, several studies have shown that delays in repair after injury contribute to poor functional recovery [155, 156]. Hence, there is a critical need to improve both the extent and rate of regeneration after peripheral nerve injury.

Synthetic biomaterial-based nerve conduits have been developed as alternatives to autografts [33, 42, 157, 158]. Across short gaps (< 8 mm), these conduits support provisional fibrin cable formation which acts as a substrate for Schwann cell (SC) and fibroblast (FB) migration into the nerve gap from proximal and distal nerve stumps [13]. These cells help reorganize the extracellular matrix (ECM) and provide the trophic support to the regenerating axons enabling bridging of the nerve gap [14]. However, nerve conduits have not been effective in bridging critically sized nerve gaps that are typically (greater than 3 cm in humans and greater than 1.3-1.5 cm in rats), and functional recovery is rarely attained [156]. Therefore, strategies to augment nerve conduit

effectiveness by including additional physical and biochemical elements within conduit lumens have been proposed.

Magnetically aligned collagen fibers [146], hydrogels [1, 159] and synthetic micro filaments [22, 160] have been tested both *in vitro* and *in vivo* and have shown promise as supporting substrates for peripheral nerve cells. Specifically, aligned electrospun fibers have been widely explored for enhancing nerve cell function. Their high surface area to volume ratio and their ability to provide contact guidance have made them an attractive scaffold for bridging peripheral nerve gaps [161, 162].

Previous studies from our laboratory have shown that poly(acrylonitrile-co-methylacrylate) (PAN-MA) based aligned fiber films stacked in a polysulfone conduit successfully bridge long peripheral nerve gaps in rats without the need of any exogenous factors by enabling efficient Schwann cell migration [33]. A subsequent study demonstrated that a single thin film of aligned PAN-MA fiber which occupied only 0.6% of the total volume of the conduit was able to bridge a 14 mm gap in rats [163].

Whereas these and other studies demonstrate the ability of electrospun films to enhance nerve regeneration, the mechanisms by which they influence regeneration and peripheral glial cells such as Schwann cells remain unclear. It is evident that surface topography significantly influences cell behavior *in vitro* and *in vivo* [164, 165]. Varying topography of electrospun fibers alters cell adhesion, spreading, proliferation, migration and differentiation in bone [166] and nerve regeneration [167] as well as in guiding stem cell fate [168]. Substrate curvature modulates neurite extension [169] and ECM may play a role in effecting this behavior of cells [142]. The present study explores the

relationship between differential protein adsorption on electrospun PAN-MA films and smooth solvent cast PAN-MA films.

## **3.2. Material and Methods**

### 3.2.1 Fabrication of polymer films with aligned and smooth topographies

Polymer solutions (7%) were made by dissolving poly(acrylonitrile-co-methylacrylate) (PAN-MA) (Sigma, MW 8000) in N,N,-dimethylformamide (DMF) at 60 °C. For electrospinning, the solution was pumped through a syringe at a rate of 1 mL/h at a voltage of 6-10 kV. The polymer stream was directed at an aluminum foil-covered metal drum rotating at 2400 rpm for 15 minutes in order to produce aligned fibers. A 2% solution of the same polymer prepared in DMF was cast on a glass coverslip to obtain smooth films with the same chemistry. A UV lamp was used to sterilize the samples. The diameter of the fibers was characterized using scanning electron microscopy (S-800 SEM, Hitachi) and quantified using Image-Pro software (Media Cybernetics). Strips of aligned and smooth films (2 cm x 1 cm) were glued to the bottom of a 35 mm petri dish for *in vitro* assessment of topography.

### 3.2.2 Harvesting of Schwann cells and dorsal root ganglia (DRG)

Schwann cells were purified from the sciatic nerves of postnatal day 1 (P1) rat pups (Harlan) using a protocol modified from Brockes et al [170]. Briefly, sciatic nerves were dissected into 1 mm segments and dissociated in 1.33% collagenase (Worthington Biochemical) solution for 30 min. The nerve segments were then treated with 0.25% Trypsin/EDTA (Invitrogen, Carlsbad, CA) for 30 min. Cells were then mechanically dissociated using a pipette and incubated in culture media (DMEM/F12 (Fisher, Hampton, NH)) supplemented with 10% fetal bovine serum (Gemini, Sacramento, CA)

and neuregulin 1 (NRG1) (R&D systems) (50 ng/mL). After 24 h, the culture media was replaced with similar media supplemented with arabinoside (Ara-C) ( $10^{-5}$ ) (Sigma) for 48 h to remove the faster proliferating fibroblasts. Purity of cells was assessed by immunostaining with S100 (DAKO). Cultures with purity of greater than 95% were used in *in vitro* assays.

DRGs were also harvested from P1 rat pups. The nerve roots were removed and the ganglia were seeded on aligned fiber based films. To encourage attachment to the films, the ganglia were first incubated for several hours with only a thin layer of medium. Afterwards, each experimental condition was fully covered with DMEM/F12 media with 10% FBS and 50 ng/mL nerve growth factor (NGF) (Roche). Effects of topography on Schwann cell migration and neurite outgrowth under different experimental conditions was characterized using these DRG cultures.

### 3.2.3 Neurite outgrowth and Schwann cell migration assay

To evaluate the effects of the underlying topography on neurite outgrowth and Schwann cell migration, DRGs were cultured for 7 days on electrospun aligned PAN-MA and solvent cast smooth PAN-MA films, fixed with Histochoice (Fisher) for 20 min and washed three times with 1X PBS. Cells were tagged overnight at 4°C with the primary antibody solutions: neurofilament 160 kDa (NF160, 1:500, mouse IgG1, Sigma) to stain for neurons and S-100 (1:250, rabbit, IgG, DakoCytomation) to stain for Schwann cells. The following secondary antibodies were used: goat anti-rabbit IgG Alexa 488/594, goat anti-mouse IgG1 Alexa 488/594. Fifteen of the longest NF160<sup>+</sup> axons and 15 furthest S100<sup>+</sup> Schwann cells were measured from the edge of the DRGs as shown in Figure 2.

ImagePro was used to quantify the migration distance of Schwann cells and the extent of neurite extension under the effects of various conditions used.

#### 3.2.4 Fibronectin adsorption assay

Fibronectin adsorption on electrospun PAN-MA and solvent-cast PAN-MA film topographies was analyzed using a modified enzyme linked immunosorbent assay (ELISA). Circular film segments 5 mm in diameter were generated using a sharp metal mask and the aligned fibers and smooth films were glued to the bottom of a 96 well tissue culture plate which was pre-coated with Protein Block (Pierce) solution to prevent protein adsorption on the dish. Fetal bovine serum (100%) was added to the films overnight. PAN-MA films were then washed thoroughly to remove unbound proteins three times with 0.1 % Tween 20 in 1X PBS. Protein block solution was applied to the substrates followed by an overnight incubation with anti-fibronectin antibody (1:3000) (Millipore). Next day; substrates were washed extensively followed by incubation with HRP conjugated secondary antibody (1:3000) for 1 hr. Substrates were washed again and incubated with TMB substrate solution and the peroxidase/TMB reaction was terminated using stop solution (Cell Signaling). A standard curve was obtained by incubating FN (0.5 ng – 10 ng,  $r^2 = 0.85$ ) in a 96 well plate by performing the above mentioned ELISA concurrently. Substrates incubated in 1X PBS were used as controls. Absorbance at 450 nm was read by using a spectrophotometer to quantify the amount of antibody bound to fibronectin adsorbed onto the different topographies. Surface area for both aligned and smooth films were characterized by Atomic Force Microscopy. 3D surface area were quantified using SPIP (nanoScience Instruments) software and used to normalize the adsorption data.

### 3.2.5 Fibronectin depletion and competition assays

To investigate whether fibronectin (FN) plays a role in affecting the migration of Schwann cells on aligned fibers, experiments were performed with FN-depleted serum. Briefly, Gelatin Sepharose media (GE healthcare) was incubated with fetal bovine serum (5 ml of Sepharose for 50 ml of Serum) overnight at 4°C. This solution was centrifuged to remove the beads and western blot analysis was performed to evaluate the percent depletion of FN. We obtained serum which was greater than 95% depleted of FN (data not shown). Fibers were incubated in FN-depleted serum before DRGs were seeded. Serum without FN depletion was used as a control. DRGs were cultured for one week in respective media and Schwann cell migration was measured as discussed previously in section 3.2.3.

To evaluate if FN adhesion motifs play a role in mediating the effects of fibers on behavior of neuronal cells, DRGs were seeded and allowed to attach to aligned fiber films overnight. Cyclo-GRGDSP (AnaSpec) was added to media (0.5 mg/mL) every two days and the DRGs were cultured for 6 days. Control cultures with no peptide were also maintained for the same amount of time. Schwann cell migration and neurite outgrowth were measured as discussed above (Section 2.3) to assess the effects of competitively binding to cell integrin.

Finally, to investigate whether fibronectin-specific adhesion motifs mediate fiber influenced cell migration, an antibody inhibition assay using the HFN7.1 anti-FN clone was performed. HFN7.1 binds to the central cell binding domain on human fibronectin with no detectable cross reactivity to rat fibronectin. DRGs were allowed to attach overnight in media containing human serum. HFN7.1 (DSHB, Iowa) and isotype control



(M18, DSHB, Iowa) antibodies were added to the cultures and maintained for 3 days. Additionally, cultures without any antibody treatment were used to determine if human serum had any negative effects on cell growth. Schwann cell migration and neurite outgrowth were quantified using methods described above (Section 2.3).

### 3.2.6 Atomic force microscopy

AFM experiments were performed using a Multimode AFM equipped with a NanoScope IIIa controller from Veeco (Manchester, U.K.) operating in tapping mode in air; the Nanoscope software was used. Si-cantilevers from Veeco (Manchester, U.K.) were used with a force constant of 2.8 N/m and resonance frequency of 89 kHz. The phase signal was set to zero at a frequency of 5% lower than the resonance one. The drive amplitude was 750 mV, and the amplitude set point  $A_{sp}$  was 1.6 V. Fibronectin from human plasma (Sigma) was adsorbed on the different substrates by immersing the material sheets in 20  $\mu\text{g}/\text{mL}$  FN in PBS for 1hr. After protein adsorption, samples were rinsed 3 times with 1X PBS to eliminate the non-adsorbed protein. Remaining drops on the surface were dried by exposing the sample to a nitrogen flow for 2-3 min. AFM was performed in the tapping mode in air immediately after sample preparation. Height, phase, and amplitude magnitudes were recorded for each image.

### 3.2.7 Fibronectin organization by Schwann cells

Purified Schwann cells were seeded at a density of  $2 \times 10^5$  cells on aligned fiber and smooth films in a 35-mm tissue culture plate and cultured for one week. Fibronectin laid down by glial cells was observed by staining with anti-rat fibronectin antibody (1:100) (Millipore). Goat anti-rabbit IgG Alexa 488 was used to stain for the matrix laid down by the glial cells.

### 3.2.8 Statistical analysis

ANOVA, combined with Tukey post hoc tests, was used to calculate the significance of differences between mean values. A p value less than 0.05 was considered statistically significant.

### 3.3 Results

#### 3.3.1 Schwann cell migration and neurite outgrowth from DRG

Aligned PAN-MA fibers were generated using an electrospinning process. Smooth PAN/MA smooth films were obtained by solvent casting the solution of the same polymer. Under SEM, aligned fibers had an average diameter of  $800 \pm 96$  nm while the smooth films' largest feature size was approximately 4 nm (Fig.3-1). Therefore, we were successful in generating a substrate with anisotropic topographical features, and another with a relatively 'smooth' topography with the same underlying substrate chemistry, PAN-MA.

DRGs were seeded on the different topographies to quantify Schwann cell migration and neurite outgrowth. Schwann cells migrated parallel to the direction of the fibers. The migration distance of S100 positive Schwann cells was significantly greater,  $1588 \pm 93$   $\mu$ m, on aligned fibers compared to the smooth films,  $371 \pm 59$   $\mu$ m, where Schwann cell migration was less and not directed ( $p < 0.05$ ) (Fig 3-2). Similar results were observed for neurite outgrowth. NF160 positive axons extended along the fibers to significantly greater extent ( $1212 \pm 131$   $\mu$ m,  $p < 0.05$ ) compared to smooth films ( $373 \pm 39$   $\mu$ m). These results demonstrate that guidance cues from aligned fibers enhanced the migration of cells as well as directed neuronal outgrowth.

#### 3.3.2 FN Adsorption from serum

We investigated the role of protein adsorption in mediating DRG and Schwann cell interactions with the underlying topography. Since fibronectin has been implicated in influencing Schwann cell migration, we characterized fibronectin adsorption from serum on aligned electrospun films relative to adsorption on smooth films. We quantified

the amount of fibronectin adsorbed on aligned fibers and smooth films using a modified ELISA based assay. Membranes of aligned PAN-MA fibers exhibited significantly ( $p < 0.05$ ) higher FN adsorption,  $4.81 \pm 0.32 \text{ ng/cm}^2$  compared to  $3.08 \pm 0.19 \text{ ng/cm}^2$  for smooth films. (Fig 3-3)

### 3.3.3 Effects of FN depletion from serum on DRG behavior

Since differential fibronectin adsorption was observed on between fibers and films, the role of FN on the migration of Schwann cell on aligned fiber films was studied to determine whether FN adsorption from serum plays an important role in stimulating Schwann cell migration. Fibronectin depleted media was used to test the effects of fibronectin on Schwann cell migration.

DRGs attached evenly on both experimental substrates but Schwann cell migration was significantly diminished on substrates incubated in fibronectin-depleted media with a migration distance of  $1144 \pm 508 \text{ }\mu\text{m}$ , as compared to control conditions,  $2146 \pm 315 \text{ }\mu\text{m}$ . DRGs showed directed growth on both conditions. However, S100 positive cells migrated faster ( $p < 0.05$ ) on substrates exposed to control serum (Fig 3-4).

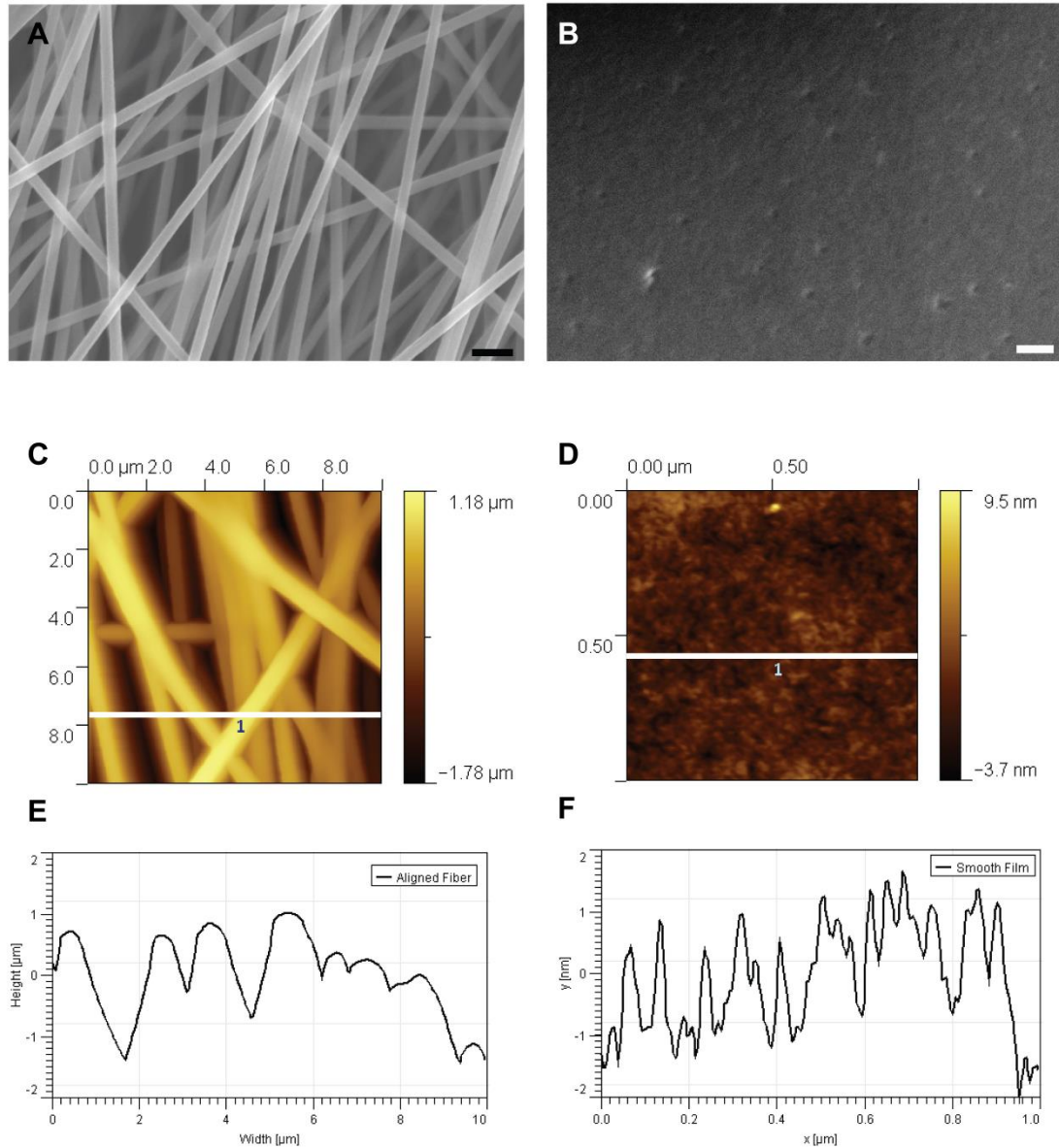


**Figure. 3-1: Characterization of electrospun fibers and smooth films.** Scanning electron microscopy images of PAN-MA aligned fibers (A) and smooth film (B). Scale bar represents 2 microns in (A) and 0.3 microns in (B). Atomic force microscope analysis of fiber topographies (C,D). Height profiles for the white lines in (C) and (D) are graphed onto (E) and (F), respectively. Scan area for (C):  $10 \times 10 \mu\text{m}^2$  and (D):  $1 \times 1 \mu\text{m}^2$ .

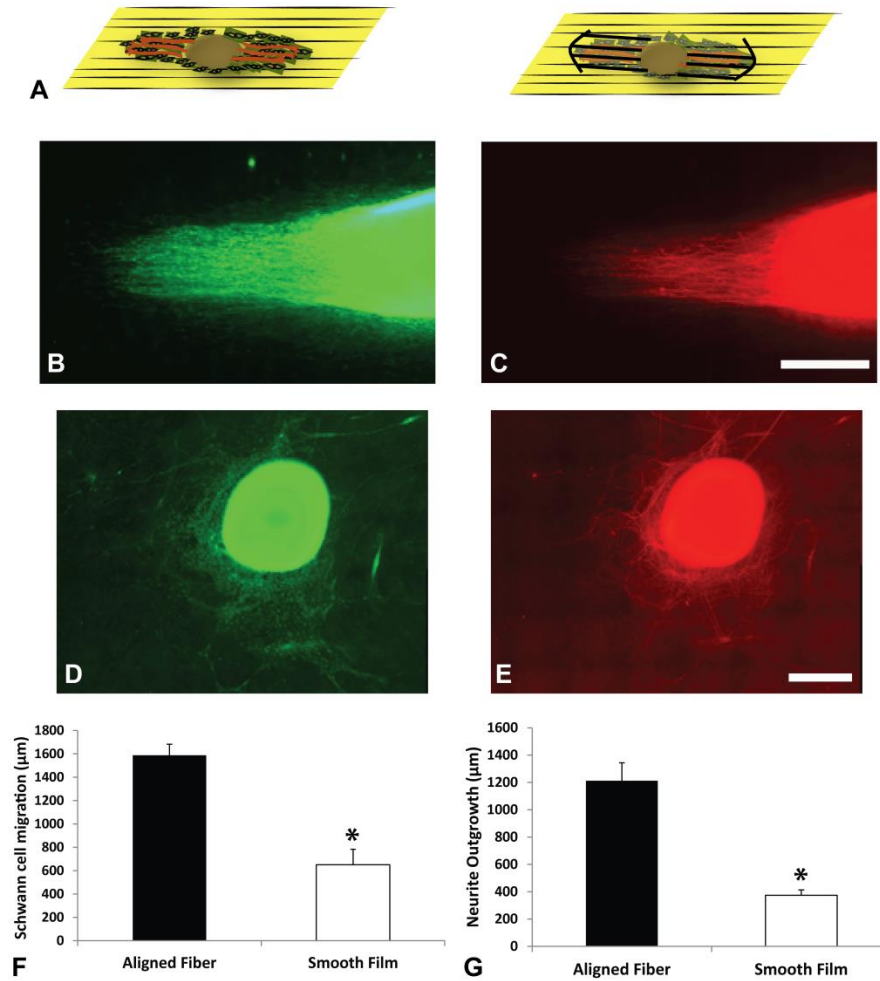


**Figure. 3-2: DRG growth on aligned and smooth thin films.** Schematic diagram illustrating how Schwann cells and neurons extend from the DRG body (A). Images of Schwann cell migration (using S100 staining, green) and neurite outgrowth (using NF160, red) on aligned fibers (B,C) and smooth film (D,E) from rat DRG in vitro. (F,G): Show the quantitative comparison of both fiber topographies in Schwann cell migration and neurite outgrowth. Aligned fibers show significantly higher migration distances and growth. \* $p < 0.05$ . Error Bars = Std. Dev.

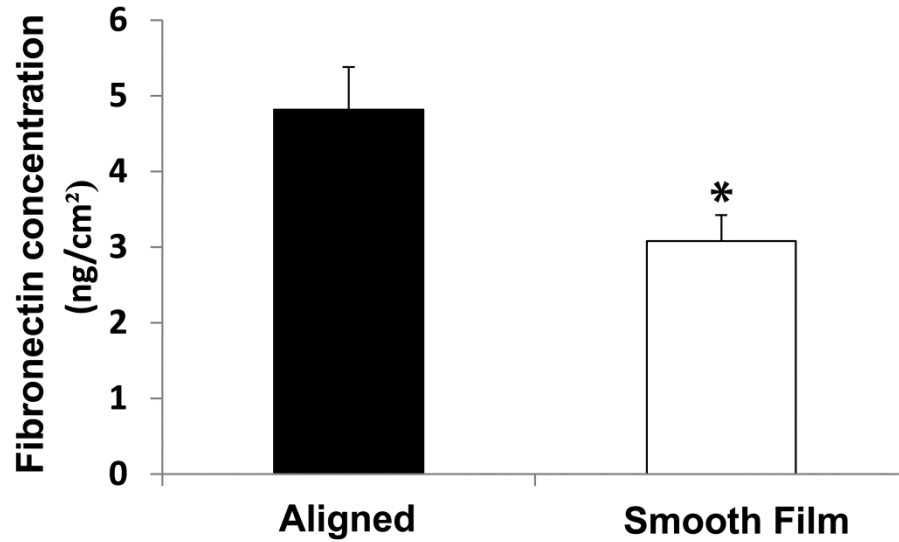


**Figure. 3-3: Fibronectin adsorption on aligned and smooth film topographies.** Analysis of fibronectin adsorption on fiber and film. Concentration of Fibronectin was normalized to the surface area of Smooth Film. Aligned fiber demonstrates significantly higher adsorption than smooth film.  $P < 0.01$ . Error bar = Std. dev.

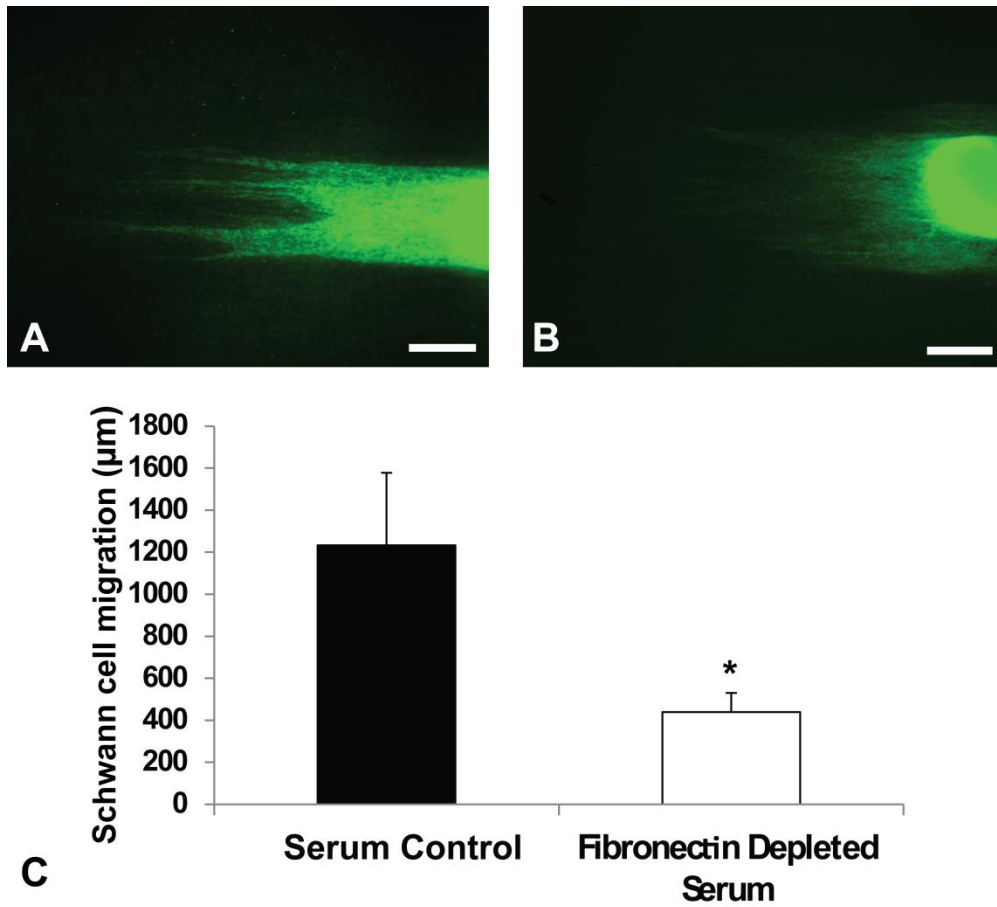


**Figure 3-4: Quantitative analysis of Schwann cell migration in fibronectin depleted serum.** Images of Schwann cell migration from DRG in normal serum (A) and fibronectin depleted serum (B). (C): Migration in serum is significantly higher than migration in depleted serum. \* $p < 0.05$ . Error bar = Std. dev.



### 3.3.4 Influence of competitive binding of Cyclo-GRGDS on FN mediated response

To further investigate the cellular interaction with adsorbed proteins on aligned fiber topographies, a Cyclo-GRGDS competitive assay was used. Cyclo-GRGDS was used to compete with the cell binding of adsorbed proteins on aligned fibers. As shown in Fig 3-5, at six days, Schwann cells migrated  $371 \pm 59 \mu\text{m}$  on substrates treated with soluble Cyclo-GRGDS compared to  $1217 \pm 73 \mu\text{m}$  on normal culture conditions. Moreover, neurite growth was significantly reduced ( $p < 0.05$ ) with GRGDS,  $269 \pm 84 \mu\text{m}$ , in comparison to normal media conditions,  $965 \pm 70 \mu\text{m}$ . These results show Schwann cell migration and neurite outgrowth on aligned nanofibers involves adhesion to an RGD-containing molecule adsorbed from serum or deposited by cells.

### 3.3.5 Inhibition of integrin binding motif of fibronectin

Next, we investigated the role of fibronectin by using antibodies specific to the central cell binding motifs of fibronectin molecule. HFN7.1 antibody was used to inhibit the effects of fibronectin adsorbed from human serum. Compared to the controls (M18 isotype control and normal human serum), HFN7.1 significantly ( $p < 0.05$ ) inhibited Schwann cell migration and neurite outgrowth ( $565 \pm 118 \mu\text{m}$  on M18,  $521 \pm 65 \mu\text{m}$  on untreated control and  $318 \pm 87 \mu\text{m}$  on HFN7.1) from DRGs. It was observed that Schwann cells migrated  $585 \pm 109 \mu\text{m}$  on substrates incubated with M18,  $572 \pm 148 \mu\text{m}$  on normal serum condition, while only  $355 \pm 80 \mu\text{m}$  on HFN7.1 incubated substrates. There was no significant difference between cell behavior on isotype treated and control condition suggesting that the antibody does not influence regular Schwann cell migration and axonal sprouting (Fig 3-6). Thus, integrin engagement of the cell binding domain of

adsorbed FN appears essential for efficient Schwann cell migration and neurite outgrowth.

### 3.3.6 Influence of topography on fibronectin organization and production

To investigate the role of topography and its effect on protein adsorption, AFM was used to understand the distribution and organization of FN on aligned fibers and smooth films. Height, amplitude and phase profiles of human plasma fibronectin adsorbed on different topographies were evaluated in tapping-mode AFM. Aligned fibers exhibited the presence of FN fibrils, mostly aligned along the length of the fiber. On smooth films, fibronectin did not form any supramolecular structure and had a more globular morphology (Fig 3-7). Together with the previous results, this phenomenon observed on aligned PANMA fibers suggests that this organized fibronectin matrix could play a vital role in aligning cells to the underlying substrates thereby affecting their migration.

The ability of the aligned fibers to organize the matrix laid down by these cells was also examined. Purified P3 rat Schwann cells were cultured on aligned fibers and smooth films. FN antibody was used to observe the organization of FN matrix laid down by these cells. Aligned fibers promoted the formation of oriented network of fibronectin in comparison to smooth films which had a more disorganized matrix (Fig 3-8). This data demonstrates that the fibers not only enhance the adsorption of proteins but also influence the production and organization of ECM produced by the cells.

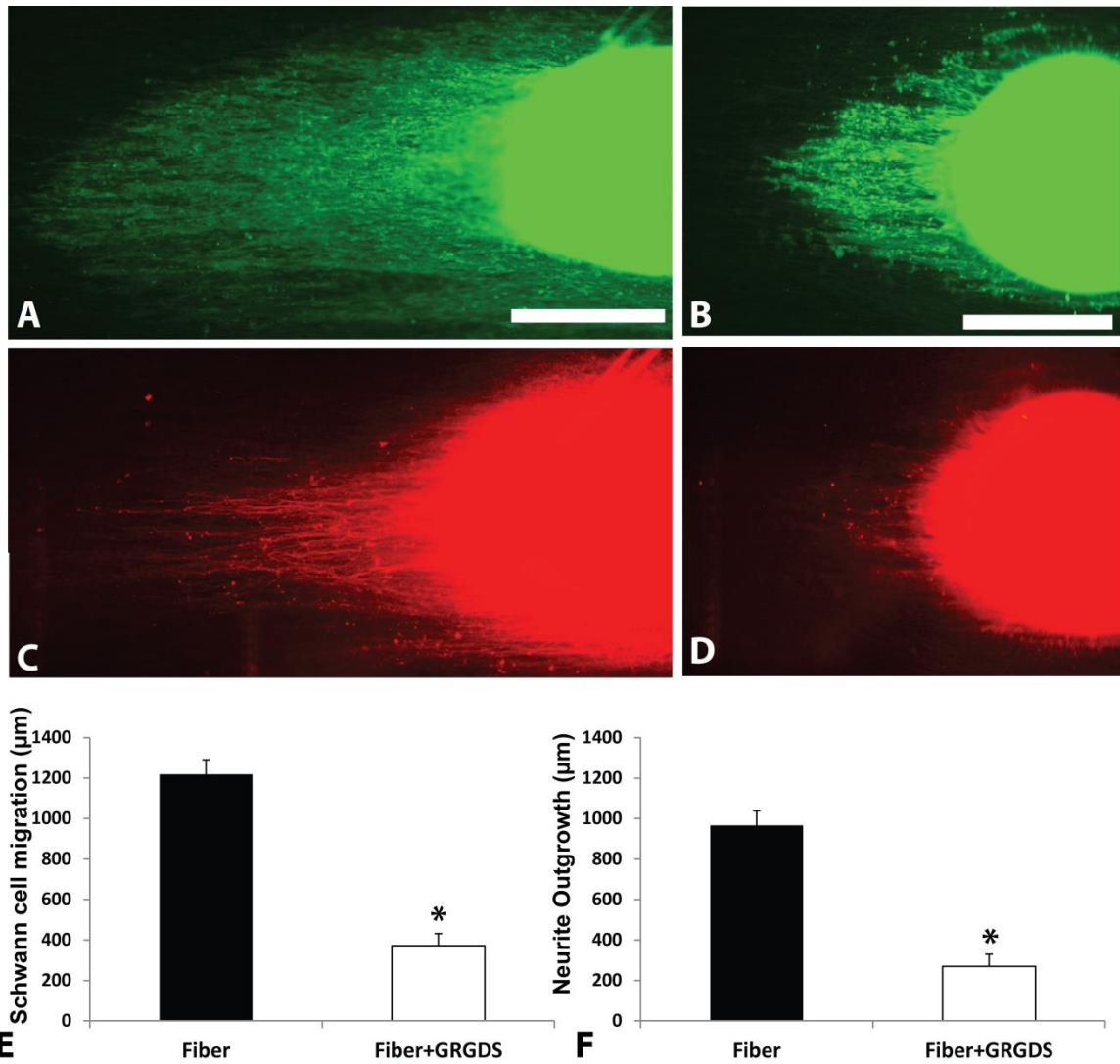


**Figure. 3.5. Schwann cell migration and neurite outgrowth analysis in GRGDSP inhibited media.** Images of Schwann cell migration from DRG in normal media (A) and GRGDSP media (B). Images of neurite outgrowth in respective conditions (C, D). Scale bars in (A) and (B) indicate 400 microns. Fibers without peptide inhibition display significantly higher migration (E) and neurite outgrowth (F). \* $p < 0.05$ . Error bar = Std. dev.

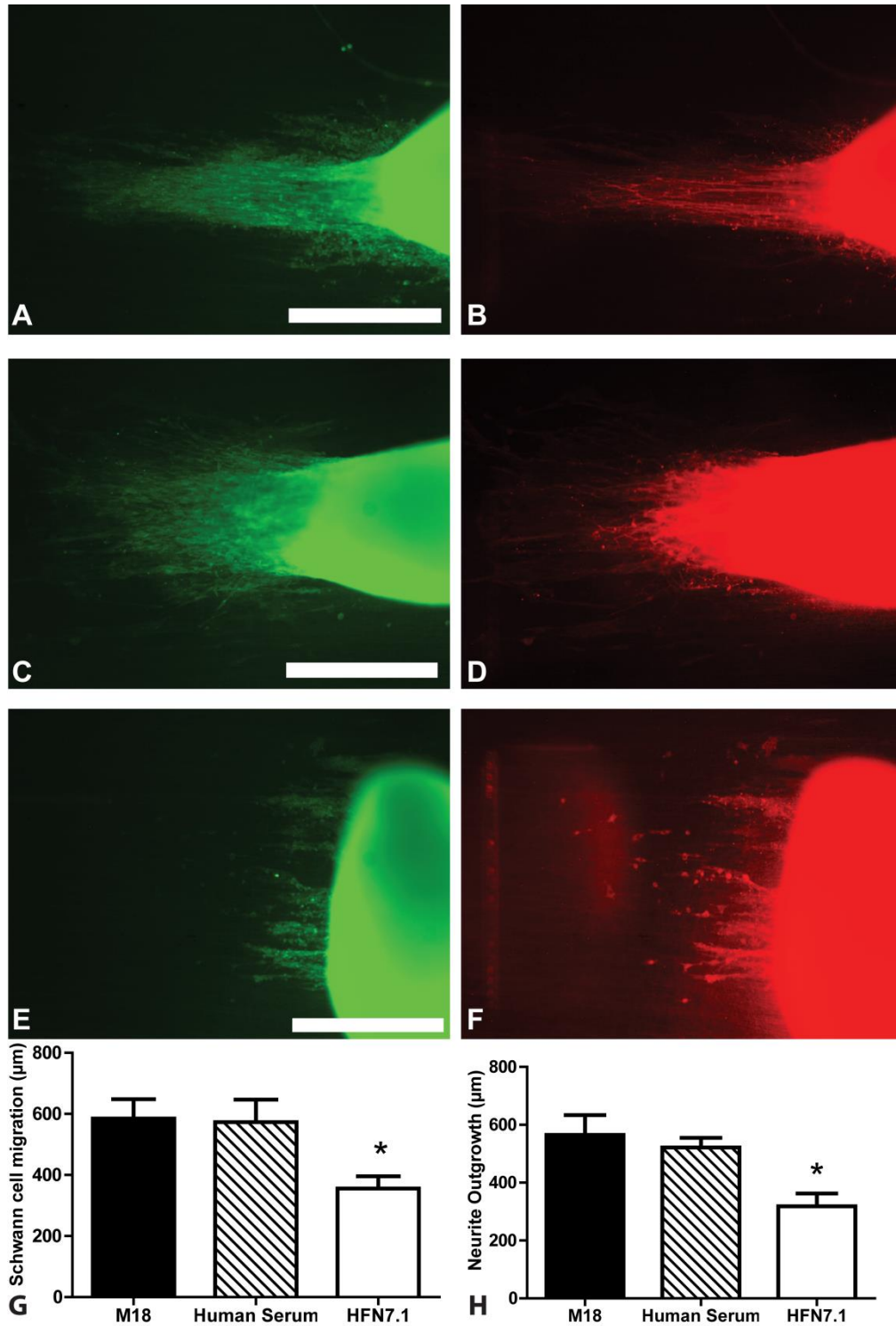


**Figure. 3.6. DRG Schwann cell migration and neurite outgrowth in HFN7.1 antibody inhibited fibers.** Migration and outgrowth in M18 isotype control (A,B), normal human serum (C,D), and HFN7.1 antibody incubated fibers (E,F). Scale bars indicate 400 microns. Both controls demonstrate significantly higher migration and outgrowth when compared to HFN7.1 incubated DRGS (G,H). \*p<0.05. Error bar = st. d.

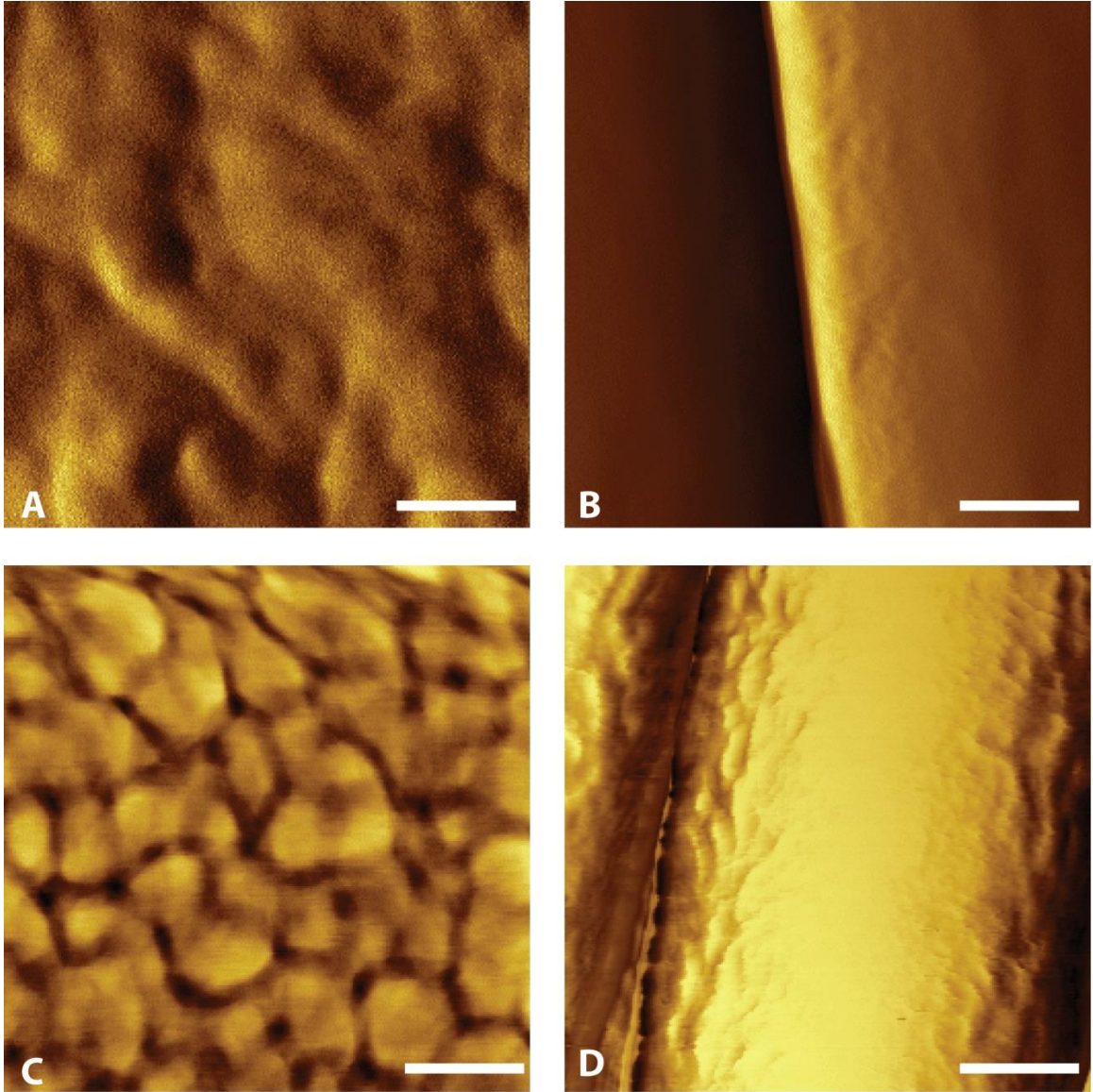


**Figure. 3.7. Atomic force microscopy images of PAN-MA polymer topography. (A):** Smooth film. (B): Aligned fiber scaffold. (C) Smooth film with fibronectin. (D) Aligned fibers with fibronectin. Scale bar = 100 nm.

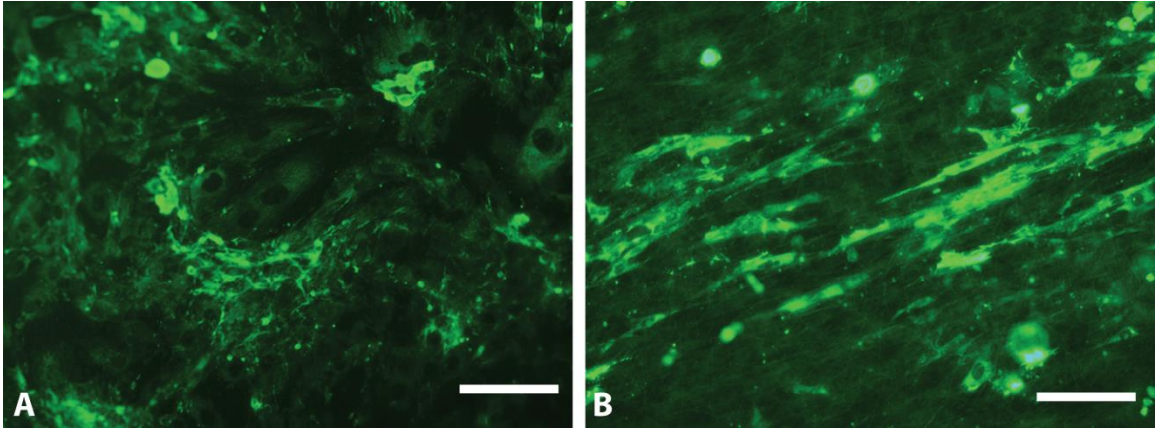


**Figure 3.8. ECM organization** on smooth film (A) and aligned fibers (B). Scale bars = 100 microns.

### 3.4. Discussion

Previous work from our laboratory as well as others has demonstrated that luminal fillers in nerve guidance channels can enhance peripheral nerve regeneration. Presumably, these luminal fillers interact with the normal regeneration process and influence the early stages of regeneration [171]. Luminal fillers may aid the formation of Bands of Bungner (longitudinal arrangement of Schwann cells and Laminin-1) by influencing the migration of Schwann cells [33, 163]. Schwann cells play an important role in the regeneration process by not only myelinating axons, but also producing growth factors such as NGF, BDNF, NT-3 and CNTF to help peripheral nerve regeneration [172]. Schwann cells also secrete and organize extra cellular matrix molecules such as vitronectin, laminin and fibronectin to enhance neurite outgrowth [173, 174]. Thus, Schwann cells have an important role in the PNS repair, and therefore, contact guidance-based strategies have been developed to enhance neurite growth have also served to enhance Schwann cell migration.

Several studies demonstrate that electrospun nanofibers align and direct Schwann cell migration as well as to guide neurite outgrowth. Electrospun PLLA fibers were used to bridge a 10 mm nerve gap in rats and showed functional recovery close to that of an autograft [160]. In another study, PCL/gelatin based aligned electrospun fibers improved Schwann cell attachment and proliferation [175]. Wang et. al fabricated aligned chitosan based nanofibers to specifically align Schwann cells for PNS repair [176]. They observed that aligned electrospun fibers promoted cell growth as well as support high axon count compared to a scaffold of non-oriented fibers in a 10 mm gap in rats. Whereas these studies show the benefits of using aligned electrospun scaffolds to repair nerve defects, it

is difficult to realize their potential since a majority of these studies are performed in non-critical gaps where spontaneous regeneration occurs in empty conduits with no fillers.

Our previous work has shown that aligned thin films fabricated from electrospun PAN-MA supported enhanced Schwann cell infiltration, axonal growth as well as improved functional recovery in a critical length (17 mm) nerve gap in rat [33]. Furthermore, a single thin film of oriented fibers which occupied only 0.6% of the total conduit volume was sufficient to enhance Schwann cell migration and bridge a 14 mm nerve gap [163]. These studies clearly show that topographical cues from aligned electrospun fibers can augment Schwann cell migration and lead to axonal regeneration. But the mechanisms by which aligned fiber based scaffolds promote neural cell or Schwann cell function are still unknown. In order to fabricate scaffolds that exceed autograph performance, an understanding of how aligned topographical cues enhance Schwann cell migration and direct neuronal growth is useful. Therefore, in the current study, we investigated how the effects of aligned fiber-based scaffolds mediate enhanced neurite extension and Schwann cell migration.

To discern the role of topography, we fabricated both aligned PAN-MA fiber-based films using an electrospinning process, and smooth PAN-MA films using solvent casting with minimal topographical cues. The topography of aligned fibers and smooth films were apparent both quantitatively and qualitatively as shown in Fig 3-1 by SEM and AFM analysis. Schwann cell migration and axonal growth are critical events for successful peripheral nerve regeneration after injury [177, 178]. We measured the extent of Schwann cell migration and DRG neurite outgrowth using cell-specific immunostaining on aligned fiber films and smooth films. Presence of aligned



topography significantly enhanced the migration of Schwann cells and directed the growth of neural cell along the long axis of the fibers (Fig 3-2). It has been speculated that nanoscale topographies alter cellular responses by controlling the elongation and alignment of the nucleus. [179]

In order to evaluate the mechanistic interplay between the topographical features of the underlying film and cellular behavior, we examined at how topography alters adsorption of fibronectin, a critical protein mediating Schwann cells behavior and neurite extension [180, 181]. During regeneration, cell interaction with ECM proteins play a vital role in controlling cell attachment, migration, proliferation and differentiation [182]. These interactions also lead to cytokine activity, cell apoptosis and are responsible for activating intracellular signaling [183]. Earlier studies have shown that nanoporous scaffolds have led to higher adsorption of serum ECM proteins such as fibronectin, laminin and vitronectin compared to solid scaffolds [184]. Protein adsorption and organization by the underlying matrix has shown to affect the alignment of cells as well as control their phenotype [85]. Specifically, in the current study we explored how fibronectin adsorption from serum is regulated by the underlying topography. Fibronectin coated tissue culture plastic increased the migration of Schwann cell *in vitro* [185]. Also, neuronal growth from DRG was influenced by fibronectin composition in another study [186]. Fibronectin fibers promoted the alignment of Schwann cell focal contacts and organized the F-actin structure in parallel to the fibers [187]. Furthermore, oriented mats from the same fibers were used to bridge a 10 mm nerve defect in rats and showed faster rate of growth compared to muscle graft. [95] Therefore, FN represents an

important ECM protein in mediating both Schwann cell and axonal response during the course of nerve regeneration.

When we quantified FN adsorption on aligned PAN-MA films compared to smooth PAN-MA films, more fibronectin adsorbed on aligned topographical films compared to smooth films. However, aligned fibers also demonstrated a higher surface area compared to smooth PAN-MA films as determined using atomic force microscopy (approximately 1.14 times higher on the aligned topography compared to smooth films, data not shown). After normalization surface area, we observed significant differences in the amount of fibronectin adsorbed per unit surface remained higher on aligned fibers compared to smooth films. At this time there are some caveats worth discussing. One of the limitations of AFM is that it has a scan depth of 5  $\mu\text{m}$  while the fiber based films are 10  $\mu\text{m}$ . Thus we may be underestimating the surface area of the fiber based films thereby exaggerating the calculation of adsorption of FN per unit surface area. Based on our calculations, even if the surface area of the fiber based films is 35% higher than that of the smooth films, the amount of FN adsorbed onto the fibers would still be statistically higher compared to the smooth films. Further the FN antibodies used in the ELISA might also interact with the adsorbed protein differently. As the dimensions of an individual Schwann cell and DRG exceed that of individual fibers, the cellular effects observed by simply be either due to greater concentration of FN being presented to cells, or the FN distribution along fibers is anisotropic compared to smooth films, causing anisotropic cellular behavior.

To investigate whether fibronectin was necessary for the observed anisotropic cell response on aligned fibers, we incubated fibers with fibronectin-depleted media and

quantified that the migration of Schwann cells from DRGs. Schwann cell migration was significantly lower on FN-depleted serum substrates (Fig 3-4). There was some migration of cell on FN-depleted serum substrates and this phenomenon is due to the cell producing their own ECM molecules that is responsible for their migration. DRG glial cells have previously been shown to synthesize their own ECM [185]. This data strongly suggests that FN plays a critical role in Schwann cell migration and neurite extension on aligned polymeric films.

To further evaluate the functional role of FN mediated enhanced Schwann cell migration and neurite extension on aligned fiber based films compared to smooth films, Cyclo-GRDSP peptide was used to competitively bind to integrins on cells. Cyclo-GRDSP exposure to Schwann cells significantly inhibited Schwann cell migration and neurite outgrowth on aligned films compared to control substrates (Fig 3-5). This suggests that cell behavior on aligned fiber topographies is mediated by integrin-based adhesion. We recognize of course that while Cyclo-GRGDSP blocks integrin binding, it is not specific to FN - RGD binding sites are found on several ECM proteins such as fibronectin, vitronectin, osteopontin, fibrinogen and laminin [188]. Receptors on cells that detect the specific RGD sequence are often structurally similar and thus the binding motifs of specific adsorbed proteins that are responsible for mediating downstream cellular activities are not easily detected with RGD based peptides. Therefore, our study demonstrates that ability of the fibers to present the cell binding motifs of fibronectin is essential to trigger downstream effects that lead to more efficient and enhanced Schwann cell migration and neuronal regeneration. Since we were interested in evaluating if the presentation of adsorbed fibronectin by aligned fibers is responsible for modulation cell

activity, we used the monoclonal antibody HFN7.1 to specifically inhibit the RGD binding site of adsorbed fibronectin from human serum. HFN7.1 inhibited Schwann cell migration from DRGs on aligned fibers suggesting that binding of fibronectin-specific RGD motifs on aligned fiber based topography are responsible for cell phenotype (Fig 3-6). Since  $\alpha_v$  integrins on Schwann cells have shown to mediate their migration on tissue culture plastic [186], we can speculate that adsorbed fibronectin on fibers also enhances Schwann cell migration via  $\alpha_v$  receptors on migrating Schwann cells. These blocking assays, when considered together, give new insights into how the effects of aligned fibers are translated to the neuronal cells.

As discussed earlier, FN's ability to mediate enhanced Schwann cell migration and neurite extension on fiber-based films could be explained either by increased FN contacting each cell, or by FN's distribution being different on fiber-based films compared to smooth PAN-MA films. Atomic force microscopy was utilized to further probe how topography influences the distribution and organization of adsorbed fibronectin. Surface chemistry, roughness and surface energy have all been shown to influence the protein adsorption process (Fig 3-7). [189] Surface roughness has shown to significantly affect fibronectin conformation which can lead to poor cell adhesion and actin reorganization. [189, 190] In our studies, aligned fibers topography promoted organized distribution of adsorbed fibronectin. Fibronectin fibrils also aligned parallel to the axis of the fibers. Since, previous studies have shown the dependence of focal contact formation to surface properties [191, 192]; it is likely that aligned PAN-MA fibers enhance the elongation of cellular processes by oriented fibronectin network formation. Smooth topography did not reveal any organization of fibronectin, suggesting that the

enhancement of Schwann cell migration and neurite outgrowth on aligned fibers is mediated by the ability of the polymer fibers to influence the organization of adsorbed fibronectin at the material interface. Fibronectin assembly into fibrils upon adsorption on some family of materials has shown to enhance its biological activity, including cytoskeleton development, focal adhesion formation, matrix secretion and differentiation. [190, 193]

Organization of fibronectin secreted by glial cells cultured on aligned fibers is also enhanced by underlying topographical cues. Aligned fibers enabled formation of organized fibronectin network compared to smooth films (Fig 3-8). Matrix organization by glial cells is a vital step in the nerve regeneration process and the ability of the aligned fibers to affect that step can be beneficial during regeneration. Even though the major focus of the present study was to elucidate the role played by fibronectin in modulating cell behavior during neuronal regeneration, it is likely that other ECM components such as laminin may also play a pivotal role in cell interaction with topography. Further studies are warranted to understand the contribution of other ECM proteins mediating topographical enhancement of neurite extension and Schwann cell migration. In this study, we demonstrate that fibronectin plays a critical role, and that blocking its function even in the presence of other ECM proteins is sufficient to decrease Schwann cell migration and neurite extension. We also demonstrate that fibronectin presentation to neuronal cells due to the protein adsorption, conformation and organization on fiber-based films may all contribute to enhanced Schwann cell migration and neurite extension.

## CHAPTER 4

### 4. EFFECTS OF TOPOGRAPHY ON THE ENDOGENOUS REGENERATIVE SEQUENCE IN LONG PERIPHERAL NERVE GAP

#### 4.1. Introduction

Peripheral nerve injuries leads to long term disability and decreased function in approximately 2.8% of all trauma patients [41]. This is followed often by neuropathic pain and significantly affects the quality of life for individuals suffering from peripheral nerve injuries. Even though there have been considerable advances made in microsurgical techniques, bridging of long peripheral nerve gaps remains a continuing clinical challenge. Autografts are the current standard technique to bridge long gaps but several drawbacks of using autografts limit their use. Use of autografts can lead to donor site complication such as sensory defect, scar, pain as well as it often requires multiple surgeries if the gaps are long [194]. Furthermore, due to modality mismatch, dimensions, etc., functional recovery even somewhat close to pre injury levels is not achieved. These limitations of autografts have led to finding substitutes to bridging peripheral nerve gaps.

Nerve conduits have been fabricated from biological materials such as veins [30, 32], ECM proteins such as collagen [76] as well as synthetic materials such as PCL [136], PGA [195], and PLGA [48]. These guidance channels have had some success in approaching autografts performance over short gaps. These conduits promote nerve bridging by first facilitating the formation of a provisional fibrin matrix which coalesce from the plasma entering the conduit space [196]. Glial cells, Schwann cells and fibroblast migrate along this provisional matrix laying down their own ECM. This

enriched matrix guides axons along with Schwann cells facilitating the bridging of the nerve gap. Axons infiltrate the denervated distal stump and eventually make neuromuscular junctions with the target muscle [41]. In larger gaps, the provisional matrix fails to coalesce and is not infiltrated by the supporting cells if it is dissolved leading to a failed regeneration [197]. This has led to their limited use in bridging clinically relevant nerve gaps.

Luminal fillers have been used to extend the bridging capacity of guidance channels [153, 160, 171]. Several designs that replicate or replace the function of the initial provisional matrix have been explored to augment the regeneration process. Cellular fillers such as Schwann cells [102], and genetically modified Schwann cell [198, 199], structural fillers such as, micro channels [200, 201], micro filaments [147, 197, 202], electrospun fibers [65, 163, 203] and neurotropic factors such as NGF [61], BDNF [86], NT-3[204] have been used individually and in combinatorial way to influence nerve bridging. In most studies, these techniques have been optimized *in vitro* for axonal growth or *in vivo* in non-challenging models. However, how these techniques interplay with the orchestrated regenerative sequence is still understudied. Thus, there are no clinically viable alternatives to autografts for critical peripheral nerve gaps.

Previous work in our lab has shown that using only 0.6% of the total volume of the guidance channel, aligned electrospun nanofibers were able to successfully bridge the nerve gap. Without the need of any exogenous factors, aligned topographical cues were able to bridge a critical length nerve gap [163, 203]. Other studies have also shown the benefits of topographical cues in nerve regeneration [164, 165, 189, 205]. While the single thin film is able to support cell migration and axonal bridging, it is still unclear

why they are able to support nerve regeneration and what is the exact role of topography in influencing the regenerative sequence in a critical length gap. It is believed by several experts in the field of PNS repair that a thorough understanding of the mechanism of how scaffolds influence the regenerative sequence is required to design next generation of PNS nerve scaffolds.

Since electrospun fibers have shown potential in bridging long gaps, in this study we evaluate how topography interacts with the different steps of regeneration. We gain insights into how luminal fillers augment the nerve regeneration process by evaluating both short term and long-term regeneration events *in vivo*. We believe that the conclusions gain from this study will pave the way for new designs of peripheral nerve graft that will utilize the body's own endogenous mechanisms to augment nerve regeneration.



## 4.2. Material and Methods

### 4.2.1 Fabrication of thin-film based scaffolds

#### 4.2.1.1 *Fabrication of Aligned, Random and Smooth thin-films*

Polymer solutions (7%) were made by dissolving poly(acrylonitrile-co-methylacrylate) (PAN-MA) (Sigma, MW 8000) in N,N,-dimethylformamide (DMF) at 60 °C. For electrospinning, the solution was pumped through a syringe at a rate of 1 mL/h at a voltage of 6-10 kV. The polymer stream was directed at an aluminum foil-covered metal drum rotating at 2400 rpm for 15 minutes in order to produce aligned fibers. A flat copper plate (McMaster Carr) was used as a collector to generate random fibers. 2% solution of the same polymer prepared in DMF was casted on a glass coverslip to obtain smooth films with the same chemistry. The diameter of the fibers was characterized using scanning electron microscopy (S-800 SEM, Hitachi) and quantified using Image-Pro software (Media Cybernetics).

#### 4.2.1.2 *Assembly for tubes for implantation*

Polysulfone nerve guidance channels (Koch Membrane Systems) were used as a carrier for the oriented fiber film scaffolding. Polysulfone tubes have a molecular weight cutoff of 50 kDa and allow for transfer of nutrients and gases while protecting the regenerating nerve against the immune cells. The semi permeable polysulfone tubing (inner diameter: 1.6 mm, outer diameter: 2.2 mm, molecular weight cutoff: 50kDa) was first cut into tubes of the 17mm, (to allow for a 15 mm gap plus 2 extra mm to allow for 1mm of both the proximal and distal stump to be pulled into the scaffold during suturing.) The polysulfone tubing was halved lengthwise using a custom-machined aluminum template. Under a fabrication microscope, a 2.2 mm wide thin-film strip was fixed on

one of the halved tubes, using medical grade UV light curing adhesive (1187-M-SV01, Dymax). To complete the scaffold, the other half of the tube was glued on top. Schematic diagrams of these tubes are shown in Figure 4-1.

The scaffolds were sterilized by immersion in 70% ethanol for 30 minutes followed by washing in sterile diH<sub>2</sub>O and overnight incubation under UV light. These scaffolds were stored in sterilized phosphate buffered saline (PBS) until the implantation surgery.

#### 4.2.2 *In vivo* Implantation

Adult Lewis male rats (250 – 300 gms) were induced to anesthetic depth with inhaled isoflurane at 3-4%. Throughout surgery, the animals were maintained at 1.5-2% isoflurane. Microscissors were used to transect the tibial nerve branch, and the nerve stumps were pulled 1mm into each end of the 17mm (aligned, random and smooth film) guidance scaffolds (leaving a 15 mm gap) and fixed into place with a single 10-0 nylon suture (Ethicon). The muscles were reapposed with 4-0 vicryl sutures (Ethicon) and the skin incision was clamped shut with wound clips (Braintree Scientific). After the surgery, the rats were placed under a warm light until sternal, and then housed separately with access to food and water ad libitum at constant temperature (19-22°C) and humidity (40-50%) on a 12:12 hr light/dark cycle. To prevent toe chewing, a bitter solution (Grannick's Bitter Apple) was applied twice daily to the affected foot. Marcaine (0.25% w/v) was administered subcutaneously for post-surgical pain relief (0.3 ml/animal). Animals were maintained in facilities approved by the Institutional Animal Care and Use Committee (IACUC) at the Georgia Institute of Technology and in accordance with the

current United States Department of Agriculture, Department of Health and Human Services, and National Institutes of Health regulations and standards.

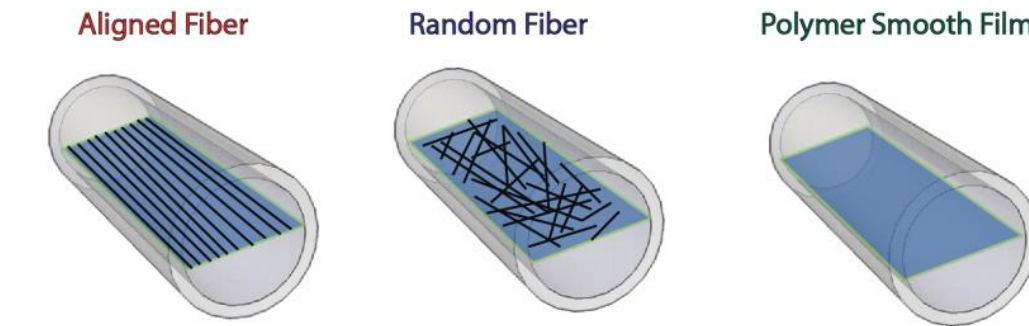


**Figure 4-1: Schematic diagram of film-based scaffolds used to bridge long peripheral nerve gaps.**

**Table 4-1: List of animals studies and outcome measures**

Studies	Conditions	# of Animals	Outcome Measures
5 Day	<ul style="list-style-type: none"> <li>• Aligned</li> <li>• Random</li> <li>• Smooth</li> </ul>	4 per condition	<b>Histology</b> <ul style="list-style-type: none"> <li>• Fibrinogen distribution</li> </ul>
5 Day	<ul style="list-style-type: none"> <li>• Empty</li> <li>• Aligned</li> <li>• Random</li> <li>• Smooth</li> </ul>	4 per condition	<b>Molecular Analysis</b> <ul style="list-style-type: none"> <li>• Cytokine Array</li> </ul>
3 Weeks	<ul style="list-style-type: none"> <li>• Aligned</li> <li>• Random</li> <li>• Smooth</li> </ul>	4 per condition	<b>Histology</b> <ul style="list-style-type: none"> <li>• Schwann cell/Axon migration</li> <li>• Fibronectin/Laminin distribution</li> </ul>
3 Weeks	<ul style="list-style-type: none"> <li>• Empty</li> <li>• Aligned</li> <li>• Random</li> <li>• Smooth</li> </ul>	4 per condition	<b>Molecular Assay</b> <ul style="list-style-type: none"> <li>• Real-time PCR</li> </ul>
22 Weeks	<ul style="list-style-type: none"> <li>• Aligned</li> <li>• Random</li> <li>• Smooth</li> </ul>	8 per condition	<b>Histology</b> <ul style="list-style-type: none"> <li>• Cable area</li> <li>• Schwann cell/Axon distribution</li> <li>• Myelin Thickness</li> <li>• Axonal Diameter</li> </ul> <b>Functional</b> <ul style="list-style-type: none"> <li>• Muscle Weight / Fibrosis</li> <li>• Electrophysiology – Conduction Velocity</li> </ul>

### 4.2.3 Evaluation of nerve bridging

#### *4.2.3.1 Experimental groups*

Nerve regeneration was evaluated at 5 days, 3 weeks and 22 weeks post-implantation (Table 4-1). Aligned, random and smooth thin-film based scaffolds were implanted for each time point. The 5 day (4 animals/condition) was chosen, based on the initial step of regeneration. During this time point, we were interested in the localization of fibrin throughout the guidance channel in response to the different topographical cues. In order to determine Schwann cell migration distances, it is important that two Schwann cell populations (proximal and distal) remain distinct. Previous work from our lab has shown that in a critical length gap, 3 weeks provide the most optimal time point to observe the infiltration of Schwann cells as well as axonal infiltration from the proximal end. We implanted 4 animal/condition for the three week time point. The 22 week time point (8 animals/condition) was chosen to allow for functional muscular reinnervation as well as to look at mature cable formation.

#### *4.2.3.2 Electrophysiology*

In the 22 week groups, electrophysiological measurements were taken of nerve conduction velocity (NCV) through the regenerated nerves. NCV measurements are positively correlated with the size of myelinated axons and degree of myelination. Measurements were taken as in previous studies [163]. Briefly, the site of nerve injury was exposed, and two pairs of stainless steel bipolar hook electrodes were positioned on the nerve. One pair of electrodes was placed on the sciatic nerve, 10 mm proximal to the implanted guidance channel, and the other pair was placed distal to the implanted guidance channel, 10 mm distal to the implanted guidance channel. A stimulator (Model

S88, Grass Technologies) and stimulus isolation unit (Model SIU5B, Grass) was used to apply supramaximal square voltage pulses of 100 $\mu$ s duration at a rate of 1Hz, through the distal pair of electrodes. The evoked compound nerve action potentials (CNAPs) were recorded upstream from the proximal pair of electrodes.

#### 4.2.3.3 Nerve Conduction Velocity

The recorded signals were filtered and amplified (Model 1700, A-M Systems) and digitally sampled at 25kHz. (Multichannel Systems DAQ card.) The recordings were averaged, and the latency of the onset of the evoked CNAP was determined off-line. The distance between the stimulating and recording electrodes divided by this latency value to calculate the conduction velocity of the CNAPs through the regenerated nerves.

#### 4.2.3.4 Relative Gastrocnemius Muscle Weight Measurement

To evaluate the change in muscle weight due to the presence of different topographical thin-films, we explanted the medial gastrocnemius muscle from the operated and the contralateral side at the end of the 22-week study. Briefly, a longitudinal cut was made in lower leg, parallel to the Achilles tendon and gastrocnemius muscle. Insertions were made in the femoral area and at the heel through the Achilles tendon and the gastrocnemius muscle was explanted. The soleus muscle was excluded from the evaluation. Medial gastrocnemius muscles (GMW) were weighed and normalized against the contralateral muscle weight (CMW). The relative gastrocnemius muscle weight (RGMW) was calculated using the following equation:

$$RGMW = \frac{GMW}{CMW} \times 100 \%$$

#### *4.2.3.5 Muscle Atrophy*

The rats' medial gastrocnemius muscle was explanted, fixed with 4% paraformaldehyde for 1 hour, soaked in a 30% sucrose solution overnight, and then frozen in Tissue-Tek Optimal Cutting Temperature compound (Sakura Finetek USA Inc.; Torrance, CA) at -80 °C. Transverse sections 10 µm thick sections of the muscle were obtained by cryosectioning the area of the muscle where the tendon of origin overlap. The muscle sections were then stained with Masson's Trichrome stain using the following method. First the sections were rinsed in distilled water and then submerged in Bouin's solution for 1 hour at 56°C. Then the sections were thoroughly washed in tap water, to remove yellow coloration, followed by a rinse in distilled water. Next, the sections were placed in Weigert's hematoxylin for 90 seconds, followed by washing in running tap water for 5 minutes and then a rinse with distilled water. Then the sections were placed in Biebrich's scarlet-acid fuchsin for 5 minutes, followed by a rinse with distilled water. Next, the sections were placed in phosphomolybdic-phosphotungstic acid for 90 seconds. Then the sections were stained in aniline blue for 5 minutes, followed by rinsing with 1% acetic acid solution for 5 minutes. Finally, the sections were dehydrated first in 95% alcohol and then 100% alcohol, twice each, cleared with 3 changes of xylene, and mounted with Cytoseal 60 (Richard-Allan Scientific; Kalamazoo, MI). The section were imaged using Axioskop 2 plus microscope (Carl Zeiss MicroImaging, Inc.; Thornwood, NY). Image-Pro Plus 7.0 (Media Cybernetics; Bethesda, MD) was used to quantify the area stained blue (representing collagen), allowing for the percent of sampled muscle area stained blue to be determined.

#### *4.2.3.6 Immunohistochemical analysis*

At the end of the prescribed regeneration times, guidance channels were explanted for histological analysis of nerve regeneration. Guidance channels from the 5 days, 3 weeks and 22 weeks regeneration group were sectioned transversely at a thickness of 10 $\mu$ m and reacted with immunofluorescent markers to quantify the different steps of regeneration. Explants were fixed in 4% paraformaldehyde in PBS (Sigma-Aldrich), washed, and stored in 30% sucrose in PBS for 24 hours. Samples were embedded in O.C.T. gel (Tissue Tek) and frozen for cryosectioning (CM30505, Leica). Using techniques previously described in [203], the sections were reacted for immunofluorescent demonstration of markers.

Fibrin cables and macrophages within each scaffolds were qualitatively measured using immuno-fluorescence. Fibrinogen antibody staining (Dako) was used to double stain for fibrin and Macrophages (ED-1, SeroTec) to evaluate the formation of provisional matrix and localization of macrophages that occurs during early regeneration (5 days). The fibrin cables in each scaffold type were characterized qualitatively in terms of (1) whether a fibrin matrix forms (for instance does it not form in the saline filled scaffolds and only forms in the scaffolds with polymer-fiber based films?), (2) whether the matrix is continuous through the length of the nerve gap, and how it affected by different topographies.

At 3 weeks and 22 weeks, transverse cryosections were taken at regular intervals through the scaffold and immunostained. To stain the scaffolds for axons, Schwann cells, and fibroblasts, the following protocol was used: Sections were immunostained for markers of 1) regenerated axons (NF160, Sigma-Aldrich); 2) Schwann cells, (anti-S-100, Dako); 3) myelin (P0, Chemicon Intl.); 4) macrophages (ED-1, CD-68, Serotec); 5)



fibroblasts: double stain of Vimentin (Sigma-Aldrich) and S-100 (to help differentiate non-specific staining of Schwann cells). Sections were double stained with the following secondary antibodies: Goat anti-rabbit IgG Alexa 488/594, and goat anti-mouse IgG1 Alexa 488/594 (Sigma-Aldrich.) A staining process as previously described were employed [203]. Briefly, sections were incubated 1 hour at room temperature in a blocking solution of goat serum (Gibco) in PBS, incubated overnight at 4°C in a mixture of primary antibody and blocking solution, washed and incubated for 1 hour at room temperature in a solution of secondary antibody mixed in .5% triton in PBS. Slides were washed once more, then dried and cover slipped for evaluation.

Transverse cryosections were used to quantitatively evaluate the migration of Schwann cells and axonal growth into the scaffolds. At the three week time point, the distance that the migration front of each cell type penetrates into the scaffold was quantified. The migration fronts Schwann cells were assessed using transverse sections taken at regular intervals through the scaffolds, with a resolution of at least 1 mm. This analysis was performed using ImagePro software. The penetration of the axonal front was quantified as well. In the 22 week study regenerated cable area of Schwann cell and axons were quantified using Image Pro. The percentage of the cable area comprised of S100 positive Schwann cells as well as NF160 positive axons were quantified to evaluate how the presence of different topographical cues lead to a differential formation of the regeneration cable.

#### 4.2.3.7 Trichrome Staining

Same procedure was utilized as previously used to stain muscles to stain for collagen presence in explanted nerve scaffolds. Collagen distribution throughout the scaffold in response to topographical cues was qualitatively observed.

#### *4.2.3.8 Myelin thickness, axonal diameter and myelinated axon count*

One millimeter long sections of regenerated nerve were removed from the center of each scaffold in the 22 week study. These explants were resin embedded, cut into 1 $\mu$ m thick slide mounted cross-sections, and stained with toluidine-blue. Images of regenerated nerve cross-sections were viewed under a Nikon Eclipse 80i light microscope (Japan), using a 100x oil-immersion objective lens. A 40x montage image was compiled for each nerve, using a NeuroLucida<sup>®</sup> system (MBF Bioscience, Williston, VT), coupled to a mechanized stage and MicroFire<sup>™</sup> camera (Optronics, Goleta, CA).

Myelinated axons were manually counted from these 40x montages, using Image-Pro<sup>®</sup> Plus software (Media Cybernetics, Inc., Bethesda, MD). Myelin thickness and axonal diameters were quantified by sampling subsets of the entire axonal population. A 25 $\times$ 25 grid was overlaid above each image, using Adobe<sup>®</sup> Photoshop<sup>®</sup> CS3 (San Jose, CA), and a cell in the upper left-hand portion of the image containing myelinated axons was selected, and grid cells spaced evenly apart from the initially selected cell were chosen for analysis. Between 5-25% of the total myelinated axon population was analyzed from each nerve cross-section. Image-Pro<sup>®</sup> Plus software was used to measure myelin thickness and axonal diameter of myelinated axons. Axonal diameters were calculated using a circle-equivalent technique, in which the cross-sectional area of each axon was measured and then converted into an axonal diameter using a formula that assumes a circular cross-section.

#### 4.2.4 Molecular analysis of explanted nerve

##### *4.2.4.1 Tissue Collection for molecular analysis*

For tissue collection, animals were anesthetized using isoflurane and euthanized by cutting the heart at 5 days and 3 weeks post-surgery. Nerve conduits were explanted from each animal and the conduits were cleaned to remove tissue on the outside. All the samples were collected in 1.5 ml polypropylene tubes (RNAase, DNAase, and pyrogen free ) and were put in dry ice immediately after collection. Finally the nerve conduits were stored at -80°C for further protein and RNA extraction.

##### *4.2.4.2 Cytokine array for 5 day samples*

1 mm of the conduit from both the proximal and distal end were precisely cut using titanium blades to leave 15 mm conduit loaded with thin film based scaffolds. An empty scaffold was also used in this study as a control to test the recruitment and production of cytokines in response to topography. The conduits were further cut into three pieces of 5 mm each to evaluate the spacial distribution of cytokines. 200µl RIPA buffer (Sigma) was used to extract the tissue within each region of the conduit. The conduit was homogenized using Bullet Blender (Next Advance) at 4°C followed by 10 min centrifugation at 10,000 rpm. The supernatants were stored at -80°C until ready for cytokine multiplex arrays.

A 9-bead based immunoassay kit for rat cytokines (BIO RAD) was used to detect the concentration of IL-1 $\alpha$ , IL-1 $\beta$ , IL-2, IL-4, IL-6, IL-10, granulocyte-macrophage colony stimulating factor, interferon  $\gamma$  and TNF- $\alpha$ . Protocol provided by the manufacturer was used to quantify the amount of cytokines present in different areas of

the conduits which were loaded with thin films as well as an empty tube. Multiwavelength fluorescence was determined with a luminometer (BIO RAD).

Concentrations of cytokines that were outside the range of the standard curve were not reported. The concentrations of these samples were observed to be below the detection limit of the assay kit.

#### *4.2.4.3 qRT-PCR for 3 week samples*

To evaluate the effects of thin films of different topographies, we evaluated the gene expression of various growth factors and receptors that play a key role in the regenerative sequence. Similar protocol to extract the conduits as used for 5 day experiment was used for 3 week samples. Instead of cutting the conduits in thirds, the conduits were cut in half following the removal of 1 mm from both the proximal and distal end of the conduits. Total RNA was extracted from each half of the nerve conduit using Qiagen RNEasy Midi-Kit (Qiagen). Briefly, aligned, random and smooth films based scaffolds, as well as empty tubes were explanted and cut in half. The tubes were homogenized using the Bullet Blender (Next Advance) and the lysis buffer provided in the RNEasy Midi-Kit. Samples were centrifuged and the supernatant was processed to extract the RNA.

5 micrograms of total RNA was converted to cDNA using high capacity cDNA reverse transcription kit (Applied Biosystems). PCR primers for BDNF, NT-3, FN, LN-1, Erbb2, Erbb3, NRG1, P75 and housekeeping gene GAPDH were designed using Primer Express software (Applied Biosystems) and obtained from Integrated DNA Technologies. qRT-PCR and primer validation were performed on StepOnePlus real-

time PCR machine (Applied Biosystems) using SYBR green mix. Fold differences were calculated using the comparative  $C_T$  method and normalized to empty tubes.

#### 4.2.5 Fiber Permeability

Constructs were created to test the ability of the thin films to allow for exchange of biomolecules. 5 mg/ml solutions of 500 kd and 70 kd FITC-Dextran (SIGMA) were added to the top chamber while 1x PBS was added to the bottom chamber to facilitate the diffusion. Samples were collected from the bottom chamber and analysed on the spectrophotometer.

#### 4.2.6 Statistical Analysis

ANOVA, combined with Tukey post hoc tests, was used to calculate the significance of differences between mean values. A p value less than 0.05 was considered statistically significant.

## 4.3. Results

### 4.3.1 Histological analysis of regenerated axons and Schwann cell migration

#### *4.3.1.1 Axonal growth and Schwann cell migration 3 weeks post implantation*

Staining of Schwann cells (S100) and axons (NF160) at 3 weeks post implantation revealed the extent of infiltration of scaffold by neuronal cells as well as the shape of the regenerating cable. At 3 weeks, the proximal area of the conduit showed that the regenerating cable was different for fiber based scaffolds versus smooth film based scaffolds. A single cable formed around the fiber-based scaffolds while separate cables were observed on either side of the smooth-film based scaffold. We also observe that in all three conditions, the regenerating cable showed positive presence of S100+ Schwann cells and NF160+ axons in the proximal end (first third, Figure 4-2) of the scaffold at 3 weeks. While in the mid-region of the scaffold (second third, Figure 4-3), the area of the regenerating cable was smaller compared to the other two regions. It was also observed that the regenerating cable was closely associated around the thin films. In case of aligned and random fibers neuronal cells were centralized around the thin-films. While in smooth films the two distinct cables that were observed to be distinctly segregated in proximal and distal thirds of the scaffolds were seen to come closer to thin film and observed to look closer in morphology as the other two conditions. But the regenerating cable still remained distinct and neither Schwann cells nor axons were found interacting with the smooth films. In the final third (Figure 4-4) of the scaffold, similar morphology of the regenerating cable was observed as in the proximal end. At the 3 week time point, no axons were present in any experimental groups. While similar Schwann cell infiltration from the distal end was observed as with the proximal end.

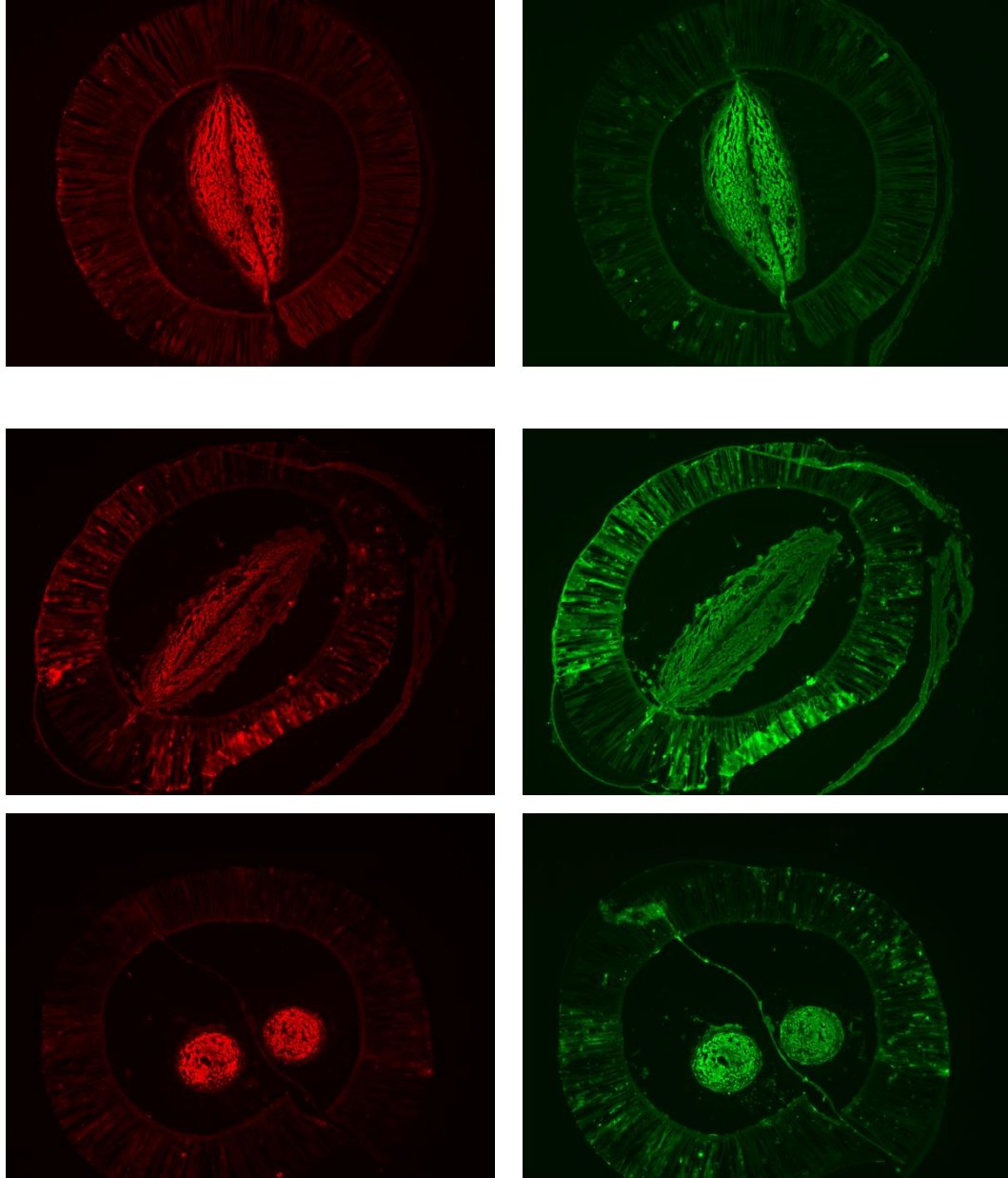
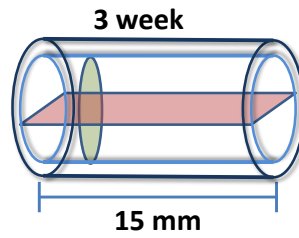


**Figure 4-2: Schwann cell cable formation at 3 weeks in the proximal section of the film-based scaffolds.** A. Schematic diagram of the location in the tube that corresponds to the stained sections. B,C. Aligned fibers based scaffold stained with NF160 (Axons) and S100 ( Schwann cells) respectively. D,E. Random fiber based scaffold stained for NF160 and S100 respectively. F,G. Smooth film based scaffold stained for NF160 and S100 respectively. Scale bar = 400 $\mu$ m

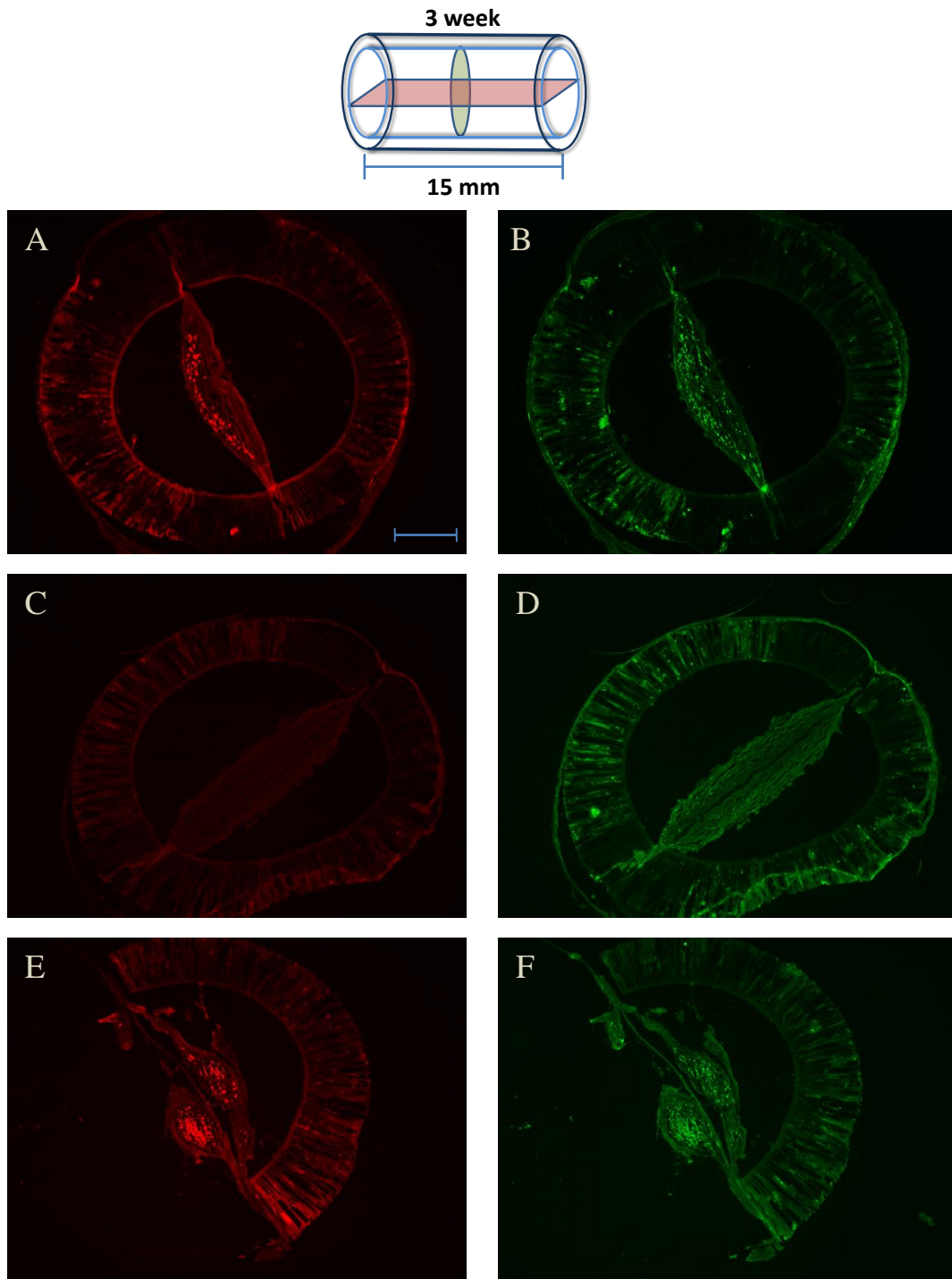


**Figure 4-3: Schwann cell cable formation at 3 weeks in the middle section of the film-based scaffolds.** A. Schematic diagram of the location in the tube that corresponds to the stained sections. B,C. Aligned fibers based scaffold stained with NF160 (Axons) and S100 (Schwann cells) respectively. D,E. Random fiber based scaffold stained for NF160 and S100 respectively. F,G. Smooth film based scaffold stained for NF160 and S100 respectively. Scale bar = 400 $\mu$ m



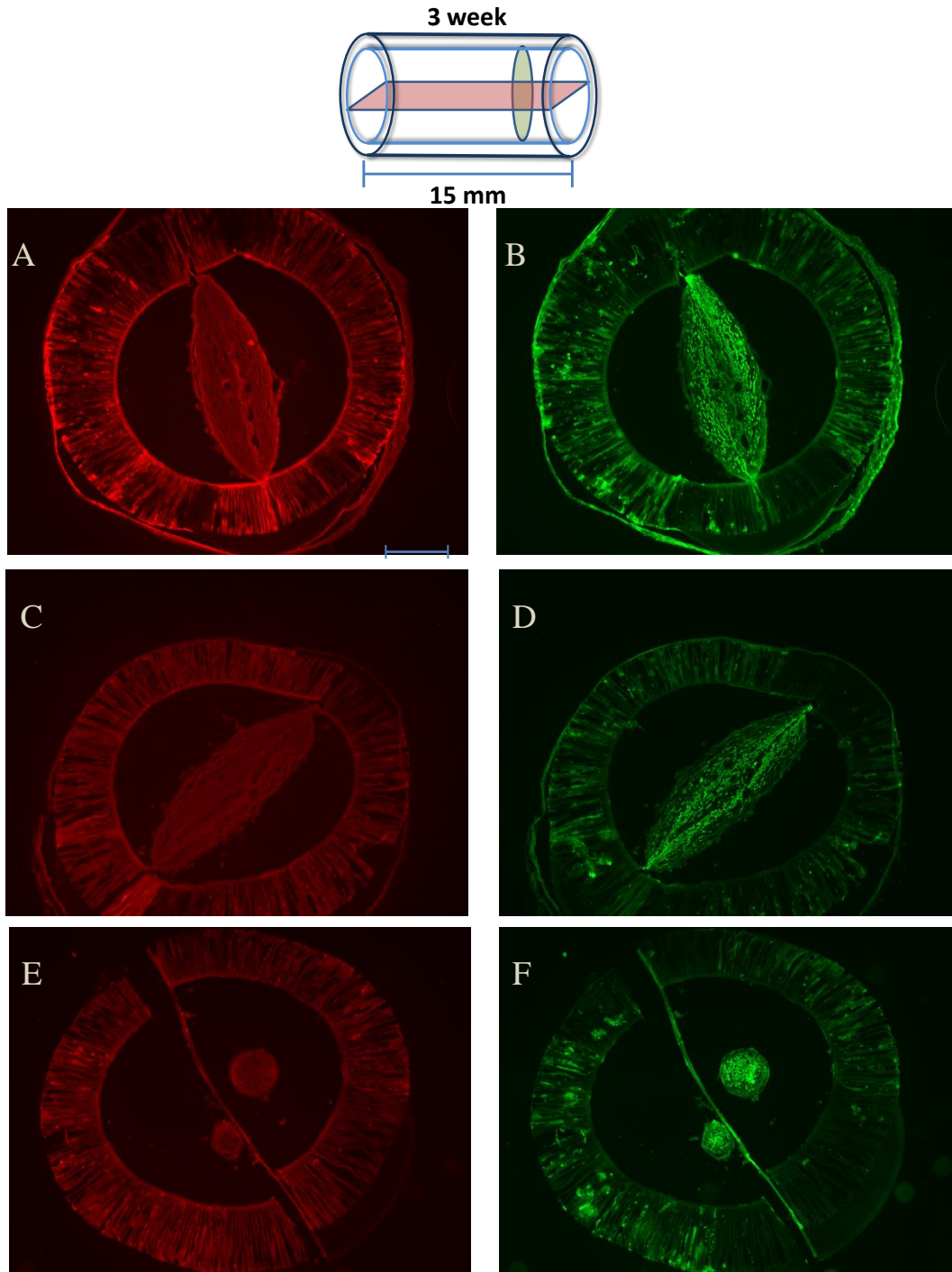


**Figure 4-4: Schwann cell cable formation at 3 weeks in the distal section of the film-based scaffolds.** A. Schematic diagram of the location in the tube that corresponds to the stained sections. B,C. Aligned fibers based scaffold stained with NF160 (Axons) and S100 ( Schwann cells) respectively. D,E. Random fiber based scaffold stained for NF160 and S100 respectively. F,G. Smooth film based scaffold stained for NF160 and S100 respectively. Scale bar = 400 $\mu$ m

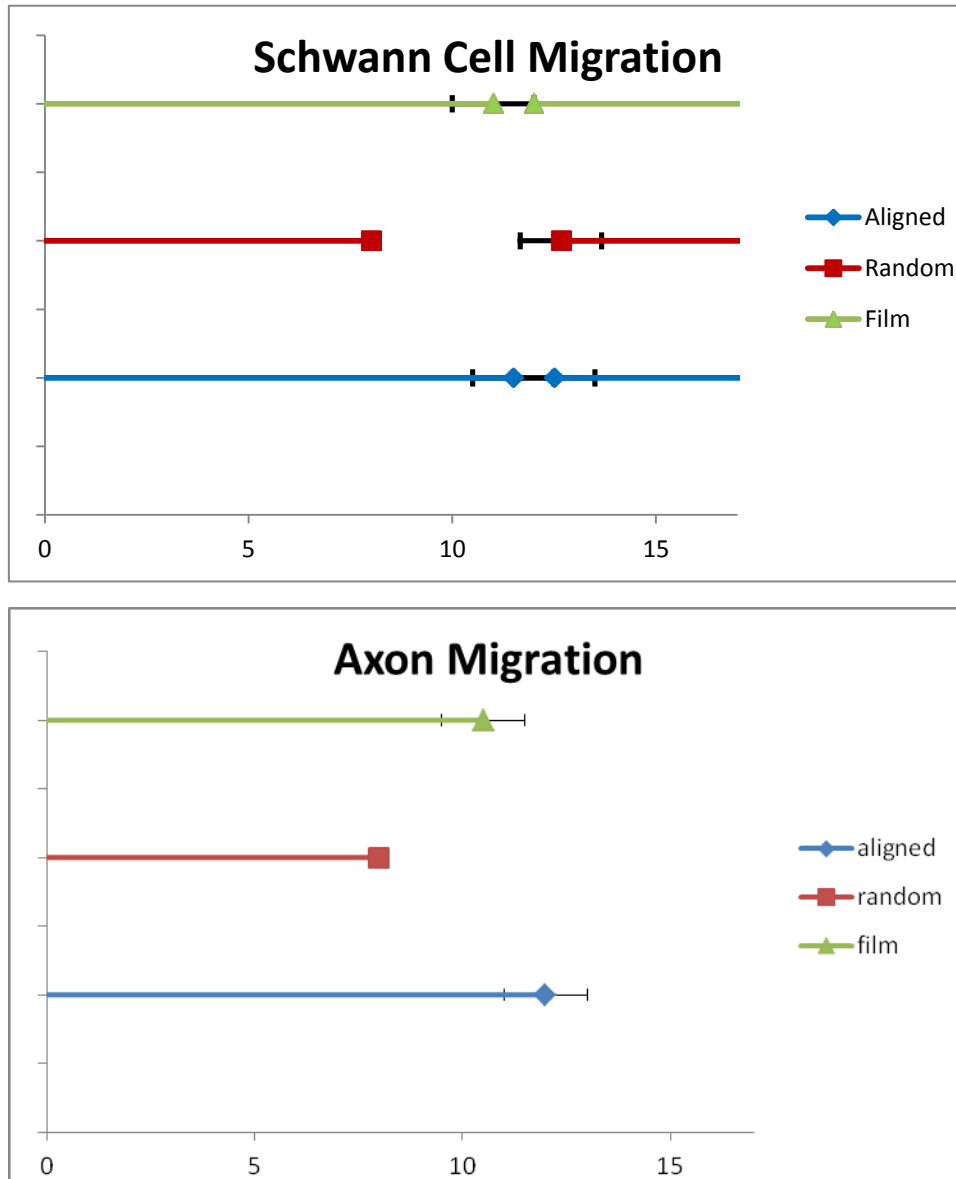


**Figure 4-5: Quantification Schwann cells migration and neurite outgrowth at 3 weeks.** Graph representing the migration of Schwann cell (top) and axonal growth (bottom) from the proximal end of the nerve graft. \*\* =  $p < 0.01$  Aligned vs Random and Smooth film condition. \*\*\* =  $p < 0.01$  for Random vs Smooth film. X-axis represents the distance within the nerve conduit.

The migration of Schwann cells and growth of axons from the proximal end of the scaffold were quantified (Figure 4-5). Schwann cell migration and axonal growth were significantly higher ( $p < 0.01$ ) in aligned fiber based scaffolds compared to smooth films and random fiber based scaffolds. The migration front of the axons was also tracked. Aligned fiber-based scaffolds promoted the axonal growth up to 13 mm in a 17 mm nerve conduit compared to smooth films and random fibers which supported infiltration of axons up to 11 mm and 9 mm respectively. Axons were observed to co-localize with the S100+ Schwann cells.

#### *4.3.1.2 Axonal growth and Schwann cell migration 22 weeks post implantation*

Long term influence of topographical cues on Schwann cell and axon maturation within the nerve conduit was qualitatively and quantitatively assessed 22 weeks post implantation. A distinct regenerative cable was observed 22 weeks post implantation in all the experimental groups. Schwann cells and axons closely associated with the fibers in the aligned fiber-based scaffolds while a layer of connective tissue was observed on the random fibers. Two distinct cables were observed in the smooth film based scaffold as previously observed in the 3 week study. The regenerative cables surrounded the thin film scaffolds and were anchored to the thin-films extending from the edge of the scaffold creating an equal tissue distribution on either side of the thin-films. Representative images from three different areas of the nerve conduit have been shown in Figures 4-6 to Figure 4-8. These areas represent the proximal third, middle third and the distal third of the nerve conduits. At 22 weeks, a complete bridging of the nerve conduit was observed in all three experimental groups. All three groups showed a bigger area of the cable in the proximal third of the conduit compared to the middle and distal thirds.

The area of the regenerative cable formed at 22 weeks post implantation was quantified to observe the how aligned, random and smooth film-based topographies lead to organization of Schwann cells and axons. Schwann cell positive area was quantified within the transverse sections at 2 mm, 4 mm, 6 mm, 11 mm, 13 mm, and 15 mm from the proximal end of the nerve conduit. Aligned fiber based scaffolds showed the highest Schwann cell area growth at 2 mm compared to smooth film-based scaffolds but not against random fibers. At 4 mm into the conduit, aligned fiber based-scaffolds had significantly higher Schwann cell area compared to both smooth films and random fiber based scaffolds. While at 6 mm into the conduit, a significantly larger Schwann cell occupied area was observed in aligned fiber based scaffolds compared to random fibers based scaffolds but not smooth film based scaffolds.

Percentage of the regenerating tissue cable comprised of Schwann cells was quantified to evaluate the effects of topography on the overall composition of the cable. Significantly higher percentage of the regenerated cable was comprised of Schwann cells compared to smooth film based scaffolds at 2, 4 and 6 mm from the proximal end of the conduit. Compared to smooth films, a significantly higher percentage of Schwann cells were present in the regenerated cable at 6 mm in the conduit in aligned fiber-based scaffolds. At conduit lengths of 11, 13 and 15 mm, no significant difference was observed between the different experimental groups. This data shows that aligned fibers based scaffolds influence the composition of Schwann cells at several locations within the conduit compared to random and smooth film based scaffolds (Figure 4-9 and Figure 4-10).

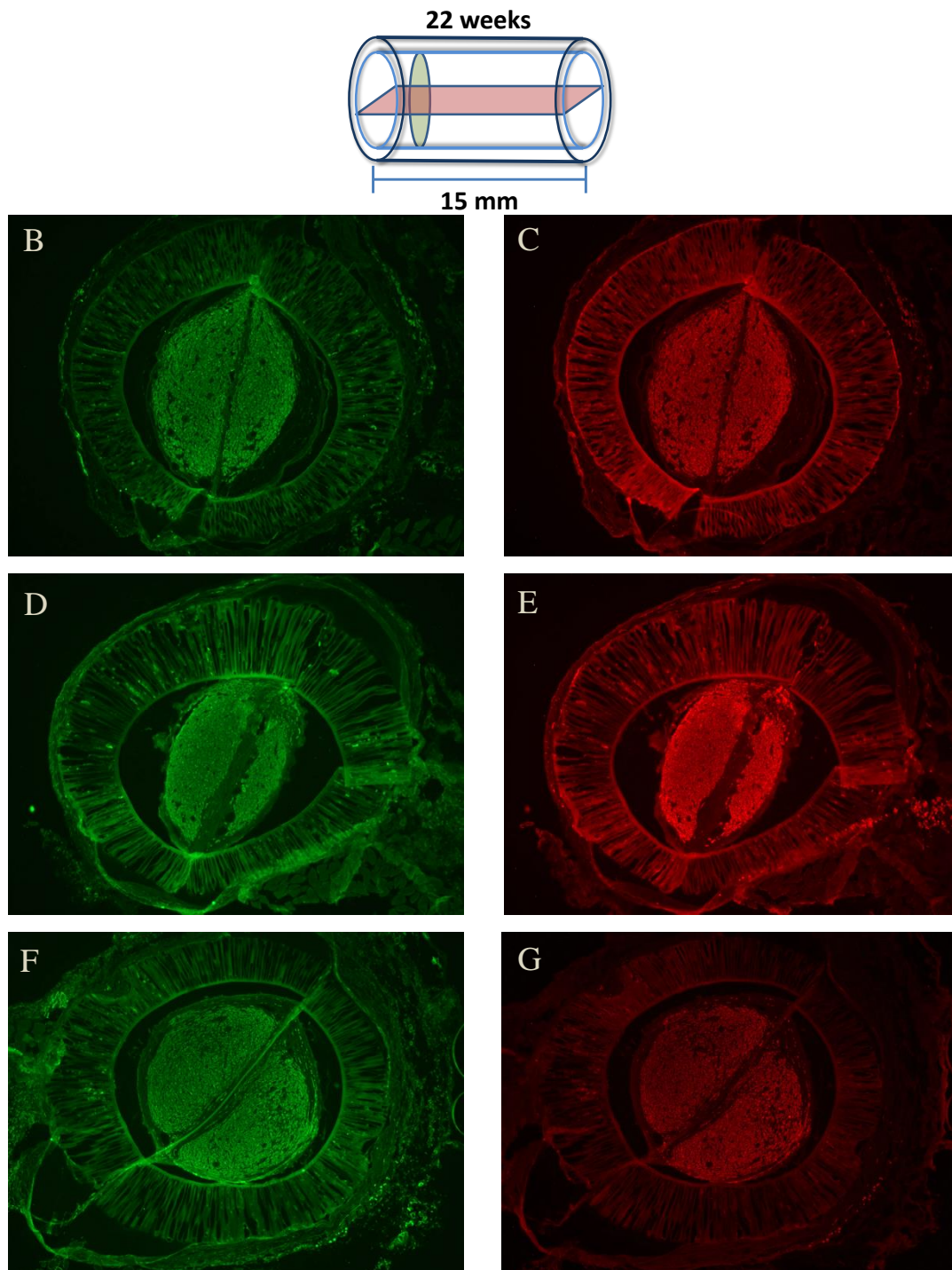


**Figure 4-6: Regenerating cable formation at 22 weeks in the proximal section of the film-based scaffolds.** A. Schematic diagram of the location in the tube that corresponds to the stained sections. B,C. Aligned fibers based scaffold stained with NF160 (Axons) and S100 ( Schwann cells) respectively. D,E. Random fiber based scaffold stained for NF160 and S100 respectively. F,G. Smooth film based scaffold stained for NF160 and S100 respectively. Scale bar = 400 $\mu$ m

B

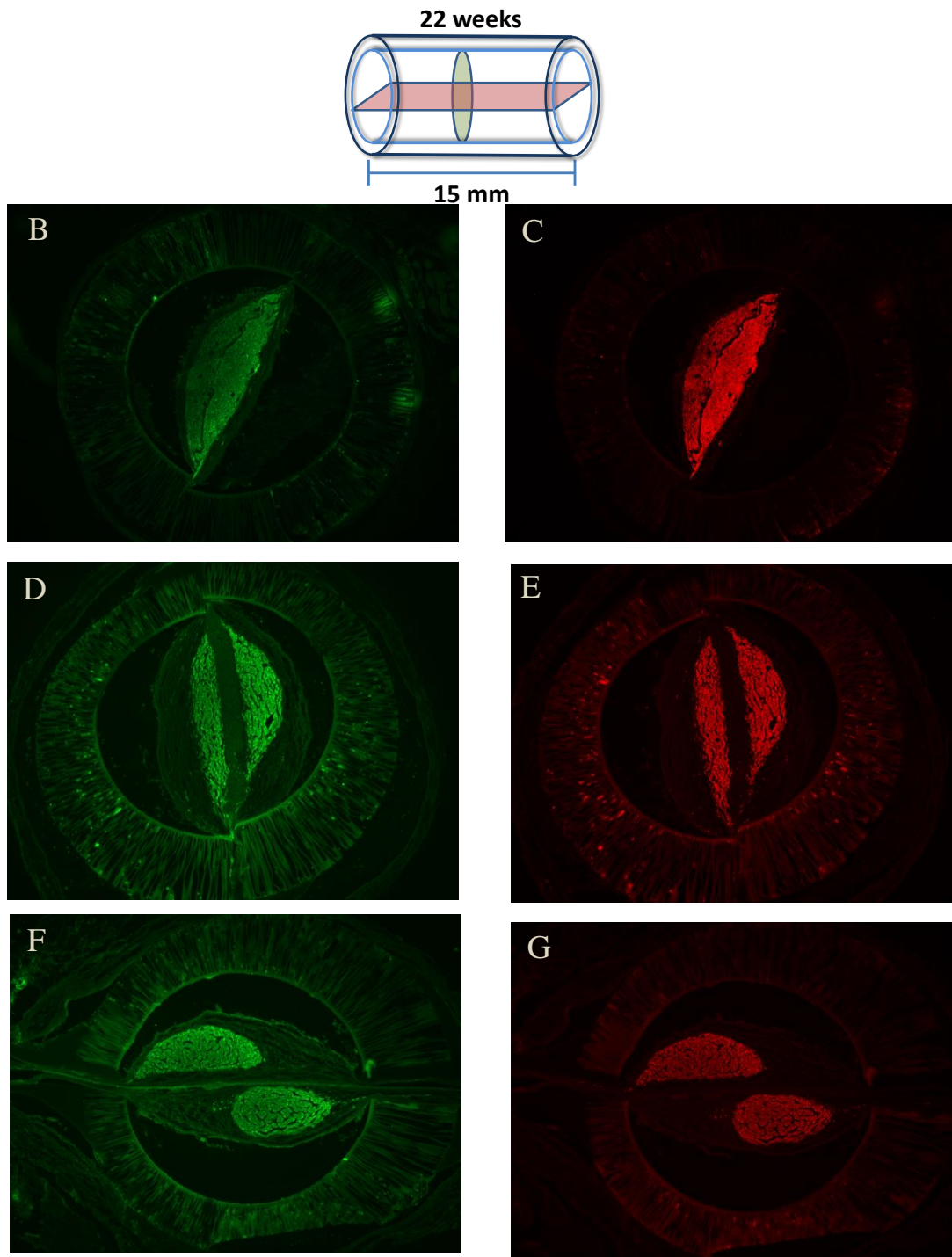


**Figure 4-7: Schwann cell cable formation at 3 weeks in the middle section of the film-based scaffolds.** A. Schematic diagram of the location in the tube that corresponds to the stained sections. B,C. Aligned fibers based scaffold stained with NF160 (Axons) and S100 ( Schwann cells) respectively. D,E. Random fiber based scaffold stained for NF160 and S100 respectively. F,G. Smooth film based scaffold stained for NF160 and S100 respectively. Scale bar = 400 $\mu$ m

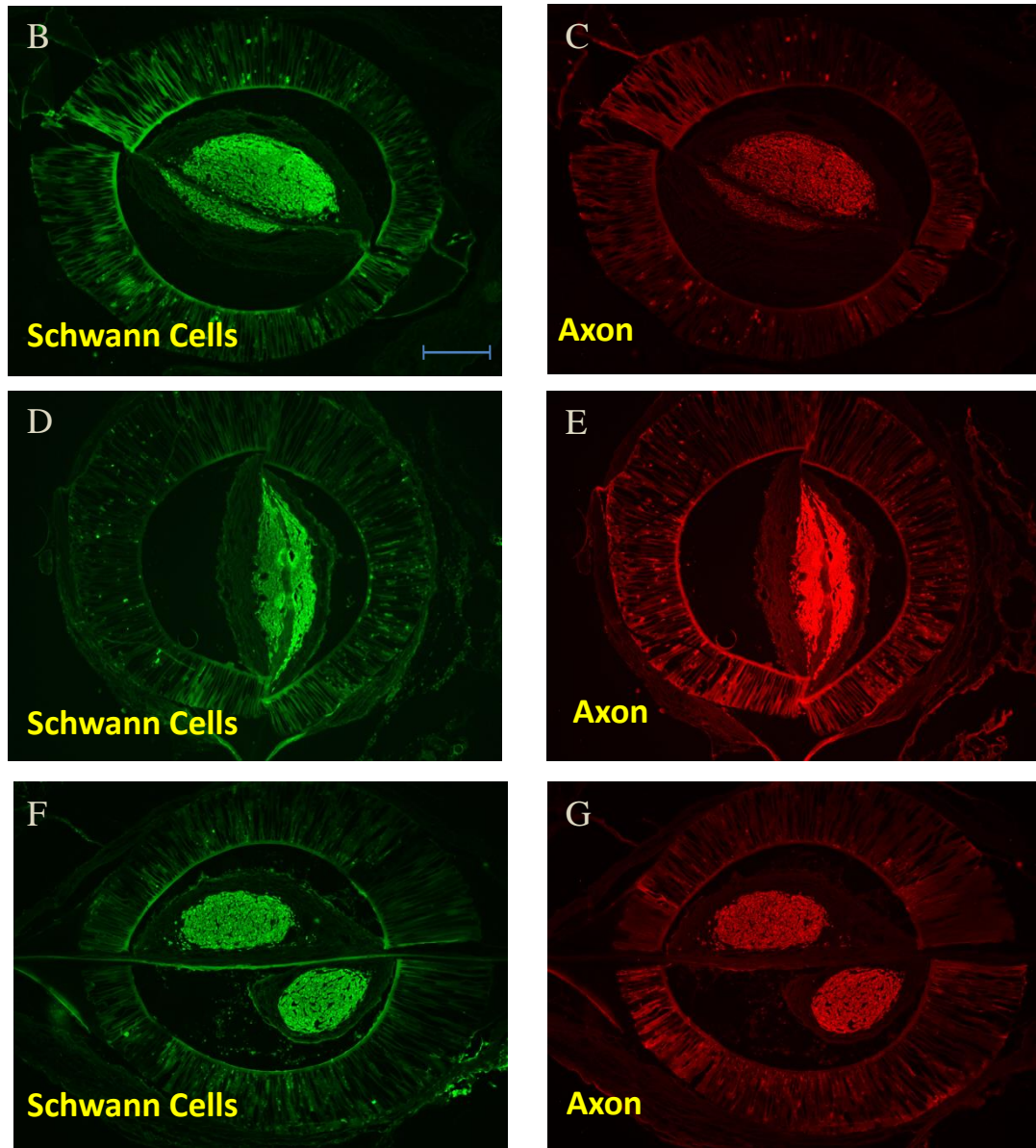
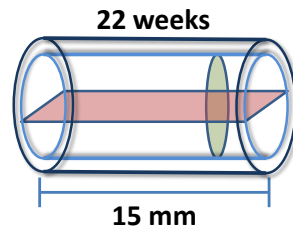


**Figure 4-8: Schwann cell cable formation at 3 weeks in the distal section of the film-based scaffolds.** A. Schematic diagram of the location in the tube that corresponds to the stained sections. B,C. Aligned fibers based scaffold stained with NF160 (Axons) and S100 ( Schwann cells) respectively. D,E. Random fiber based scaffold stained for NF160 and S100 respectively. F,G. Smooth film based scaffold stained for NF160 and S100 respectively. Scale bar = 400 $\mu$ m

Similar analysis as done for Schwann cells was performed for the axonal growth within the transverse sections of the different groups at 22 weeks. This was performed to show the effects of topography on late stage maturation of the axonal cable. Significantly higher area of NF160+ axons were present in oriented fiber based scaffolds at 2 mm into the conduit compared to smooth film based scaffolds and at 4 mm into the conduit compared to random fiber based scaffolds. This data shows that higher presence of axonal growth was observed in the proximal end of the nerve conduit in the aligned fiber based group. There was no significant difference observed from 6 mm onwards into the conduit between the different experimental conditions (Figure 4-11).

Percentage of the cable comprised of axons was also quantified to observe the influence of topographical cues on long term neuronal growth. Percentage of axonal area within the aligned fiber based scaffolds was significantly higher compared to smooth films up to 11 mm into the conduit. Percentage of the area was also significantly higher in the aligned fiber based scaffold compared to random scaffold at 2 mm and 11 mm into the conduit. Since this data represents the composition of axons in the regenerated cable, it suggests that oriented topographical features support higher number axons compared to other cells/tissue within the nerve conduit compared to random and smooth film based topographies. Beyond 11 mm, there is no significant difference found between the different experimental groups (Figure 4-12).



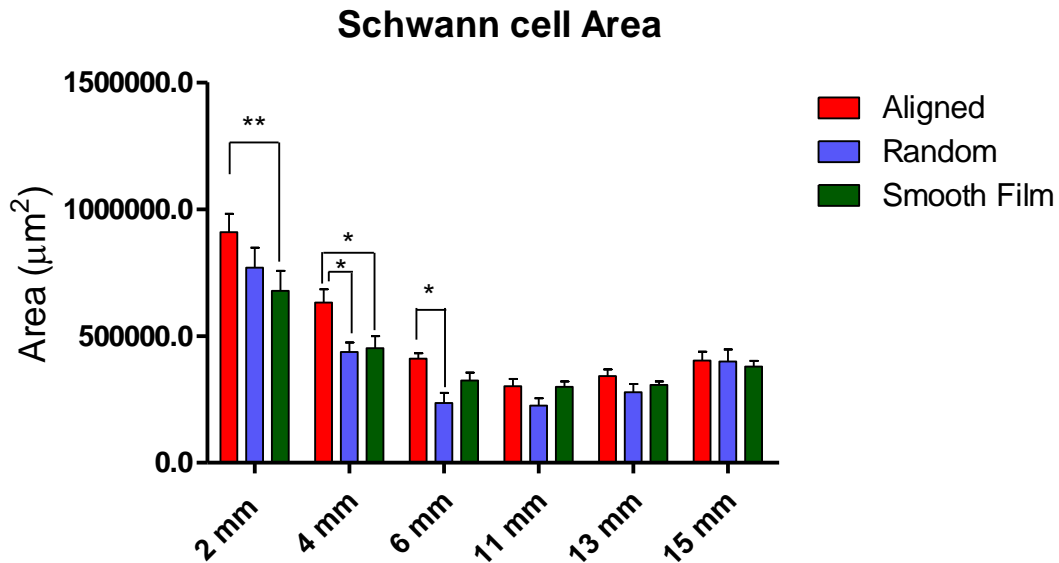


**Figure 4-9: Quantification of Schwann cell area at 22 weeks.** Total area that was positively stained for S100 (Schwann cells) at different locations in a nerve conduit 22 weeks after implantation. \*\* =  $p < 0.01$  and \* =  $p < 0.05$ .

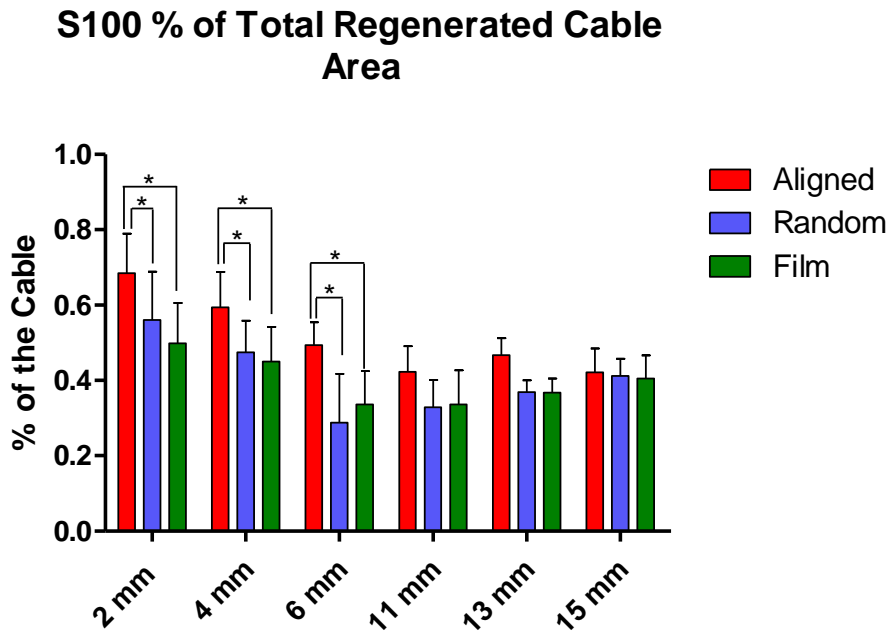


**Figure 4-10: Percentage of Schwann are in the total regenerated cable at 22 weeks.** Percentage of the total cable area positive for S100 (Schwann cells) at different locations in a nerve conduit 22 weeks after implantation. \* =  $p < 0.05$

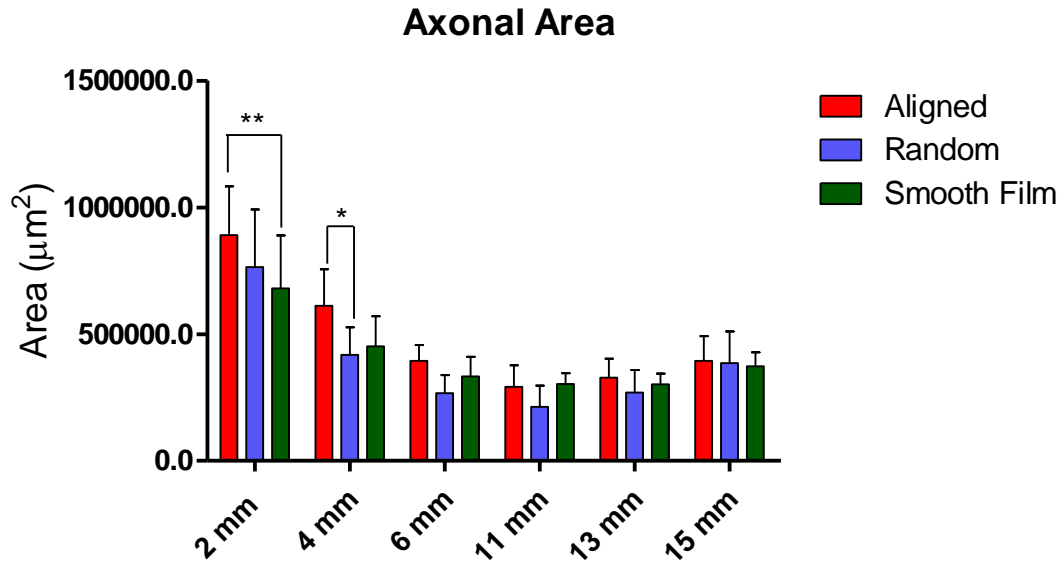


**Figure 4-11. Quantification of Axonal area at 22 weeks.** Total area that was positively stained for NF160 (Axons) at different locations in a nerve conduit 22 weeks after implantation. \*\* =  $p < 0.01$  and \* =  $p < 0.05$ .

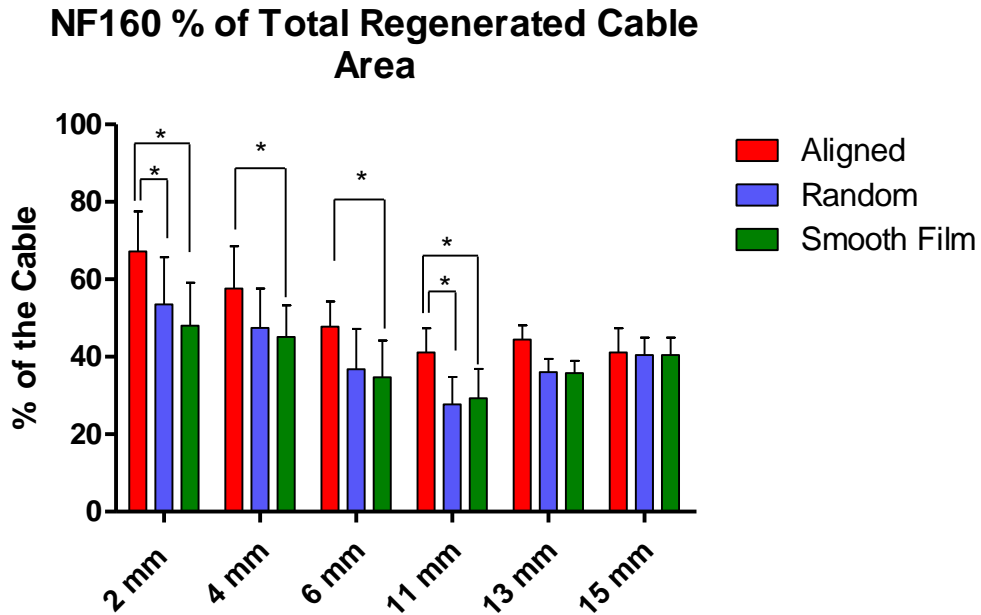


**Figure 4-12: : Percentage of Axonal area in the total regenerated cable at 22 weeks.** Percentage of the total cable area positive for NF160 (Axons) at different locations in a nerve conduit 22 weeks after implantation. \* =  $p < 0.05$

#### 4.3.2 Number of myelinated axons

To further investigate the maturation of the regenerated axons in response to different topographical cues, transverse sections from the center of the scaffolds were quantified for number of toluidine blue stained myelinated axons. Within the epineurium style connective tissue, aligned fiber-based scaffold showed a significant higher number of myelinated axons compared to random fiber based scaffolds. There was no difference observed between aligned and smooth film or between smooth film and random fiber based scaffolds in the total number of myelinated axons. It was observed that axons were closely associated with the fiber based scaffolds and even penetrated the aligned fibers. A thin layers of connective tissue was observed on the random fibers while two distinct epineurial cables were observed on either side of the smooth films. Axons were not present in the vicinity of the smooth films at higher magnification. Aligned fiber-based scaffolds also exhibited a higher density of axons as showed by Figure 4-13.

#### 4.3.3 Myelinated sheath thickness and axonal diameter

The scaffolds were further investigated to elucidate the axonal width and myelin thickness as measures for the level of growth of axon within the thin film based scaffolds. There was no significant difference observed between the different experimental groups for myelin thickness. This data suggests that axons were myelinated equally in response to topographical cues provided by aligned, random and smooth thin films (Figure 4-14 D).

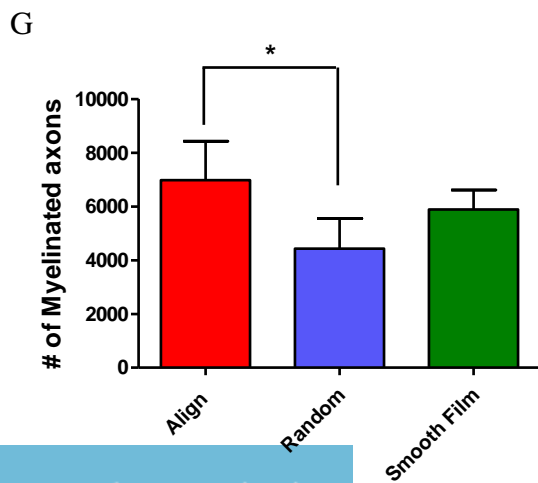
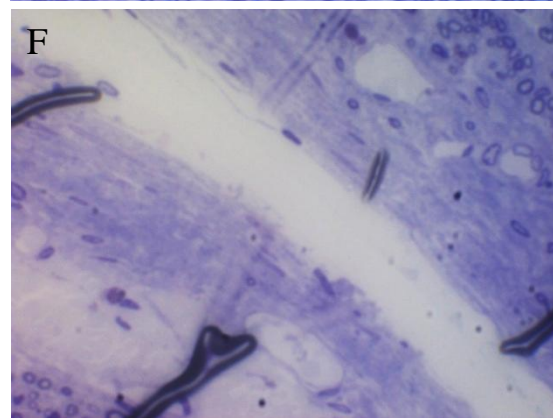
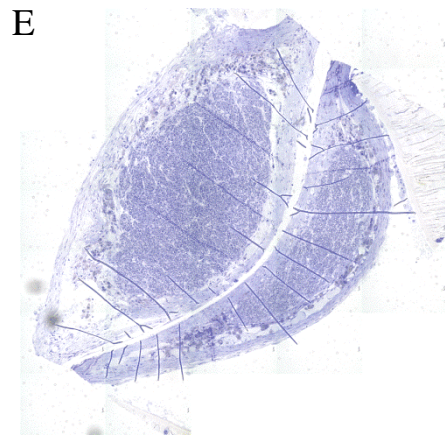
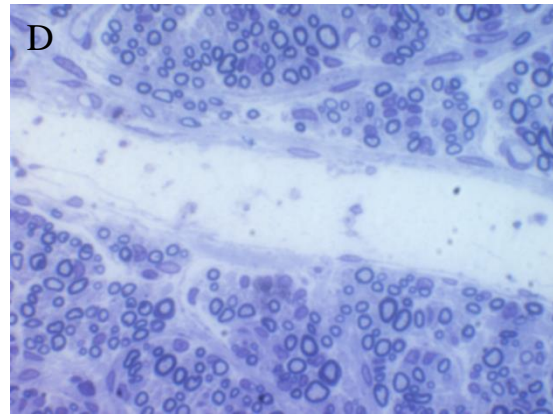
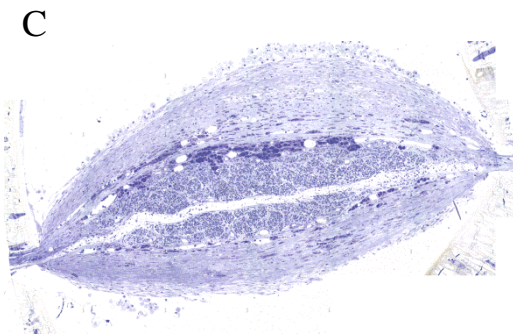
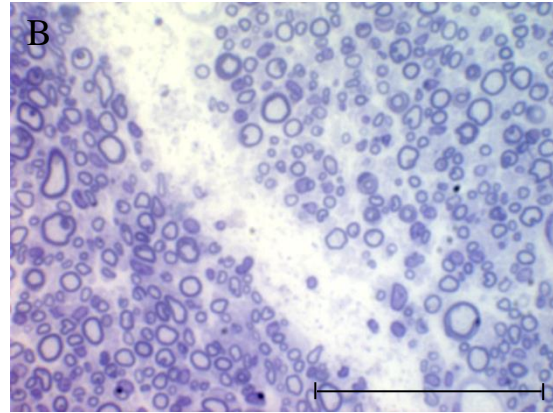
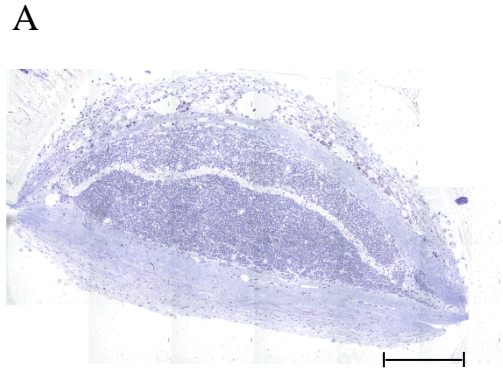


**Figure 4-13: Axonal myelination.**

Toluidine blue stained cross sections from the middle of the scaffold 22 weeks post injury. A. Aligned. B. Random. C. Smooth film. D, E, F represent 40X images of the tissue close to the thin films. G. Number of myelinated axons. \* =  $p < 0.05$ . Scale bar =  $250\mu\text{m}$

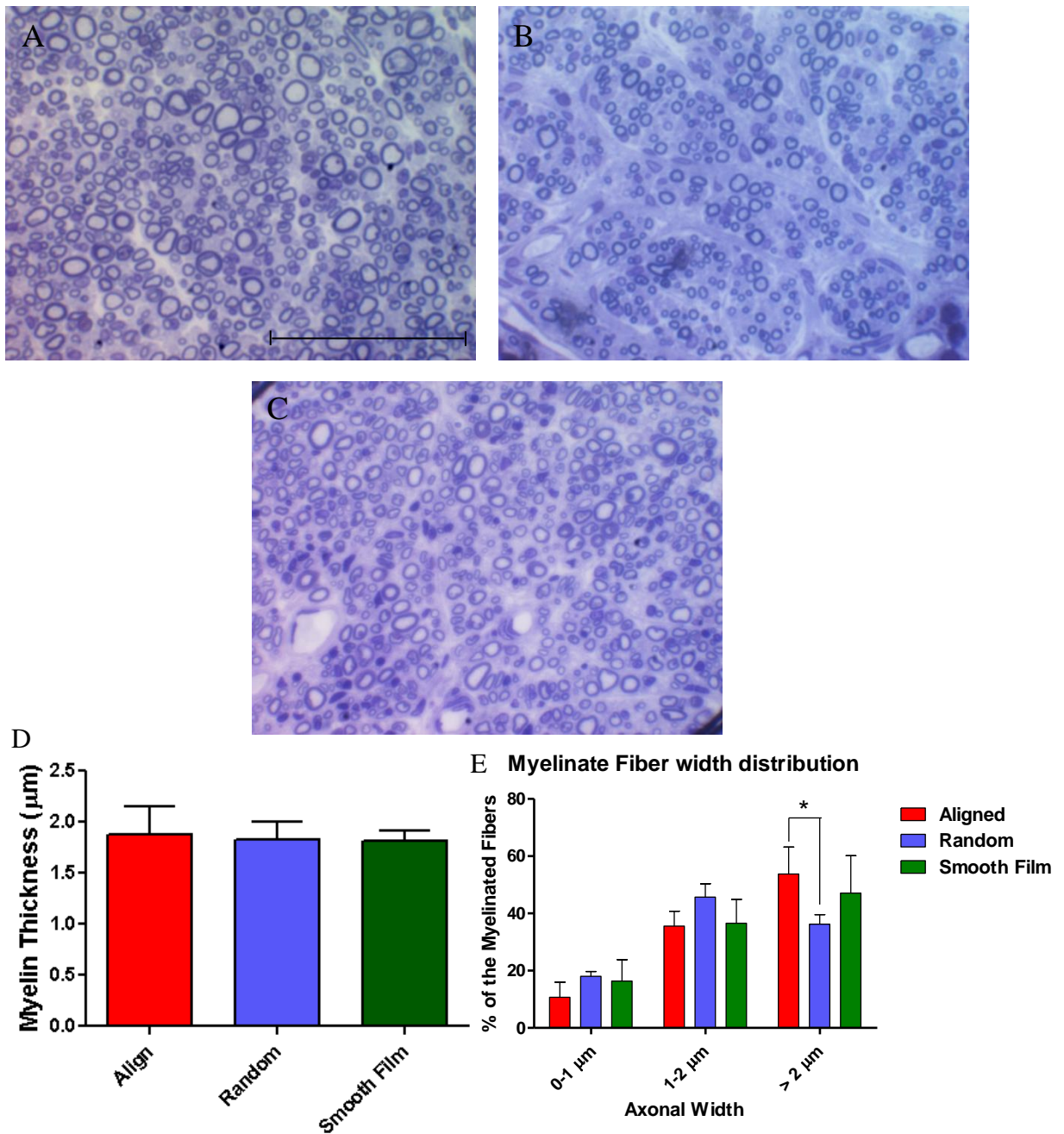


**Figure 4-14: Quantification of myelin thickness and axonal width.** Myelinated axons in A. Aligned, B. Random, and C. Smooth Film based scaffolds. D. Quantification of myelin thickness. E. Quantification of Myelinated fiber diameter. Scale bar = 25 µm

Axon maturity was also quantified within the conduit by evaluating the axonal width. Percentage distribution of axonal width was quantified. A significantly higher percentage of >2mm diameter fibers were observed in aligned fiber based scaffold compared to random fiber based scaffold but not smooth film based scaffolds (Figure 4-14 E). These observations show that 22 weeks post implantation, topographical cues influence the regenerative capacity of peripheral nerve and lead to axonal maturation compared to non-oriented fiber based scaffolds.

#### 4.3.4 Muscle weight and muscle fiber diameter

Functional evaluation of axonal reinnervation into the muscle was indirectly tested by performing muscle weight analysis. The innervated muscle weight ratio was significantly higher in aligned fiber based scaffolds compared to random and smooth films based scaffolds (Figure 4-15 D). Furthermore, trichrome staining of sectioned muscle tissue showed that amount of atrophy, measured by the shrinking of the bundle of muscle fibers was significantly higher in random fiber based scaffolds compared to smooth films and aligned fiber based scaffolds (Figure 4-15 E). This data suggest that muscle innervation was enhanced by oriented topography.

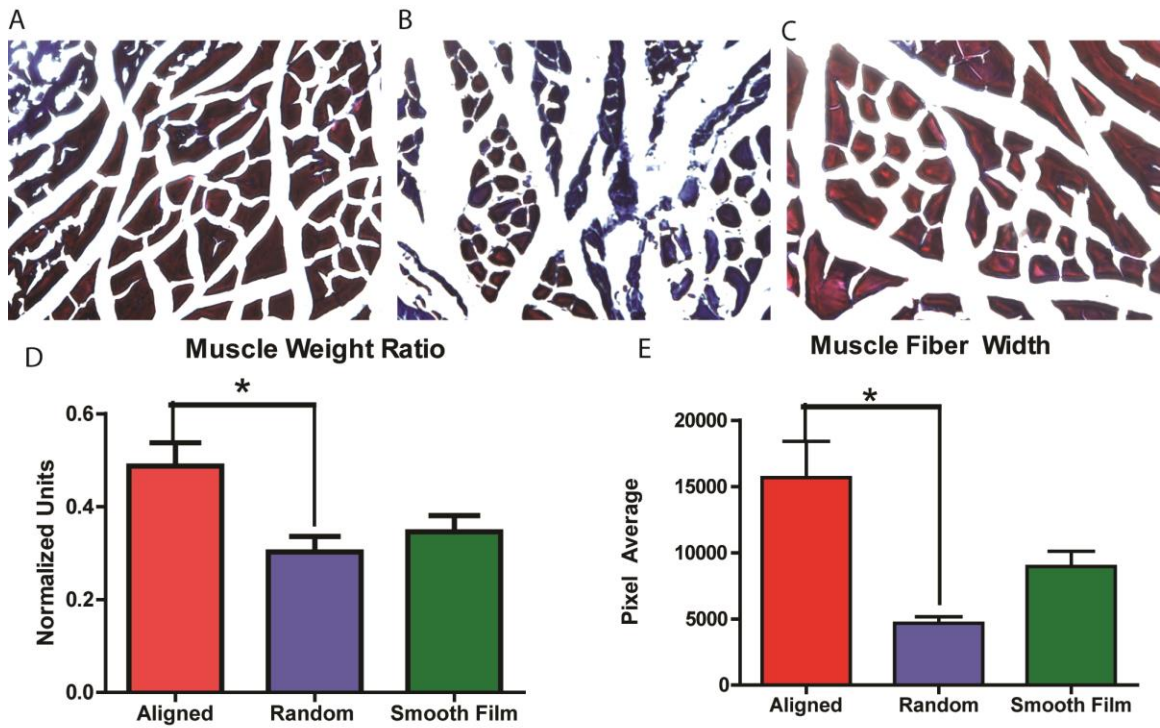


**Figure 4-15: Cross section analysis of gastrocnemius muscle.** A. Aligned B. Random C. Smooth Film. D. Quantification of relative Gastrocnemius muscle weight ratio. \* =  $p < 0.05$ . E. Pixel average diameter of muscle fibers. \* =  $p < 0.05$ .

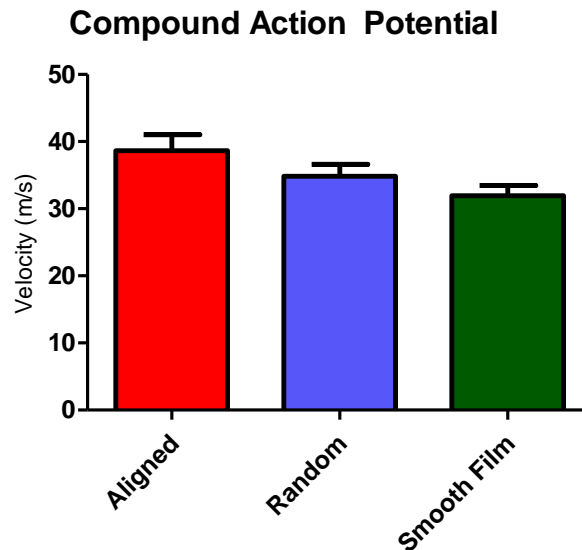


**Figure 4-16: Compound action potential velocity.** Nerves were stimulated distal to the injury site and the signal was recorded proximal to the site of injury.

#### 4.3.5 Compound action potential velocity

To further understand the functional implication of the presence of different topographical cues within the nerve guide, the ability of the regenerated nerve cable to transmit electrical signals was measured. Compound action potentials were measured and the conduction velocity in response to various topographies was calculated. The compound action potential velocity was not significantly different between all three experimental groups (Figure 4-16). All the conditions supported the transport of electrical signals suggesting that they supported the growth of axons which were functionally active.

#### 4.3.6. Fibrin organization 5 days post injury

Presence of the fibrin matrix was observed in all conditions throughout the length of the conduit. A denser fibrin matrix was observed in the smooth film based scaffolds. A more disrupted provisional matrix was observed in random fibers based scaffolds compared to smooth film based scaffold. A representative image from the center of the scaffold is showed in Figure 4-17

#### 4.3.7. ECM Organization at 3 weeks and 22 weeks post injury

Cryosectioned samples were stained for Laminin at 22 weeks and collagen at 3 weeks and 22 weeks post-surgery using trichrome staining. In all thin film based scaffolds (aligned, smooth film and random) positive Laminin signal was observed within the area where Schwann cells were observed. Laminin also localized on the fiber based thin films. Compared to that, Laminin was not observed on smooth films within the cross section (Figure 4-18).



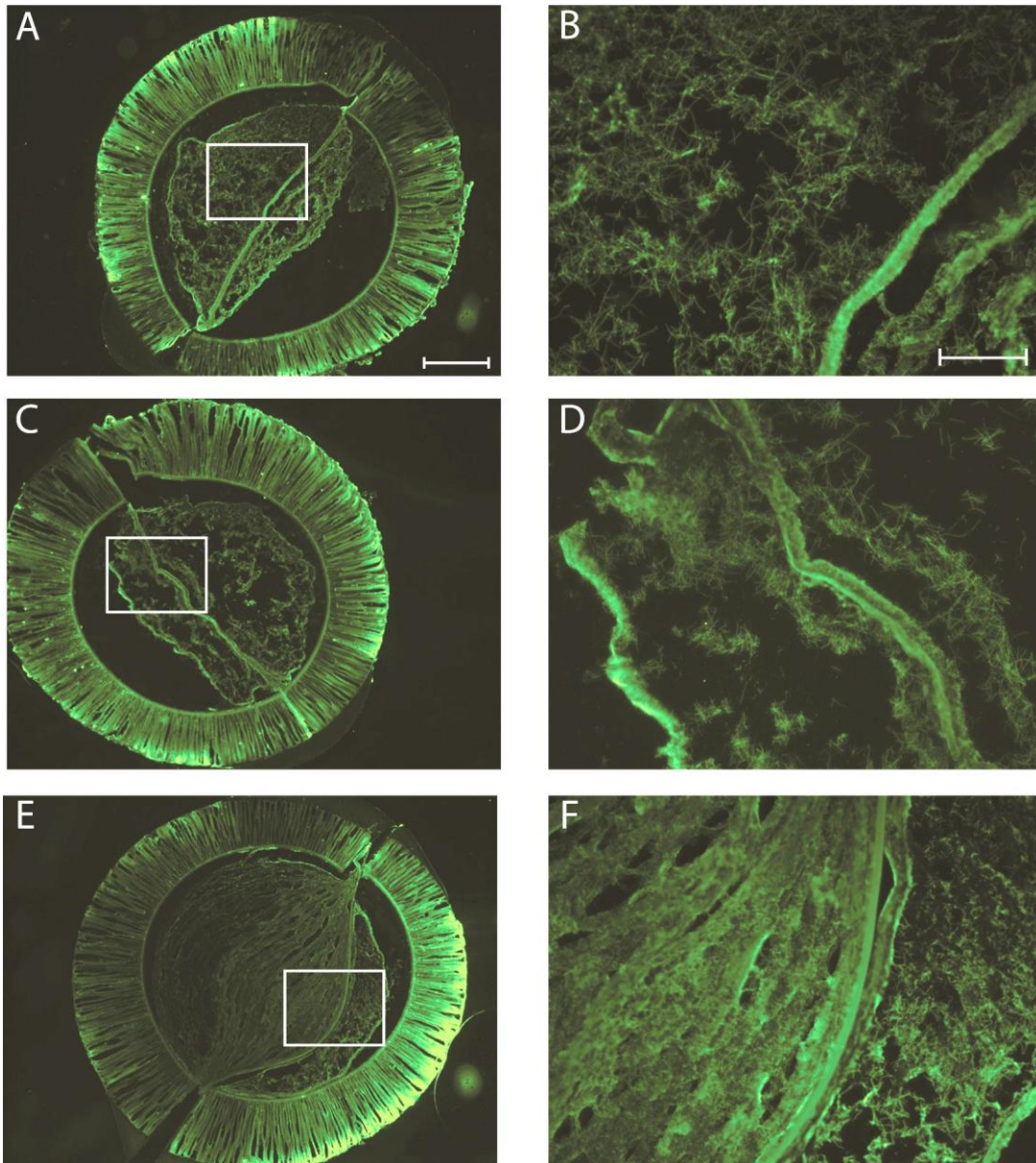


**Figure 4-17: Fibrinogen staining 5 days post-surgery near the proximal end of the conduit.** A. Aligned. C. Random. E. Smooth film. Scale Bar = 400  $\mu\text{m}$ . B,D,F represent 20X magnification of A, C and F respectively. Scale bar= 100 $\mu\text{m}$

Tissue sections were further observed using Trichrome staining to evaluate the presence of collagen within the regenerating cable at 3 weeks and 22 weeks post injury. As shown in Figure 4-19, collagen (blue) fibers surrounded the regenerating cable comprised of Schwann cells, axons and other supporting cells creating a epineurial like coating. A higher density of collagen fibers were observed encapsulating the random fiber based scaffolds compared to aligned fiber based scaffolds and smooth films. The maturation of the nerve cable can also be observed by the presence of increased red (cell cytoplasm) staining in 22 weeks samples compared to 3 week samples. Trichrome staining also confirms our previous observations where two distinct cables are observed on each halves of the smooth film both at 3 weeks and 22 weeks post injury. The Figure 4-19 shows a cross section from the proximal third of the scaffold but similar observations were made throughout the scaffold length.

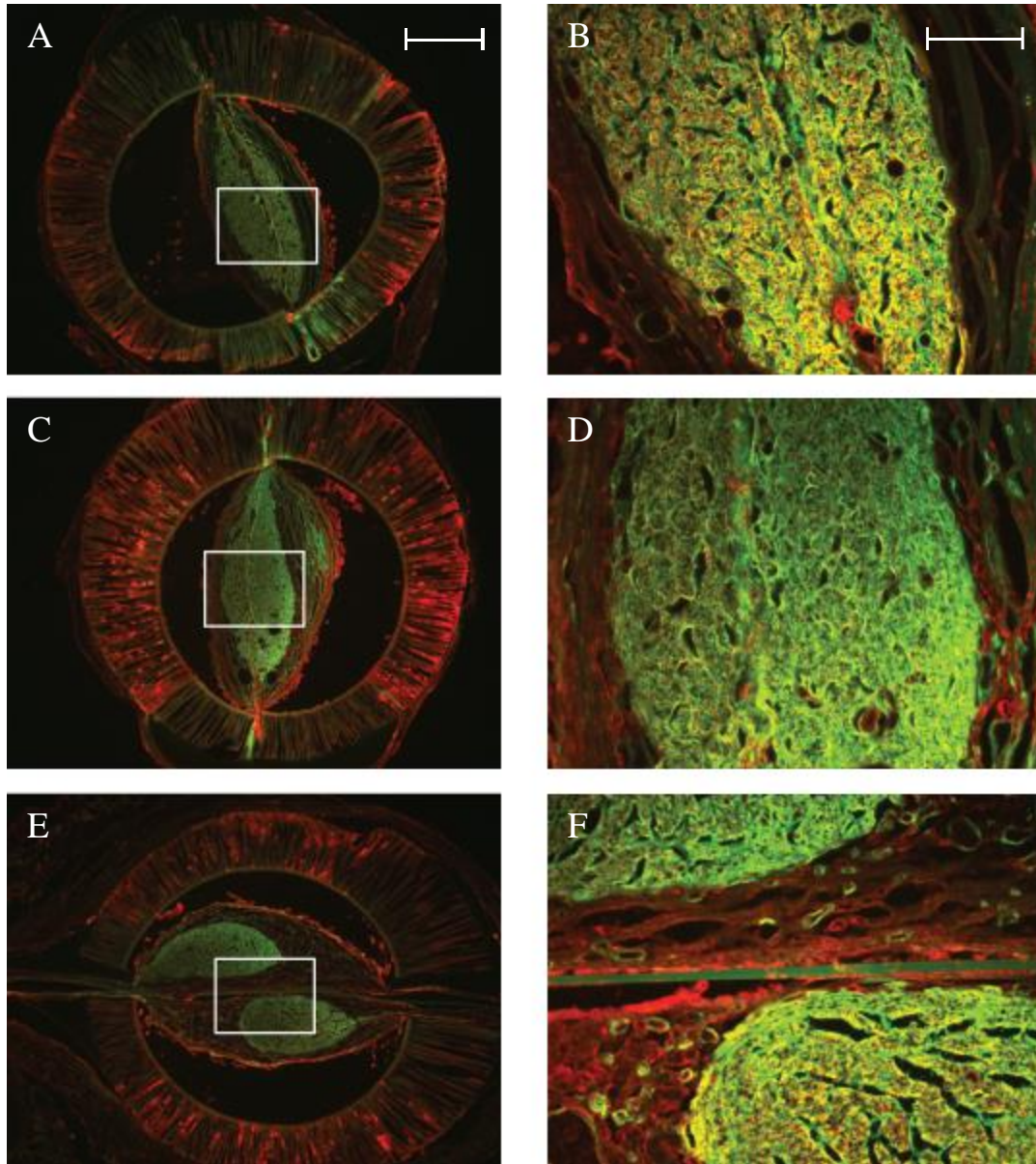


**Figure 4-18: Fibroblast and Laminin localization in a mature regenerated cable.** Laminin (Green) and Fibroblast (red) localization center of the nerve conduit 22 weeks post-surgery. A (Aligned),C (Random),E (Smooth film) : 4X image on upright scope. Scale bar = 400µm. B,D,F: 20X of A, C and E respectively. Scale bar= 100µm

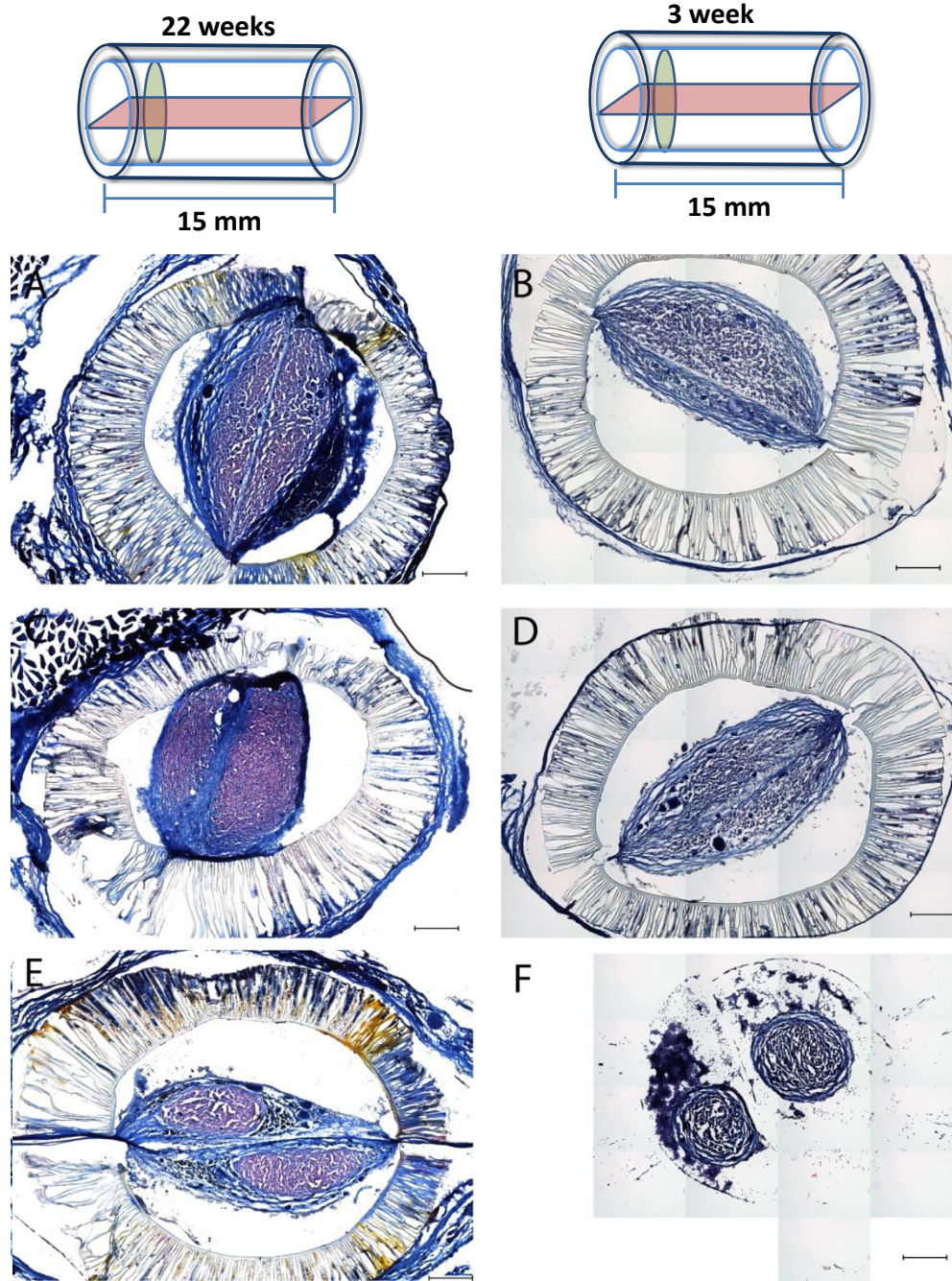


**Figure 4-19: Trichrome staining to evaluate the localization of Collagen within the nerve conduit.** Left column represents cross sections from near the proximal end of the scaffold 22 weeks post-surgery. Right column represents cross sections from near the proximal end of the conduit 3 weeks post-surgery. A-B aligned, C-D random, E-F Smooth film. Scale bar = 400  $\mu\text{m}$ .

#### 4.3.8 Macrophage response to topography in a long gap

Localization of macrophages within the nerve conduits was also evaluated at all three time points (5 days, 3 weeks and 22 weeks). Qualitative analysis of macrophage density within the conduit suggests that macrophage presence within the conduit 5 days post-surgery was minimal in all three conditions. Macrophages were mainly localized at the thin films and near the periphery of the fibrin cable 5 days post-surgery. At three weeks, a higher density of macrophages was observed throughout the regenerating cable in all three conditions. Finally at 22 weeks post-surgery, aligned fiber based scaffolds contained the least macrophages in the vicinity of the thin film compared to random fibers and smooth films (Data only shown for crosssections near the distal end). A higher density of macrophages were seen encapsulating the random fiber based scaffolds throughout the length of the nerve gap compared to the other conditions. Figure 4-20 shows the localization of macrophages close to the distal end of the scaffold for each time-point

#### 4.3.9 Cytokine array

To gain mechanistic insights into the role of topography in augmenting nerve bridging within the conduit, presence of cytokines at various locations within the nerve conduits were analyzed. We observed that IL-1 $\alpha$ , IL-1 $\beta$ , IL-6 and TNF- $\alpha$  were present in detectable amounts at all three locations within the aligned, random, smooth film loaded thin film conduits as well as empty tube. Concentrations of IL-2, IL-4, IL-10, GM-CSF and IFN- $\gamma$  could not be assessed because their levels were below the detection limit of the cytokine array kit. This suggests that these cytokines were not present compared to the other cytokines that were detected. IL-1 $\alpha$  was observed to be significantly higher in

conduits loaded with thin films compared to empty tubes in the proximal region of the nerve. However, levels of IL-1 $\alpha$  were not significantly different between the various conditions in the middle portion. In the distal 5 mm segment of the conduits, IL-1 $\alpha$  amounts were significantly higher in comparison to random fiber and smooth film loaded scaffolds as well as empty conduits. IL-1 $\beta$  levels were not significantly different between all the conditions as well as for all locations within the nerve conduits. Presence of IL-6 was not significantly different in the proximal and middle regions of the conduits in all the conditions, but a significantly higher concentration of IL-6 was observed in the aligned fiber based scaffolds in relation to the rest of the conditions in the distal 5 mm section of the conduits. Finally TNF- $\alpha$  concentration were observed to be significantly higher in aligned fiber based scaffolds with respect to empty conduits in all three locations within the conduits. In the proximal region, both random fibers and smooth film loaded conduits contained higher concentration of TNF-  $\alpha$  as compared to empty tubes. This data (Figure 4-21) suggests that certain cytokines are differentially present in conduits loaded with different surface topography based films and this could lead to the distinct maturation of the nerve.

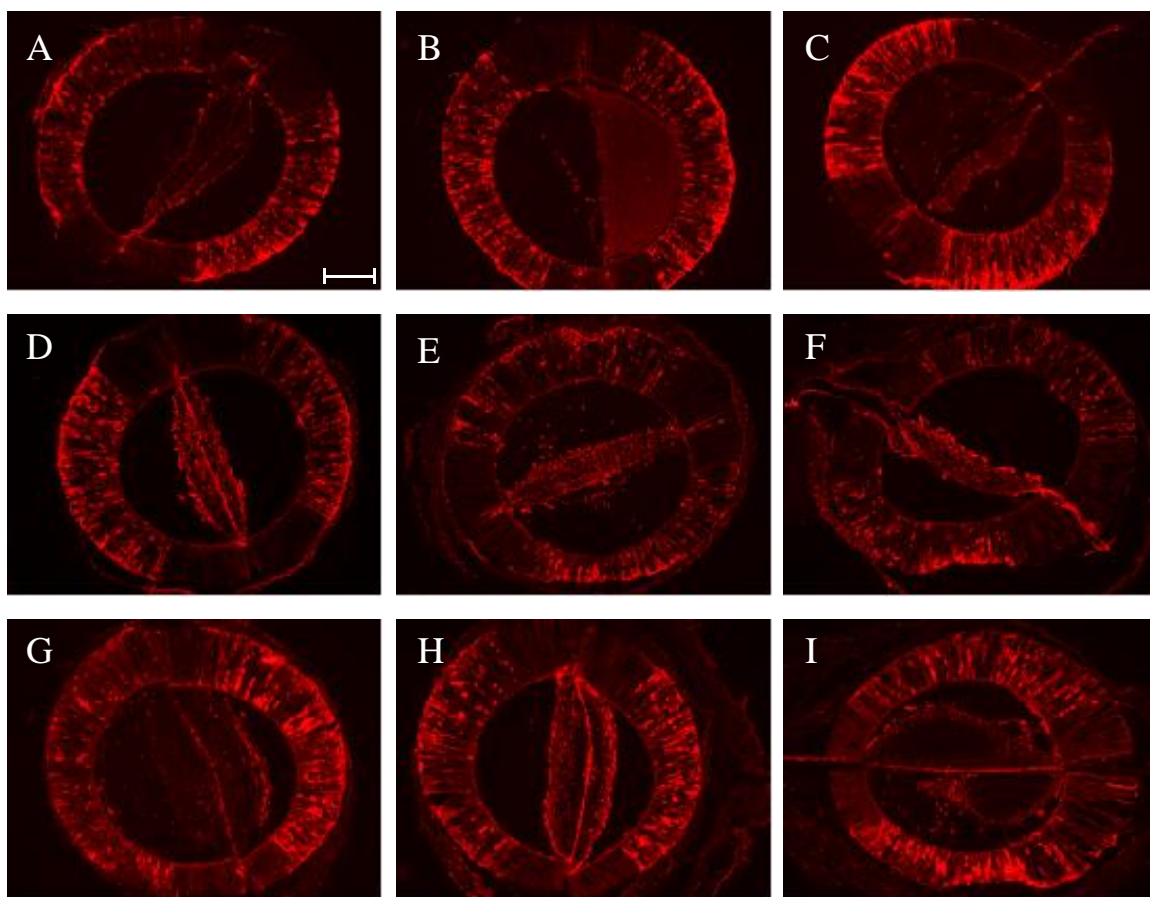


**Figure 4-20: Macrophage localization at different location and time points.**

Representative histological sections from near the distal end of the conduit stained for ED-1 (macrophages). Left column: Aligned fiber based scaffolds at A-5 days, D-3 weeks and G-22 weeks. Middle column: Random fiber based scaffolds at B-5 days, E-3 weeks and H-22 weeks. Right column: Smooth Film based scaffolds at C-5 days, F-3 weeks and I-22 weeks. the 4X image on upright scope. Scale bar = 400 $\mu$ m

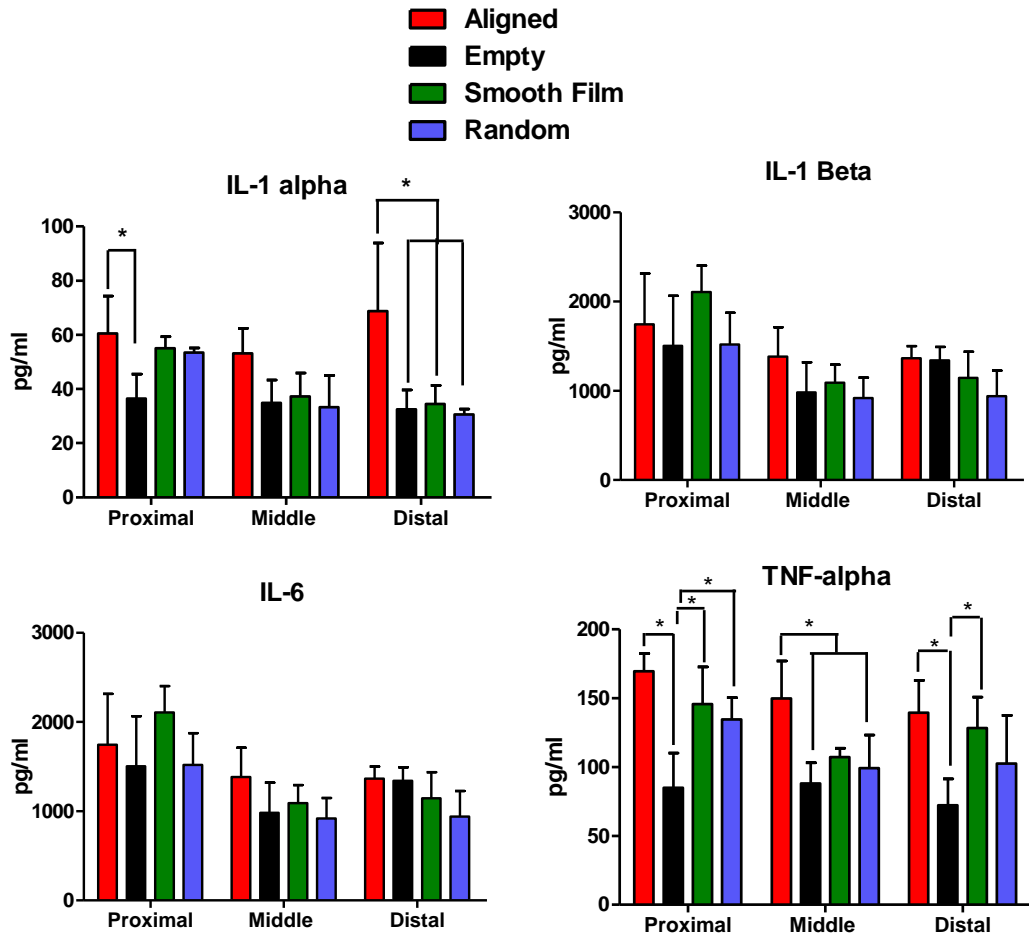


Figure 4-21: Cytokine array analysis five days after injury. \* =  $p < 0.05$ .



#### 4.3.10 qRT-PCR

qRT-PCR was performed to evaluate the differential expression of regeneration specific markers in response to the various topographies. The two halves (distal and proximal) of the nerve conduits were evaluated to understand the phenotype of cells migrating from both the proximal and distal stumps. Empty tube implantation as controls were used to normalize the expression levels of the various markers comparing expression in different thin film topographies.

The markers can be classified in two categories. First we analyzed the change in expression of growth factors and ECM proteins expressed by the infiltrating glial cells as well as axons within the nerve conduit. We also evaluated the expression of receptors on neuronal cells which play an active role in the signaling of regenerative events during nerve bridging.

We observed that on the proximal half of the conduit BDNF expression was approximately two-fold higher in cells on aligned fiber loaded conduits in comparison to empty tube, while the expression of BDNF in random fibers based scaffolds was significantly less compared to empty tube controls. There was no significant difference observed in the expression of BDNF in smooth film based scaffolds and empty tubes on the proximal side. Laminin and Fibronectin expression trends were similar at three weeks after injury. Both ECM protein expression was not significantly different in random fiber based scaffolds and smooth films, while it was significantly lower in aligned fiber based scaffolds and smooth film based scaffolds in relation to empty tubes on the proximal end. Analyzing samples for NT-3 was excluded as the  $C_T$  values were high (> 35 cycles). This suggested that significant expression of NT-3 does not occur in

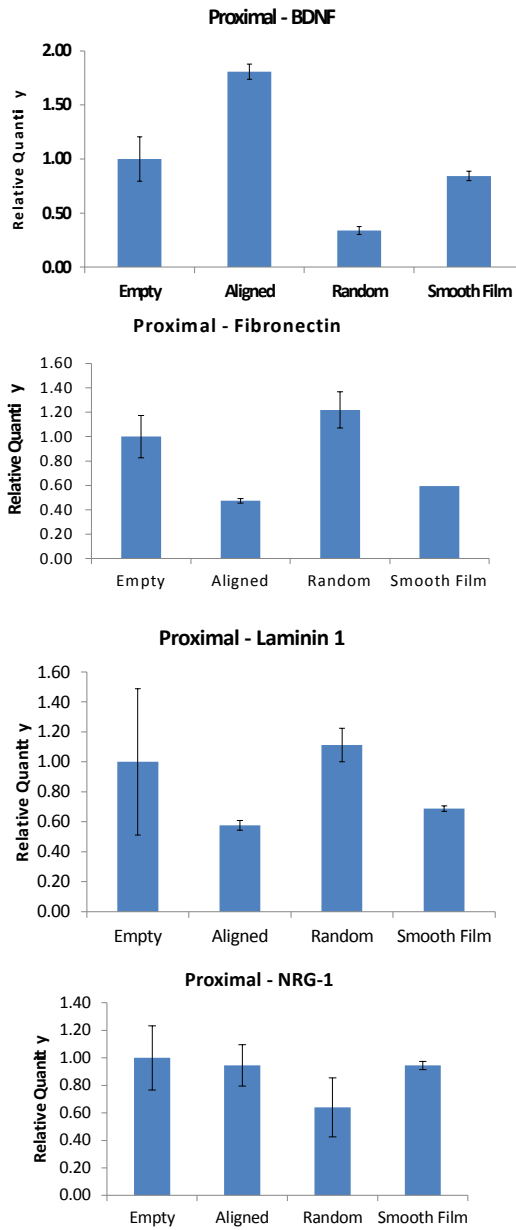
response to all conditions three weeks post injury in both the proximal and distal part of the conduits.

Change in Erbb2 and Erbb3 gene expression trends were similar in all conditions in the proximal and distal region of the nerve conduits. Both Erbb2 and Erbb3 expression were significantly lower in aligned fiber based scaffolds compared to random and smooth film based scaffolds and empty tubes. While P75 expression was observed to be significantly higher in aligned and random fiber based scaffolds as compared to smooth films loaded scaffolds and empty tubes on the proximal half. There was no difference between all the conditions in respect to the expression levels of NRG-1 on the proximal half of the nerve conduits (Figure 4-22).

On the distal half of the scaffolds, BDNF expression was greater than two fold higher in aligned fiber and random fiber loaded scaffolds in comparison to smooth film conduits and empty tubes. There was no significant difference between the expression of Laminin and fibronectin in all the conditions on the distal half of the scaffold.

Expression profiles of Erbb2 and Erbb3 were similar in all conditions in the distal region of the nerve conduits. Erbb2 and Erbb3 expression was relatively higher in random fiber based scaffolds as compared to empty tubes. There was no difference in the expression of both Erbb2 and Erbb3 between aligned fibers based scaffolds and empty tubes. While Erbb2 and Erbb3 was significantly down regulated in smooth film based scaffolds when compared to empty tube control. P75 expression was greater than four-fold higher for aligned and random fiber based scaffold in relation to empty scaffold. While the NGFR expression was significantly lower compared in empty tube controls and in smooth film based scaffolds (Figure 4-23).

## Growth Factors and ECM proteins



## Receptors

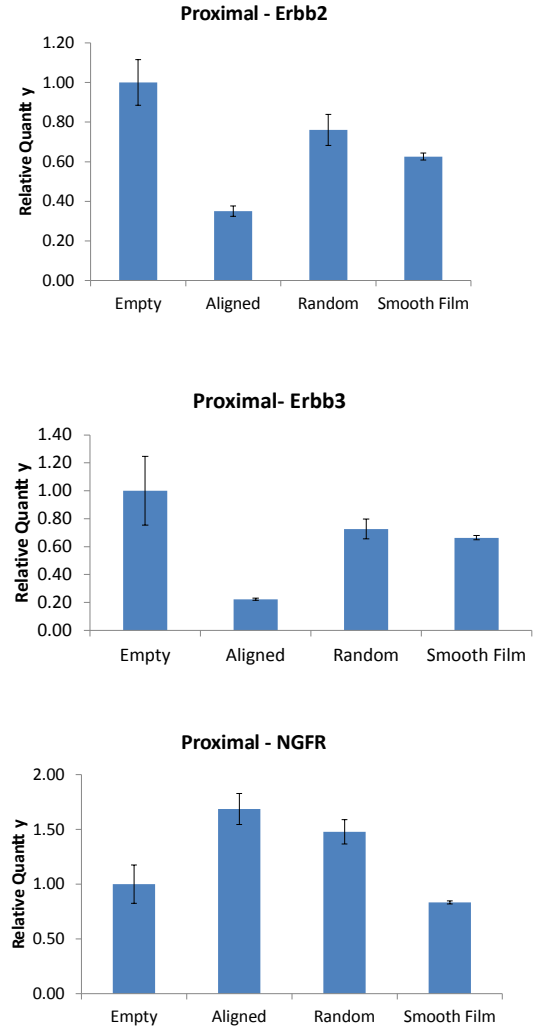


**Figure 4-22: Gene expression analysis using real-time PCR analysis from the proximal half of the 15 mm conduit at 3 weeks.**

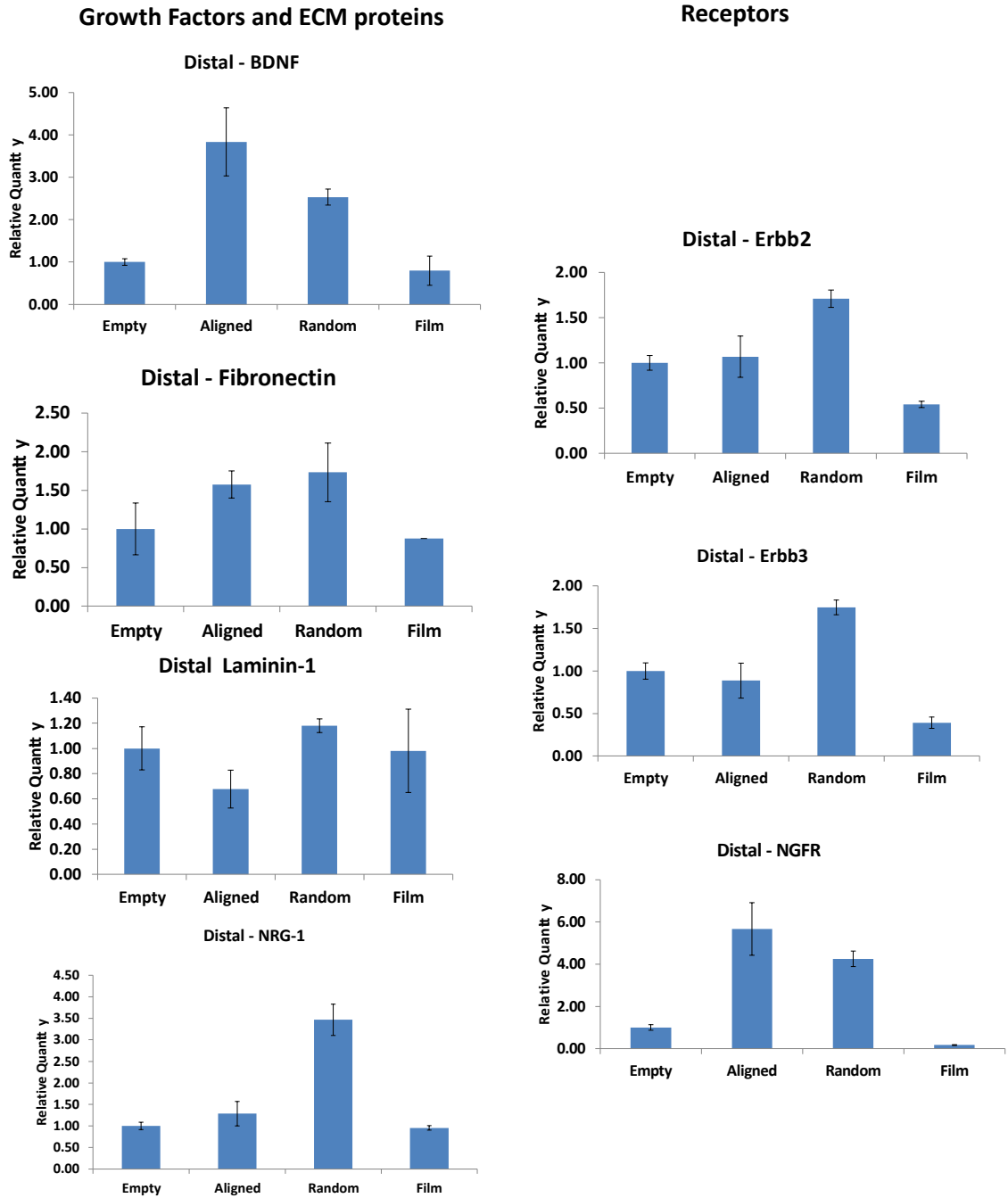


**Figure 4-23: Gene expression analysis using real-time PCR analysis from the distal half of the 15 mm conduit at 3 weeks.**

#### 4.3.11 Scaffold permeability

In vitro analysis of scaffold permeability was performed to observe the difference in fiber and smooth films to transport of different molecular weight proteins. We observed that fiber based scaffolds were permeable to proteins up 500 kda while smooth films were impermeable to both 70 kda and 500 kda proteins (Figure 4-23).

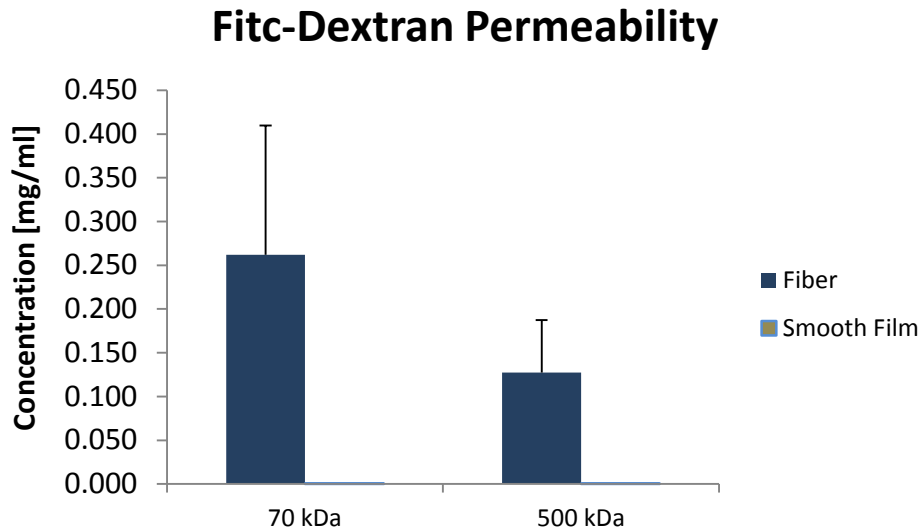


**Figure 4-23: Fiber permeability study.** Smooth film based scaffolds were impermeable to Fitc-Dextran molecules of 70 kDa and 500 kDa.

#### 4.4. Discussion

It has been widely known that synthetic filler materials can enhance nerve growth within guidance channels [153, 200, 206]. Several studies that utilize synthetic micro fibers, microchannels and electrospun fibers have shown to augment bridging of non-critical gaps after peripheral nerve injuries. These studies have focused on the effects of different treatments on axonal growth in small gaps, but it is not clear if they would work in critically sized gaps. Furthermore, interactions of these luminal fillers with different components of the endogenous regenerative sequence are largely understudied in critical nerve gap models.

Previous work from our group has shown that minimal topographical cues provided by electrospun thin-film scaffolds have led to bridging of nerve gaps in critically sized defects [163, 203]. These studies showed that the presence of oriented environmental cues from electrospun nanofibers as well as the organization of thin films within the nerve conduits influences regenerative events. These scaffolds also support and optimize the function of glial cells and help guide axons to bridge the nerve gap. While these studies give us insights into the role of electrospun fibers in eliciting the endogenous regenerative sequence, it is still unclear if it is the presence of topographical cues or the orientation of thin films within the scaffold that leads to successful bridging of the critical size nerve gaps. Furthermore, the temporal progression of the regenerative sequence in response to different topographical cues is still unknown in long gaps. Thus, in this study we explore the influence of topographical cues on the regenerative sequence in critical size gaps. The insights gained here will help develop rational designs to augment nerve regeneration using thin film synthetic fillers.

Based on histological analysis, all aligned, random, and smooth film based scaffolds supported bridging of axons over 22 weeks in the long gap model. Previous studies have shown that gaps larger than 10 mm in rats are not bridged without the presence of exogenous factors. Synthetic micro fibers have been used to extend nerve regeneration to 15 mm previously. Previous study from our lab and this one are the only instance where the thin films which occupied only 0.6% of the conduit space were able to bridge a critical length gap. Furthermore, in this study, we observe that independent of surface topography, the nerve gap is bridged in all cases. This suggest that single thin film based scaffolds are successful in bridging critical length gaps without the need for an exogenous factors.

Since the original organization of the cable is vital to long term regeneration, we evaluated the composition of the cable at 3 weeks. To further elucidate the role that topographical features play in augmenting nerve regeneration, we looked closely at how Schwann cell migration and neurite outgrowth were influence during the course of nerve bridging the gap. The short term migration of Schwann cells and axons were analyzed while the composition of the cable comprised of Schwann cells and axons was elucidated at longer time points. We observed that at 3 weeks, oriented topographical cues enhance the migration of Schwann cells and infiltration of axons within the conduit compared to random and smooth film scaffolds. This suggests that oriented topographical cues lead to the acceleration of regeneration in a critical gap model. Histological evaluation of the regeneration at three weeks also showed that the localization of Schwann cells and axons was greatly influence by the topography, suggesting that the differential interaction with the thin films could have led to the difference in migration that we have observed.

Several studies have stressed the importance of the speed of regeneration and not just the quality of regeneration [207] [113]. While all topographies supported axonal growth the acceleration of the initial regeneration process is an important design criterion that needs to be considered while designing scaffold to repair long nerve gaps. Here we show that topographical guidance by oriented scaffold plays an important role in achieving faster bridging of the gap.

Temporal progression of the localization of Schwann cells and axons suggest that different thin film topographies lead to a very distinct regenerating cable. Histological analysis via immunofluorescence of Schwann cell, axons, fibroblast, Laminin, and fibrin as well as Trichrome staining suggest that aligned, random and smooth film based scaffolds cause a differential cable formation and influence the regenerative sequence. As suggested by fibrin staining at 5 day post injury, all the thin film based scaffolds were able to sustain some form of the provisional matrix throughout the length of the conduit. While previously it has only been hypothesized that the thin films play a role in either replacing or aiding in the function of the provisional matrix, this is the first instance where it has been shown that thin films promote the stabilization of the fibrin matrix by being the scaffolding around which the matrix forms. We observe that the provisional matrix has a similar shape to that of the mature cable leading us to conclude that the long-term maturation of the nerve cable is dependent on the ability of the thin films to organize the fibrin matrix.

We also observe that in the random film based scaffolds, there is more disruption in the fibrin matrix compared to aligned fibers and smooth film based scaffolds. This could have caused the slow migration of Schwann cells and neurite outgrowth that we



have observed in the *in vivo* studies. Studies have shown that varying crosslinking and density of fibrin gels has shown to affect neurite outgrowth and Schwann cell migration. [208-210] While the aligned and smooth film based scaffolds both exhibit a contiguous fibrin cable, a difference in the density of the fibrin is observed in cross-sections at different locations within the random conduit. This could be one of the major reasons why we see a difference in initial migration of Schwann cell and neurite outgrowth between aligned and smooth film based scaffolds vs. random fibers based scaffolds. This is a speculation based on the histology and looking at previous studies involving fibrin matrix characterizations and warrants a more thorough investigation of the crosslinking as well as density of the provisional matrix needs to further investigate the role that the properties of provisional matrix play in influencing the regenerative sequence in nerve conduits.

In contrast to smooth film based scaffolds, both random and aligned fiber based scaffolds promote the formation of a consolidated axon/Schwann cell cable surrounded by collagen bands of epineurial-like tissue. Both fiber based scaffolds lead to a unified cable surrounding the thin films compared to smooth films whereas segregated cables on either side of the smooth thin films based scaffolds are observed. One factor contributing to this difference in organization of the regenerating cable is the permeability of the thin films. FITC-dextran based permeability studies suggested that fiber based topographies are permeable to biomolecules of up to 500 kDa while smooth films were impermeable. This could promote the diffusion of growth factors, ECM proteins and other signaling molecules in fiber-based scaffolds and lead to a differential maturation of the nerve cable from smooth films.

While thin film topography plays an important role in the organization of the regenerative cable, we also evaluated the quality of the cable to evaluate long term regenerative potential. All thin film based scaffolds were able to bridge the critical length gap irrespective of the topography. Evaluation of the percentage of both Schwann cells and axonal area within the cross section suggested that aligned fibers promoted significantly higher percentage of regenerating axons and Schwann cells compared to the other conditions. We also observed that aligned fiber based scaffolds support the highest number of myelinated axons compared to the other conditions suggesting that aligned topographical cues provide the ideal conditions to maximize nerve growth. The ability of the topographical cues to affect long term myelination of the nerve was also quantified. Previous work has stressed that myelin thickness directly affects conduction velocity [211]. Our observations indicate that the myelin thickness was similar for all conditions. This suggests that while topography affects the number of axon infiltration in the conduit, it does not affect the myelination of the axons. Myelin thickness for each condition was similar to normal nerve [1]. Thus we can speculate that the 22 week time point might have been too long to observe any differences in myelin thickness due to the presence of topographical cues. Final evaluation of the quality of regenerating axons was performed by quantifying the axonal diameter. Highest numbers of axons with width greater than 2  $\mu\text{m}$  were observed in aligned fiber based scaffolds. While in this study we did not measure the amplitude of the action potential, we can hypothesize based on previous studies that higher numbers of larger diameter axons would lead to a larger action potential in the aligned case compared to other conditions. This suggests that even though

thin films with various topographies can be used to bridge long gaps, aligned fiber based scaffolds are able to optimize the regenerating cable and are ideal for nerve repair.

Characterizing the maturation of the nerve cable gives us insight into how topographical cues influence the bridging of critical gaps and modulate the regenerative sequence. Further tests were done to see the extent of long term functional recovery in response to different topographical cues. Compound action potential velocity was measured to evaluate the ability of the regenerated cable to carry electrophysiological signals. All thin film based scaffolds were able to sustain the signal through the tube. Nerve conduction velocity was slightly higher but not significantly different in aligned fiber based films compared to the other conditions. This is likely because of our previous observations that showed that aligned fiber based scaffolds promoted the highest number of myelinated axon growth and axon diameter which could together lead to a higher nerve conduction velocity. Furthermore, comparing to a previous study from our lab, the velocity that we achieved is similar to the gold standard autographs in a similar gap [1]. Thus this data suggests that all thin film based scaffolds are able to generate a functional cable. Since measurements were performed 5 mm past the distal end, it is not clear if all conditions would support such nerve conduction velocities closer to the innervation site.

To further evaluate the functional differences in response to topographical cues, we measured RGMW and muscle fiber diameter. Several studies have stressed that, the final goal of all PNS injuries therapy is accelerating nerve growth and achieving functional recovery to the reinnervated muscle. We use muscle atrophy as a measure to evaluate the speed of reinnervation, because muscle atrophy will increase if axons growth is slower in any of the conditions tested. We observed that RGMW was significantly

improved in aligned fiber based scaffolds compared to the other conditions. To further validate this we quantified the individual muscle fiber area. This data also suggests that aligned topographical cues are able to accelerate axonal growth and lead to the arrest of muscle atrophy compared to other conditions. This data also correlates to our earlier observation where we see a direct relationship between the trends observed in Schwann cell migration and axonal growth for all conditions and the levels of RGMW. Thus our results strongly suggest that aligned topographical cues enhance the endogenous regenerative sequence to accelerate nerve growth.

To further elucidate the role of topographical cues in influencing the infiltrating cells and changing the regenerating micro environment, we performed molecular assays to evaluate the recruitment and production of cytokines at 5 days and changes in the regeneration specific genes at 3 weeks post implantation. Several molecular and cellular events occur directly following nerve injury that lead to Wallerian degeneration as well as prime the proximal and distal end of the severed nerve for repair. Following nerve injury, non-immune cells and macrophages work together to remove degenerated myelin [212]. Histological assessment at all three time points showed the presence of Schwann cells and macrophages interacting with the thin films in our study. Since long term regeneration depends on the efficient removal of inhibitory molecules from the injury site, we evaluated the effects of topography on the production of cytokines at the five day time point.

Previous work has shown that IL-1 $\alpha$  and TNF- $\alpha$ , pro inflammatory cytokines that help in the recruitment of macrophages and clearance of myelin debris are first produced by Schwann cells directly after injury [213, 214]. Our study shows that IL-1 $\alpha$  and TNF- $\alpha$

production was influenced by the nature of topography. We observed that higher quantities of IL-1 $\alpha$  and TNF- $\alpha$  were detected in aligned fiber based scaffolds when compared to other conditions. This suggests that aligned topographical cues augment the pro inflammatory phenotype of Schwann cells. Saino et. Al. have also shown that topographical cues from fibers and smooth films are capable of inducing macrophage activation and secretion of proinflammatory cytokines [215]. Furthermore, in our study all thin film based scaffolds (aligned, random and smooth film) increased the production of TNF- $\alpha$  at the proximal end of the scaffold as compared to empty tube control. This phenomenon could further explain why thin film based scaffolds are able to support nerve bridging while it fails in an empty tube. TNF- $\alpha$  has also been shown to cause IL-1 $\beta$  production in Schwann cells via autocrine effects [213]. Even though we did not observe any differences between any of the conditions, our data confirms this phenomenon as we observe detectable quantities of IL-1 $\beta$  throughout the conduit at day 5. We believe this is most likely cause by the TNF- $\alpha$ 's effect on Schwann cell in the conduit.

It has also been shown that Wallerian degeneration is a biphasic process where during the first phase, M2 phenotype macrophages are recruited due to the actions of pro inflammatory cytokines such as TNF- $\alpha$ , IL-1 $\alpha$ , IL-1 $\beta$ , IL-6 and GM-CSF [212, 213, 216]. These macrophages have been implicated to influence nerve repair. Second phase is predominantly anti-inflammatory where IL-1 $\beta$  and TNF- $\alpha$  levels are reduced and the production of IL-6 and IL-10 is increased. Quantity of IL-10 in our assay was under the detection limit suggesting that at 5 days, we were still in the first phase of Wallerian degeneration. Overall, this data suggest that the presence of topographical cues alters the

cytokine production after nerve injury. Topographical cues also augment the pro-inflammatory phenotype of glial cells which helps clear the inhibitory environment and enhance the overall nerve regeneration. We can thus conclude that some of the long term gains we have observed in earlier studies with the aligned topographical cues are most likely due to their ability to modulate the pro-inflammatory phenotype of Schwann cells compared to other topographies. Since we limited our study to 5 days, we were not able to observe the effects of topography on the second phase of Wallerian degeneration which is usually observed between 7 days and 3 weeks post injury.

RT-PCR study was performed at 3 weeks to understand the effects of topography on gene expression of ECM proteins, growth factors and Schwann cell receptors involved in nerve repair. Since previous studies have shown that Schwann cells migrating from proximal and distal ends have different phenotypes, we characterized the levels of expression of the different markers due to the underlying topography in the two halves of the conduits separately. Earlier we observed that both IL-1 $\beta$  and TNF- $\alpha$  are present in all conditions after injury. Previous studies have shown that IL-1 $\beta$  and TNF- $\alpha$  leads to NGF synthesis [217]. Therefore, we can hypothesize that the presence of these cytokines in our conduits could lead to NGF production from the infiltrating cells. RT-PCR analysis showed that NGFR mRNA from the proximal end was relatively upregulated in scaffolds with fiber based topographies and down regulated in smooth film based scaffold when compared to an empty tube control. This suggests that P75 expression is modulated by surface topography. Work by Anton et. Al. has emphasized that NGF and P75 together stimulate Schwann cell migration [218]. Thus the ability of aligned topographical cues to increase TNF- $\alpha$  production leading to increased NGF release combined with topography

induced upregulation of P75 could explain the increase in the short term Schwann cell migration and neurite outgrowth at 3 weeks. Our earlier studies also indicated that smooth film also enhance Schwann cell migration compared to random fibers but RT-PCR analysis suggests that they relatively downregulate P75 production. Therefore we believe that smooth film induced Schwann cell migration might be due to alternative pathways. Earlier work has suggested that increased P75 expression might lead to increased myelination [219]. Studies have shown that Schwann cell with a myelinary phenotype do not migrate as well [85, 90] and lower expression of P75 observed in smooth film scaffolds could keep the infiltrating Schwann cells in a more migratory phenotype and lead to migration of glial cells that we observe histologically.

Previous work has shown that NT-3 increases Schwann cell migration [90, 220]. NT-3 was not expressed in any of the conditions in our study based on real-time PCR analysis. Since topographical cues are not able to influence NT-3 expression, future therapies could incorporate exogenous NT-3 to synergistically work with aligned topographies to enhance regeneration.

We also observe downregulation of Erbb2 and Erbb3, which are receptors that are involved in Schwann cell proliferation [221], compared to empty tube controls in the proximal side. Previous work by others have speculated that Erbb2 and Erbb3 have the ability to keep Schwann cells in a non-myelinating phenotype and their downregulation could initiate the onset Schwann cell transition into myelinating stage [90]. The highest downregulation of Erbb2 and Erbb3 was observed in aligned fiber based scaffolds suggesting that migrating Schwann cells on aligned topographical cues could be maturing faster and transitioning into their myelinary phenotype compared to other conditions.

This supplements our earlier observations that histology showed where aligned fibers demonstrated enhanced maturation of the nerve cable.

Thus results from the entire study indicate that there are multiple mechanisms that concurrently work to help bridge a critical gap using thin films of different topographies. While it is an extremely complex system which warrants further studies, our data indicates that the enhanced outcomes observed on aligned films are due to their ability to create the most regeneration friendly environment and influence the pro regeneration phenotype of the different components of the regenerative sequence.



## CHAPTER 5

### 5. CONCLUSIONS AND FUTURE DIRECTIONS

In 4<sup>th</sup> century BC, Hippocrates wrote the first written description of the peripheral nervous system. Herophilus in the 3<sup>rd</sup> century BC identified nerve as being separate from the tendons and identified the motor and sensory components. [222] Paul of Aegina (625-690 A.D.) provided the first reference of nerve suturing. [222] Historically not much has been documented since then during the middle ages. It is believed by experts that without the understanding of anatomy, physiology and the regenerative potential of nerves, it was not a normal practice undertaken by surgeons during that era. It was not until during the 16<sup>th</sup> - 18<sup>th</sup> century that a deeper understanding of the nervous system was achieved. Antonj van Leewenhoek (1632 A.D. – 1723 A.D.) elucidated the microscopic structure of the nerve while Fontana in the 18<sup>th</sup> century gave the first account of myelin sheaths. [222] Also in the 18<sup>th</sup> century, Galvani (1774 AD – 1798 AD) showed the functional aspects of the nervous system by stimulating frogs with electrical stimulation. [222]

In 19<sup>th</sup> century, a deeper understanding of the components of the peripheral nerves was elucidated. Theodore Schwann (1810-1887) published the first studies on Schwann cells. Works of Purkinje and Robert Remak uncovered the differences in the nerve connections as well at myelinated and un-myelinated fibers. Augustus Waller provided a major boost to the field in 1850 when he described the process of Wallerian degeneration where there is loss of the distal nerve following injuries. These studies increased the understanding of the peripheral nervous system and over the following century, influenced the field of nerve repair. [222, 223]

Traumatic injuries during the World Wars in the first half of the last century influenced many of the current surgical techniques that are used for nerve repair. Sydney Sunderland in the 1940s published studies on the intraneural topography of the radial, median and ulnar nerves as well as of the sciatic nerves and provided the anatomic foundation for peripheral nerve repair. [222, 223] With the advent of micro surgical techniques and advancement of technology, several strides in the field of nerve repair have been achieved. For small gap, close to normal functional recovery can be achieved today. For longer gaps, we still face some of the same challenges that have been around for the past century. The gold standard to bridging long gaps for the past century has been autografts. However, there are several drawbacks of using autografts that prevent them from achieving full functional recovery after nerve injury.

With the advances made in the field of regenerative medicine, alternatives to using autografts have been explored. Several synthetic and natural guidance channels are currently used in clinical as well as research settings to bridge nerve gaps. These techniques have shown to improve nerve regeneration in small gaps (<10 mm in rats and <30 mm in human and primates) but fail when the gaps are longer. Even after the last 150 years of innovation and development of refined surgical techniques and understanding nerve injury, we do not have a suitable replacement for autografts. Historically, advances in the field of regenerative medicine and even in peripheral nerve repair have come due to a greater understanding of the physiology and the underlying mechanism that affect the regeneration process. Tissue engineering strategies to bridge long gaps have shown promise but very little is known in regards to how these technologies interact with the endogenous repair mechanism. Previous work from our lab has shown that

aligned topographical cues from electrospun thin films have helped bridge long peripheral nerve gaps. Other labs have also utilized aligned topographical cues and showed their positive influence on neuronal cells. While these studies have utilized the topographical cues to augment nerve regeneration, it is still unclear how these scaffolds interact with the natural regenerative sequence. Thus, the goal of this thesis was to gain insights into how topographical cues from electrospun nanofibers based scaffolds are able to bridge long gaps so that we can provide rational approaches to future designs.

To evaluate the role of topography in influencing neuronal cells and the regenerative sequence, we divided the thesis into two specific aims. 1) We examined the effects of fiber topography on Schwann cells to understand their role in the nerve regeneration process *in vitro*. 2) We evaluated the interplay between polymer fiber-based thin films topography and the different steps of the regeneration process during repair of critically sized nerve gaps.

Our main goal of Aim 1 was to understand how the effects of topography from the aligned electrospun fibers are mediated to the neuronal cells to affect their migration and phenotype. While previous studies have focused on optimizing materials for just axonal growth, here we evaluate the ability of different topographical cues to augment both Schwann cell migration and neurite outgrowth. Thin film scaffolds with aligned, random and smooth film based topographies were fabricated to evaluate how these topographies were able to influence purified Schwann cells and Dorsal root ganglion cultures. Quantification of neurite out growth and Schwann cell migration lead us to conclude that aligned topographical cues are able to enhance directed growth compared to random fibers and smooth films. To further elucidate this phenomenon, we probed the

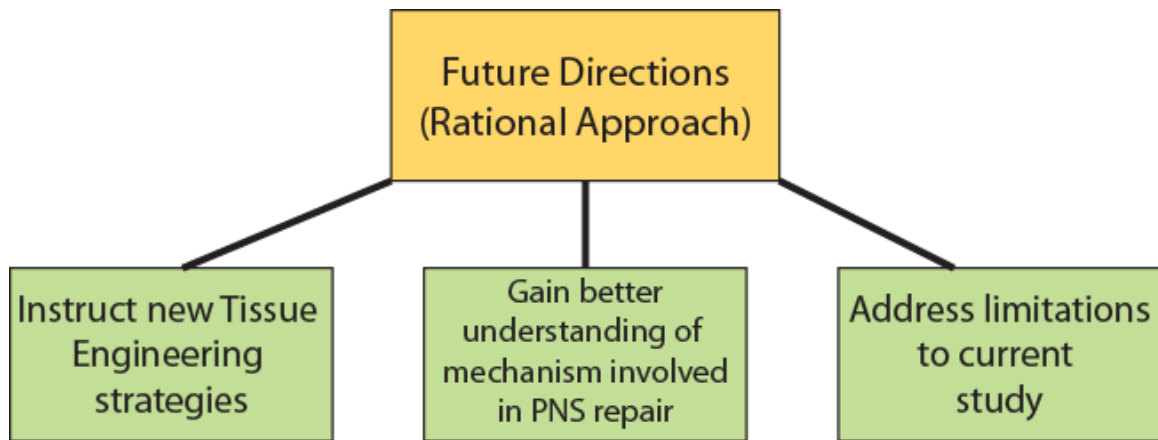
adsorption of ECM molecules as well as observed the effects of blocking adsorbed protein on the cells seeded on these surfaces. These studies showed that fiber based topography was able to efficiently adsorb fibronectin from serum and this adsorbed fibronectin is able to mediate the gains in migration and neurite outgrowth that we see on aligned fibers. We also observe that fiber based topography is able to guide the organization of the fibronectin fibers compared to smooth film based topography and this could have influenced the directed growth that we observe. Thus data from this aim suggests that fibronectin presentation, conformation and organization contributes heavily to enhanced Schwann cell migration and neurite outgrowth on fiber-based films compared to smooth films of the same composition. In order to develop scaffolds that match or exceed the performance of autografts, a deeper understanding of the mechanisms by which scaffold properties affect the nerve regeneration is critical. Thus in the second aim of this study we pursued to understand the role of topography in influencing the long term nerve regeneration through a critical sized gap using electrospun fibers.

While Aim 1 gave us insights into how cues from various topographical films are mediated to the overlaying cells, in Aim 2 we focused our efforts on understanding the interplay between the different steps of regeneration and the various topographies. In this aim, we tested the hypothesis that, presence of different topographies will lead to a change in the regenerative sequence by altering the organization of the initial fibrin matrix, cellular signaling and the rate of regeneration. Our results show that topographical cues affect the normal regeneration process significantly both spatially and temporally. Short term molecular assays and histological assessment show that thin film

based scaffolds are able to aid in the function of the fibrin matrix and help stabilize it. The different topographies do this uniquely but compared to empty scaffolds, are able to guide migration of axons and glial cells after injury. We also observe that thin films create a proinflammatory environment by influencing the phenotype of Schwann cells and macrophages to speed up the removal of inhibitory debris from around the injury sites. This ability of the fiber-based scaffolds can be utilized in spinal cord repair as well, where an inhibitory glial scar prevents regeneration. Along with their ability to direct growth, fiber based thin films can be used to modulate the local microenvironment to influence repair. Histological studies also show that topographical cues from aligned, random and smooth film based scaffold alter the organization of the cable within the nerve conduit. Thus based on the results from this study we can conclude that topographical cues create a pro-regeneration environment needed to support bridging in long peripheral nerve gaps. While random and smooth films based scaffolds support nerve bridging over critically sized gaps, aligned fiber based films are the best at augmenting phenotype of Schwann cells and providing the environment for accelerated nerve growth and innervation of the target muscle.

### **Future Directions**

The main goal of this thesis was to understand the mechanism via which topographical cues influence the endogenous regenerative sequence. The conclusions that we draw as well as the tools developed in these studies will help future designs of biomaterials for peripheral nerve regeneration as well for other tissue engineering applications. There are three major areas where the lessons learnt from this thesis can be applied in the future and are shown in the schematic below.

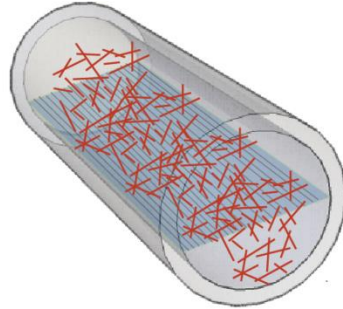


### **New tissue Engineering Strategies**

Based on the previous studies and the current study from our lab, we can conclude that thin films of PAN-MA fibers can be used to bridge critical length gaps in rat sciatic nerve. As discussed previously the speed of bridging is equally as important as guiding axons to the distal stump. Thus, the gains from using aligned topographical cues can be combined with other strategies to synergistically increase the rate of peripheral nerve regeneration.

Based on our observations from Aim 2, we concluded that the pro-inflammatory environment created by topographical cues could help in the early migration of peripheral neuronal cells. We can deliver factors such as TNF- $\alpha$  and other pro-inflammatory cytokines to evaluate if the presence of these cytokines can aid in the recruitment of macrophages and along with the ability of the fibers to influence their phenotype, increase the migration of Schwann cells and eventually affect the rate of PNS repair. Previous work by others in the field has shown how to deliver small molecules from electrospun fibers [81]. Previous work in our lab has also developed delivery vehicles that are capable of sustained release of growth factors and other bio-molecules [224-226]

from lipid microtubes. These delivery vehicles can be used to release cytokines, growth factors during the early stages of repair to speed the regeneration process.



*Schematic diagram of nerve conduits loaded with thin films of aligned fibers and fibrin gel to enhance functional outcomes*

Our studies also show that fibrin matrix stabilization within the nerve conduit is vital for successful repair and the differences in the provisional matrix formation can influence the rate of repair. Previous work has stated the benefits of using fibrin within nerve conduits to improve functional outcomes [18, 227] and perhaps using the aligned topographical cues in conjunction with an in situ gelled fibrin matrix could help improve regeneration. Evaluation of cross-linking as well as density of fibrin within the conduit could give us more insights into how the initial provisional matrix aids in the nerve regeneration process.

### **Assays to understand mechanisms in response to topographical cues**

Results from the two Aims in this thesis help elucidate several key mechanisms of how topographical cues from electrospun fibers help in the regeneration of a critical length nerve gap. However, several other key events, which could be further explored to gain a deeper understanding of how topographical cues alter signaling events that lead to the pro-regenerative phenotype of infiltrating cells.

In the second Aim, we developed techniques to harvest RNA and cytokines with good yield. We evaluated the influence of cytokines and expression of regeneration

specific markers but did not look at downstream effects of these markers. Previous works has suggested that activation of TrkC receptors by growth factors can lead to Schwann cell migration. Since one of the key events in the regenerative sequence is the ability of the Schwann cells to guide repair, understanding their signaling could provide further insights into their role. Future studies can thus evaluate the change in phosphorylation of the TrkC receptors in response to the various topographies that have been developed in this study using a Phosphosensor kinase assay.

We also believe that the assays developed in this study can be applied for evaluation of the role of topography in other fields of regenerative medicine. Electrospun fibers have been used to repair bone, cartilage, vascular tissue etc. While these systems are different from nervous system tissue, there are specific regenerative events that lead to repair in these systems. It would be interesting to evaluate how electrospun fibers guide some of the initial stages of repair in these systems and compare them to the results obtained in this thesis. This will provide a basis of how topographical cues influence cells in tissue engineering applications and could lead to new designs of biomaterials for tissue repair.

#### **Address the limitation of current study**

While we were able to gain important insights into how topographical cues augment PNS repair in this thesis, there were several outcomes that led to many new interesting questions that we propose should be done in the future to further elucidate the role of topographical cues. In this section, we go over various studies that will address some of the limitations of the current thesis.



One of the most interesting findings in the first Aim was the ability of the fibers to efficiently adsorb fibronectin compared to smooth films in vitro. We also evaluated the effects of blocking adhesion sites on adsorbed proteins that would lead to arrest of Schwann cell migration. While fibronectin is an important molecule which can mediate the effects of fibers, there are several other ECM molecules like Laminin, vitronectin, etc., that can also play a significant role in influencing the phenotype of neuronal cells. Since we have already developed the techniques to evaluate the role of fibronectin on different topographies, future studies can translate some of these techniques to evaluate the effects of other ECM proteins and biomolecules that interact with the topographical cues.

In Aim 2, we evaluate the effects of topography on cytokine production at day 5. Our observations lead us to conclude that during this time point, the Wallerian degeneration is in the first pro-inflammatory phase. The thin films are able to influence the release of several cytokines that help recruit macrophages and alter their phenotype. Both Schwann cells and macrophages work together to clear the inhibitory environment debris and provide the necessary signaling molecules to start the regeneration process. The analysis on a later time point was not performed to evaluate the production of cytokines and their profile. Our data also indicates that at the 5-day time point, the cytokines specific to the second phase were not expressed. Based on these results we can instruct that future studies should also involve a later time point (7 day – 3 weeks) where the secondary phase of the Wallerian degeneration can also be evaluated via cytokine array.

## APPENDIX A: OPTIMIZATION OF FIBER DIAMETER

### Fabrication of aligned fibers with different diameter

Similar method as discussed in Chapter 3 and Chapter 4 to fabricate thin films of aligned PAN-MA fiber was used to create electrospun fibers film with different diameters. Briefly, polymer solutions of different concentrations were used to generate fibers of different diameters. PAN-MA was dissolved in DMF at 12%, 14%, 16% and 18% (w/v) to use for electrospinning. A rotating drum was used to collect the electrospun jet to create fibers that had aligned topography. As shown in figure a.1 we were able to fabricated fibers with average diameter of 350 nm, 430 nm, 720 nm and 1029 nm.

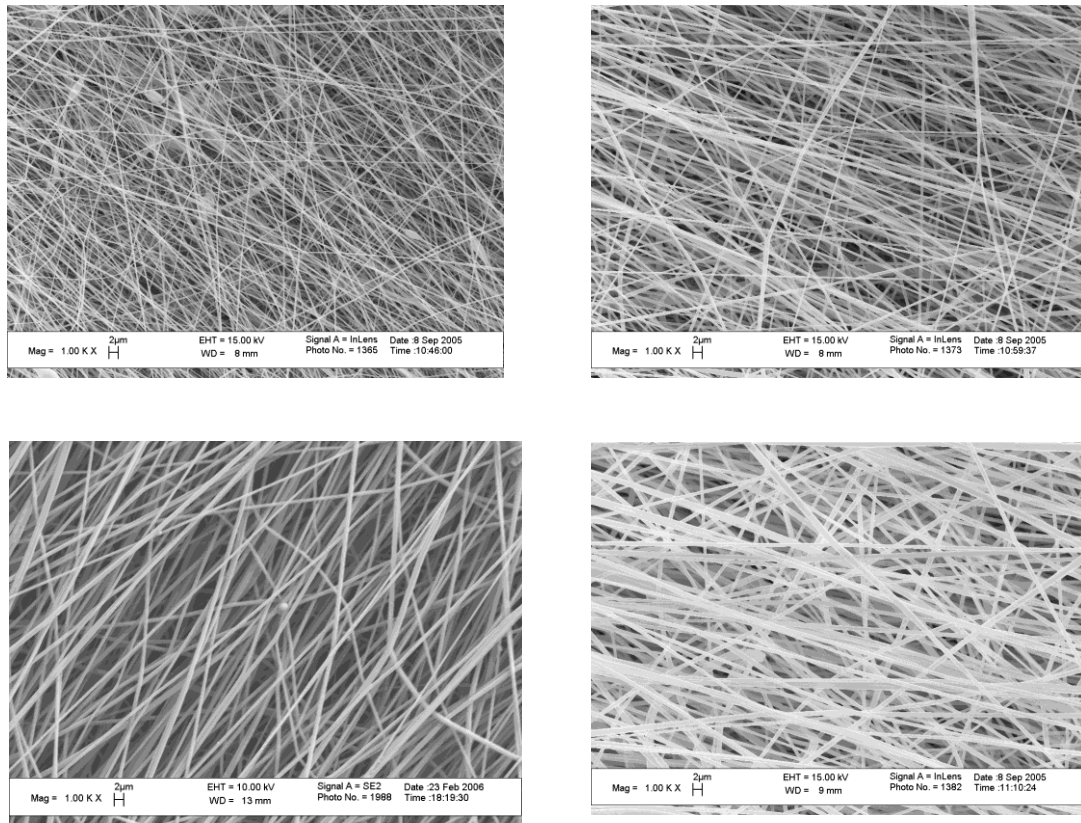


**Figure A-1. Aligned electrospun fibers fabricated using polymeric solutions of different concentrations.**

### Evaluation of Schwann cell migration and neurite outgrowth

In order to evaluate how different diameter fibers are able to influence the migration of neuronal cells, we harvested dorsal root ganglion from P2 rat pups and seeded them on the thin films. These cultures were allowed to grow for 3 days, 6 days and 9 days. Schwann cell migration and neurite outgrowth were quantified at each timepoint by staining for S100 and N160 cell markers respectively.

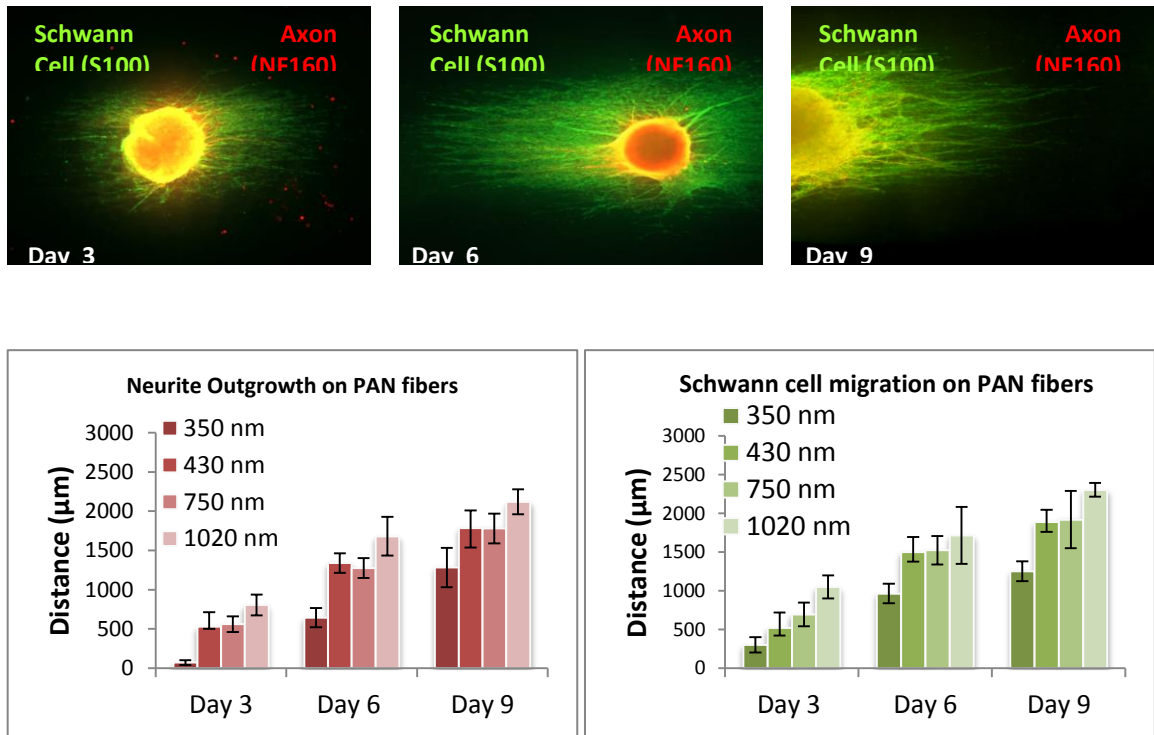


**Figure A-2: DRG study in response to fiber diameter.** Representative image of DRG seeded on aligned electrospun fibers at three time points. Graphs represent the neurite outgrowth and Schwann cell migration on four different fiber diameter

We observed that fibers greater than 500 nm supported similar neuronal cell migration. These fibers were effective in directing Schwann cell migration and neuronal outgrowth in a directed fashion. This data led us to fabricate fibers of approximately 800 nm for the rest of the studies.

## APPENDIX B

### APPENDIX B: DEVELOPMENT OF A COMPLETELY BIODEGRADABLE SCAFFOLD FOR NERVE REGENERATION

#### Fabrication of PLLA aligned fibers

The PLLA solution was prepared by dissolving the PLLA polymer pellets (4% w/v, M.W. =300kDa) into a solution of Methylene Chloride (MC). The polymer solution was fed into a syringe and the feeding rate was controlled by a syringe pump at 1ml/hour via an 18 gauge stainless steel needle. For making aligned polymer fibers, a high speed rotating metal drum, wrapped with an aluminum foil, was used. A high voltage of 15 kV was applied between the needle and the collecting metal drum to generate the polymer fiber jet from the needle tip. The collected polymer fibers on the aluminum foil was sterilized by UV lamp and stored in a desiccator until ready for use.

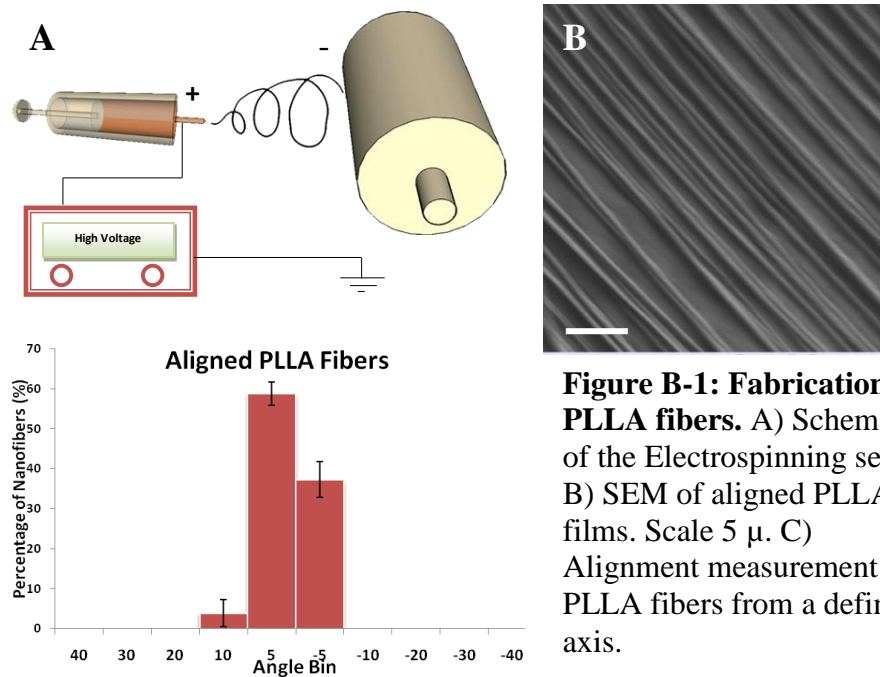


**Figure B-1: Fabrication of PLLA fibers.** A) Schematic of the Electrospinning setup. B) SEM of aligned PLLA films. Scale 5 μ. C) Alignment measurement of PLLA fibers from a defined axis.

Diameter and alignment of the resulting fibers were obtained using a Scanning electron microscope (DeLong Instruments). The degree of orientation was measured by quantifying the angle that individual polymer fibers make with respect to the longitudinal direction. As shown in Figure B1, we were able to fabricate highly aligned PLLA fibers with diameter of approximately 600 nm. We also show that 90% of the fibers were within 5 deg from the defined axis.

### Cell compatibility and alignment on PLLA fibers

Primary Schwann cell cultures were used to test the ability of oriented PLLA fibers to align cells. Schwann cells are important for nerve regeneration because they organize the extracellular matrix as well as provide neurotrophic support to the regenerating nerve. They are also involved in the myelination process and are essential in peripheral nerve regeneration. We purified Schwann cells from P1-P3 rat sciatic nerve and harvested on aligned fibers as well as tissue culture plastic (TCPS). We observed that oriented PLLA films were able to align cell more efficiently than TCPS (Fig.3).

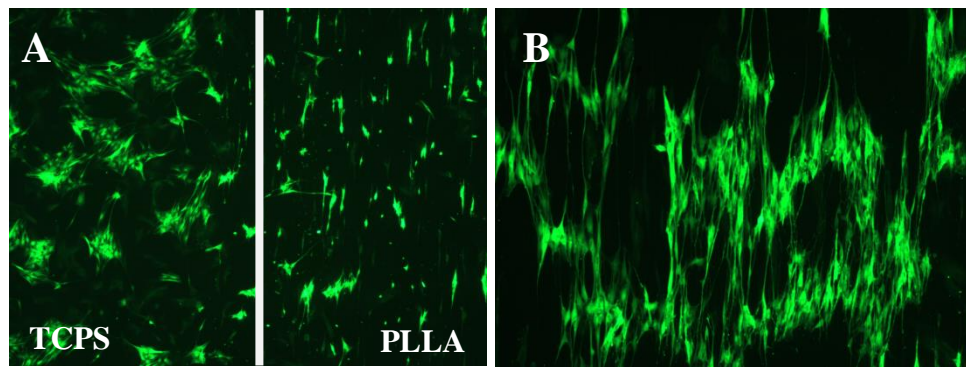


**Figure B-2: A. Schwann cells on TCPS and aligned PLLA films. 10x . B) Schwann cell on aligned PLLA films. 20x. S100 (green) was used to stain for Schwann cells**

### Fabrication of porous PCL conduit as a carrier for aligned fiber thin films

In order to provide a suitable environment for the regenerative cable to form, we fabricated a biodegradable PCL conduit. This conduit will be used as a carrier for the aligned PLLA fibers which were fabricated in the previous section to enhance nerve regeneration in vivo. PCL conduits were prepared by consecutive-dip technique using a glass mandrel. Mandrel tip was submerged in 10% PCL/DCM solution containing suspension of Sodium Bicarbonate at concentration of 1:4 (salt:PCL by weight). After the composite solidified, we leached the salt to obtain a porous semipermeable conduit as is evident from SEM in Figure. B3.

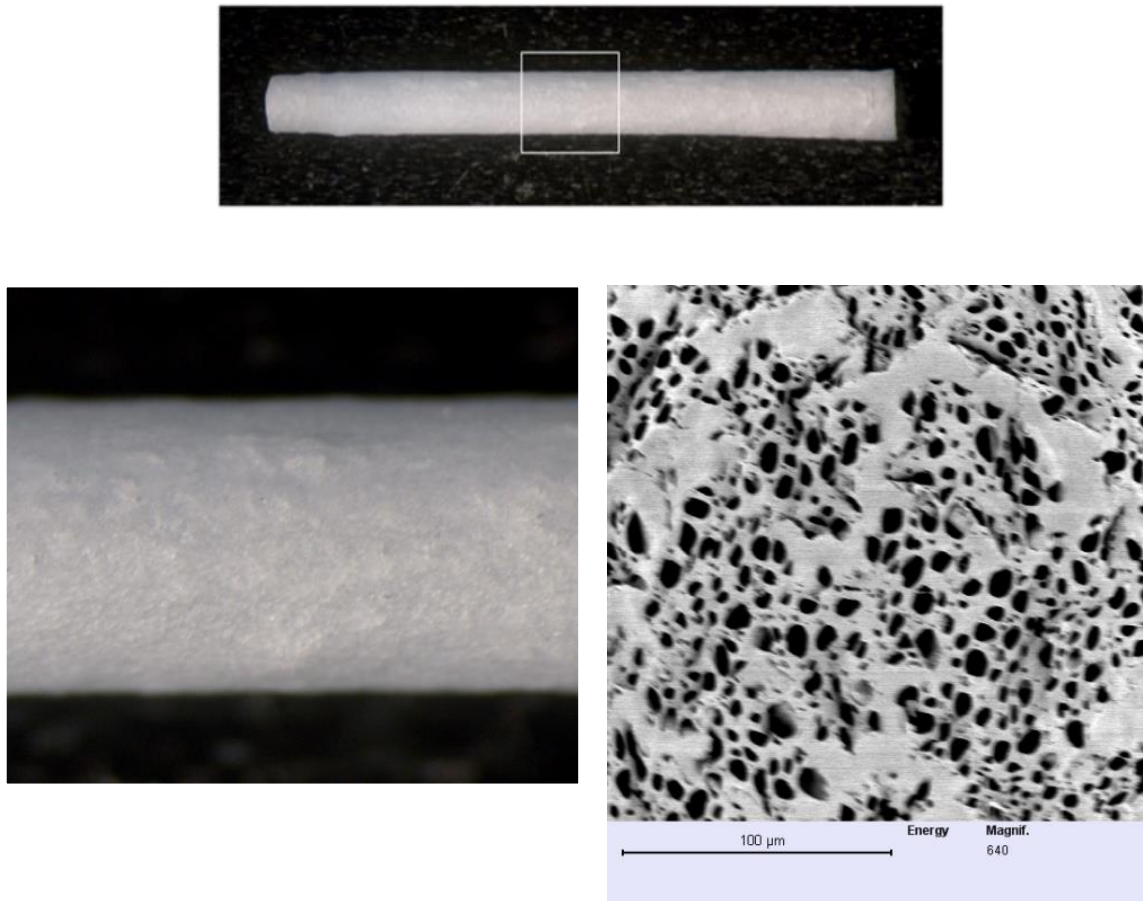


**Figure B-3. PCL nerve guidance channel fabricated using dip coating technique.** Bottom right: SEM image of porous structure suggesting that we have pores of approximately 50  $\mu\text{m}$ .

## **APPENDIX C: FABRICATION OF LONG LIPIDMICROTUBES FOR SUSTAINED DELIVERY OF BIOMOLECULES**

### **INTRODCUTION**

Providing an efficient, biocompatible, sustained drug delivery system to a localized site in the body poses a challenge to the scientific community. Drug delivery systems have the potential to deliver proteins, antibodies, or even DNA to injured organs and provide the appropriate aid. Current advances in the medical field have identified proteins and genetic agents with great therapeutic potential; however, during administration with current delivery mechanisms the protein or genetic material is easily denatured and inactivated. This alteration can be due to exposure to harsh organic solvents during the loading procedure. While current systems such as liposomes, polymer-based systems, and biodegradable systems such as polylactides are commonly-used options available, they include a great drawback in that once they deliver the drug, its effectiveness is reduced. Therefore, there is an unmet for an alternative efficient drug delivery method. One option being researched is using lipid-based microtubules as a drug transportation vehicle. [225, 226] Lipid microtubules made from a lipid such as diacetylenic lipid 1,2-bis(tricoso-10,12-diynoyl)-sn-3-phosphocholine (DC<sub>8,9</sub>PC) self-assemble into hollow cylinders (diameter ~0.5µm and length ~46µm) when the lipid passes through a phase transition temperature of 43°C during a controlled cooling process.[228, 229] Previous research has shown that the length of the tubules can be controlled by altering the rate at which the lipid passes through its transition temperature of 43°C. Furthermore, by altering the ethanol/water ratio into which the lipid is mixed, the length can be controlled.[229, 230] Research in the Bellamkonda lab has shown that lipid microtubules to be an efficient and biocompatible drug delivery method. By altering the fabrication

process, characteristics of the microtubules were altered and further characterized to understand how the release of a protein was altered.



## MATERIALS AND METHODS

### Standard Protocol

DC<sub>8,9</sub>PC (diacetylenic lipid 1,2-bis(tricoso-10,12-diynoyl)-sn-3-phosphocholine ) was mixed in a 70:30 ethanol to water solution held at 55°C. The solution was cooled to 25°C at 1°C/40 min, heated to 33°C, and finally cooled to 25°C in a controlled heating bath. At the end of a two week stabilizing period, cyroprotectant trehalose was added to the solution. Once the trehalose had one day to take effect, the tubule mixture was centrifuged, and the supernatant was removed. [230] Deionized water was added to the tubules to aid in removing the lipid from the tube, and the mixture was rotary evaporated until dry. Lastly, the tubules were loaded with the protein of interest by exposing a protein-concentrated phosphate buffered saline (PBS) solution to the dried tubules. In order to determine the amount of protein released from both ends of the tubules over time, they were embedded in an agarose hydrogel (SeaPlaque) in a 96 well plate. The hydrogel system localized the microtubules and allowed the protein to diffuse through the pores to the surface of the hydrogel and into the PBS placed on top. This protein and PBS mixture was collected and replaced with fresh PBS every 48 hrs to determine protein concentration by using a BioRad protein assay. [226] To understand how length changed with altering cooling rate and mixture of ethanol:water, all studies were compared to the standard protocol.

### Alterations Cooling Rate:

Two batches of microtubules were created in the 70:30 ethanol water ratio as per standard protocol. However, one batch was cooled at 1°C/40 min and the other at 1°C/20

min from 55°C to 25°C. Lengths were calculated by taking images of the microtubules on an AxioSkop2 Zeiss microscope and analyzed using ImagePro Software.

### **Altering Cooling Solution Composition:**

Four batches of microtubules were created as per standard protocol at a cooling rate of 1°C/40 min. However, each was mixed into a different ethanol:water solution of 50:50, 60:40, 70:30, and 80:20. Length was then determined by taking images of the microtubules on an AxioSkop2 Zeiss microscope and analyzed using ImagePro Software.

### **Needle Studies**

Preliminary studies were conducted to determine if passage of microtubules through a needle would affect the length of the tubule. Two batches of microtubules were created in 70:30 ethanol/water solution. One was cooled at 1°C/20 min and the other at 1°C/40 min. They were then passed through various needle gauges (18, 23, 27). Final lengths were analyzed by taking images on an AxioSkop2 Zeiss microscope and measured using ImagePro Software.

### **Release Profile Comparisons**

Based on results from altering the cooling rate and solution composition, four batches of tubules were created under various conditions:

- Batch A: cooled at 1°C/40 min and mixed in 70:30 ethanol: water
- Batch B: cooled at 1°C/20 min and mixed in 70:30 ethanol: water
- Batch C: cooled at 1°C/40 min and mixed in 60:40 ethanol: water
- Batch D: cooled at 1°C/20 min and mixed in 60:40 ethanol: water

All batches were loaded with 10 mg/ml Bovine Serum Albumin (BSA) protein and embedded in the hydrogel as per standard protocol. The plate was stored in an

incubator held at 37°C. The protein-PBS solution was collected every 48 hrs for two weeks. Samples of tubules were collected before loading to determine the length. Images were taken on an AxioSkop2 Ziess microscope and analyzed using ImagePro Software.

### *Statistics*

To determine statistical significance in the difference of lengths by just altering the cooling rate but keeping the standard 70:30 ethanol water ratio (Type A and B), a Wilcoxon Sum Rank test was used to make no assumptions about variance. To determine statistical significance on altering ethanol: water ratios and the release profiles of all types of microtubules on each day, a one-way ANOVA test was employed on a 95% confidence interval ( $\alpha = 0.05$ ). To further understand statistical significance between each group on each day, a Tukey test was conducted on a 95% confidence interval.

## RESULTS

### Altering Cooling Rate

It was found that the length of microtubules formed could be significantly changed by altering the rate of which the lipid in 70:30 solution passed through its transition temperature. The average length of those cooled at  $1^{\circ}\text{C}/40$  min ranged from  $60.5 \pm 25$   $\mu\text{m}$  and the average length of those cooled at  $1^{\circ}\text{C}/20$  min ranged from  $90.7 \pm 42$   $\mu\text{m}$ . Figure C1 illustrates the effect of altering the cooling rate on microtubule length. Figure C2 displays images of the microtubules.

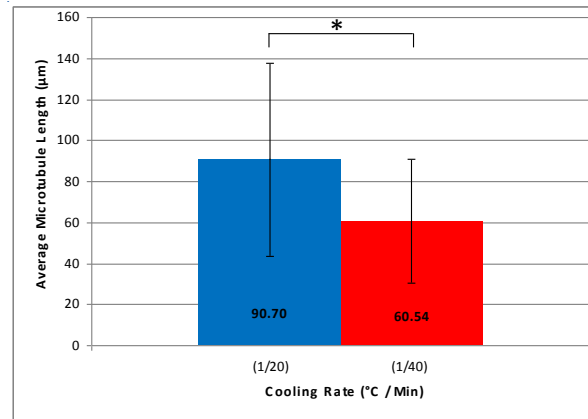


**Figure C-1: Average Lipid Microtubule Length at two Cooling Rates.** The average length of microtubules cooled at  $1^{\circ}\text{C}/40$  and  $1^{\circ}\text{C}/20$  min was  $60.5 \pm 25$   $\mu\text{m}$  and  $90.7 \pm 42$   $\mu\text{m}$  respectively. A significant difference was determined with a two sampled Wilcoxon Sum Rank test resulting in a  $p\text{-value} = 0.0075 < \alpha = 0.05$ .

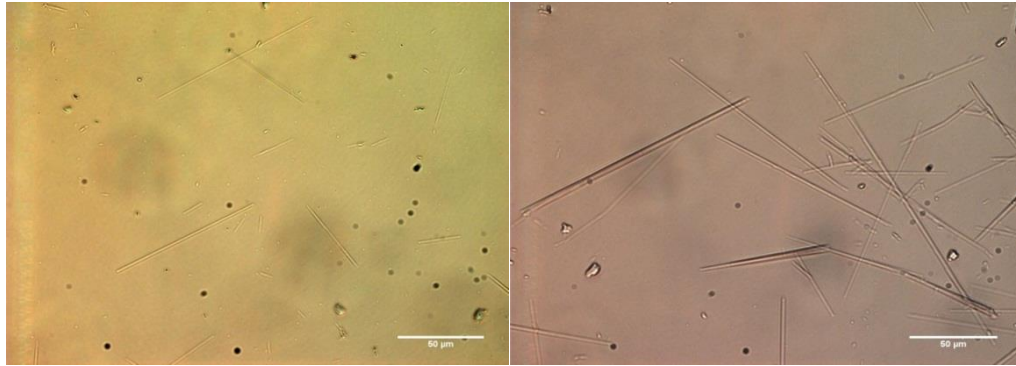


**Figure C-2: Images of Microtubules at Two Cooling Rates.** Scale bar is at 50 µm. Images taken at 40x with AxioSkop2 Zeiss microscope **A)** Microtubules formed at cooling rate of 1°C/40 min **B)** Microtubules formed at cooling rate of 1°C/20 min.

### **Altering Cooling Solution Composition**

It was found that the length of microtubules formed could be changed by altering the ethanol, water ratio into which the lipid is dissolved. Four microtubule batches were created in either 50:50, 60:40, 70:30, 80:20 ethanol/water solution and cooled at 1°C/40 min. Results determined the average length of microtubules created in 70:30 ethanol: water is statistically different to that of microtubules formed in 50:50 and 80:20 (Figure C3 & C4). There was no difference found between 70:30 and 60:40 with values of  $92.2 \pm 14$  and  $79.7 \pm 15$  respectively.

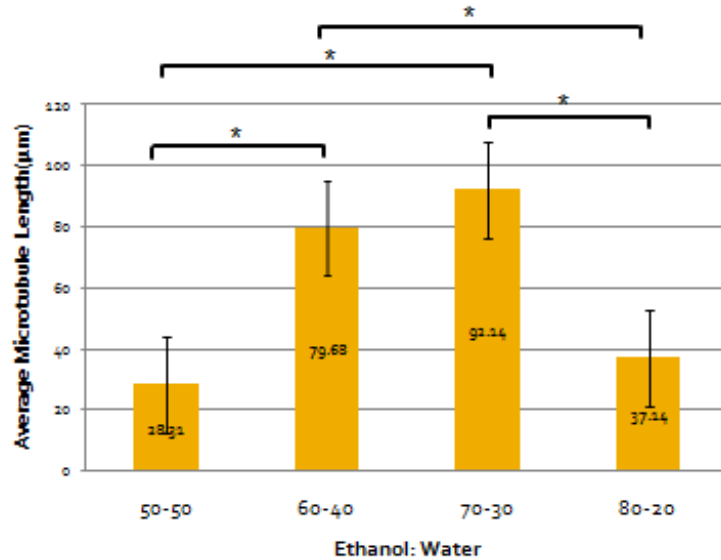


**Figure C-3: Average Lipid Microtubule Length After Altering Solution Ratio.** The average length of microtubules created in 50:50, 60:40, 70:30, 80:20 ethanol water solution was  $18.3 \pm 9 \mu\text{m}$ ,  $79.7 \pm 15 \mu\text{m}$ ,  $92.2 \pm 14 \mu\text{m}$ , and  $37.2 \pm 18 \mu\text{m}$  respectively. A statistically significant difference was found between the groups with a one way ANOVA test. No significant difference found between 60:40 and 70:30

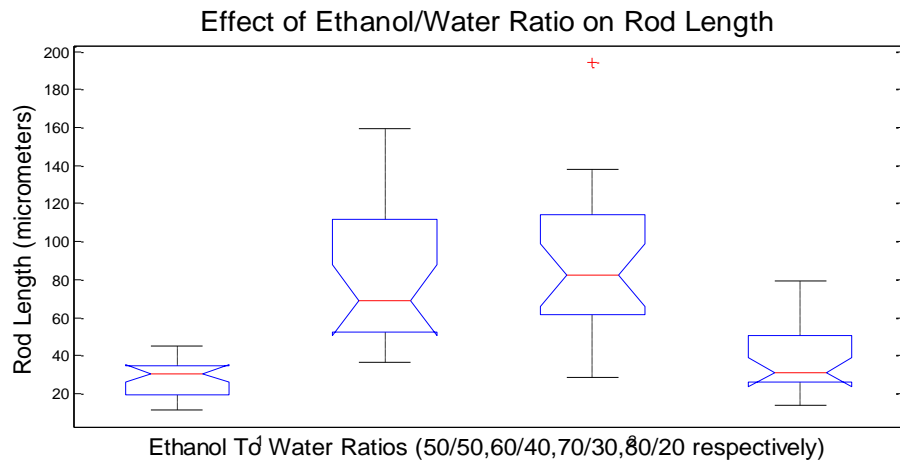


**Figure C-4: ANOVA results of Average Lipid Microtubule Length After Altering Solution Ratio.** A significant difference was determined between the groups with a one way ANOVA test. The average length of microtubules created in 70:30 ethanol: water is statistically different to that of microtubules formed in 50:50 and 80:20. There was no difference found between 70:30 and 60:40 with values of  $92.2 \pm 14$  and  $79.7 \pm 15$  respectively.

## Needle Studies

Microtubules created in 70:30 solution and cooled at either 1°C/20min or 1°C/40 min were passed through various needle gauges (18, 23, 27). Following passage, lengths were measured and results are displayed in Figure C5.

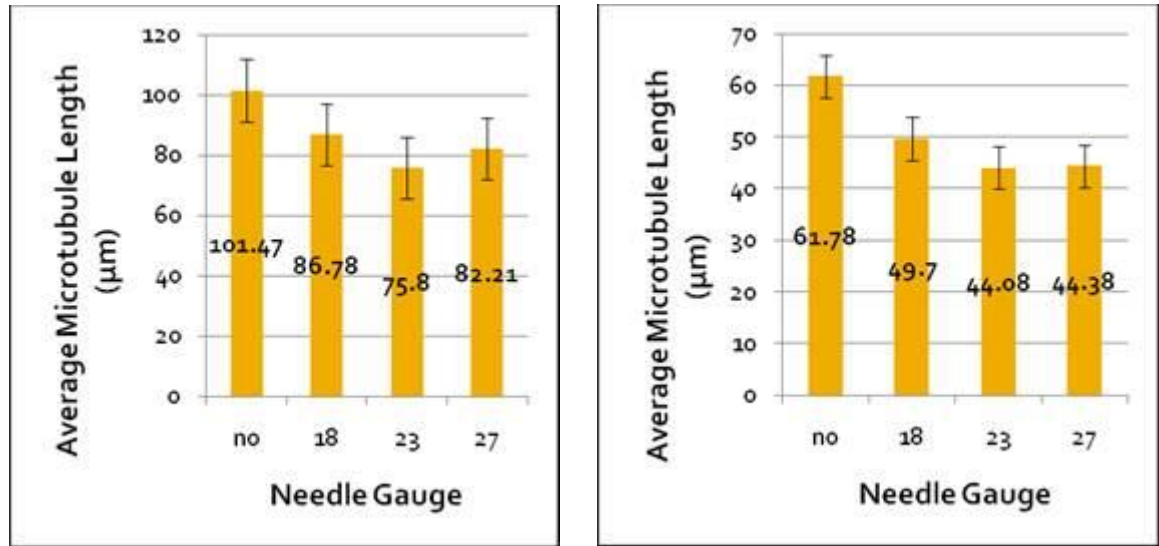


**Figure C-5: Average Microtubule Length after Passage through Needles.**

Microtubules were passed through needles of various gauges: 18, 23, and 27. A significant difference was found after passing microtubules through 18gauge; however, no significant difference was found between the 18,23, and 27 needle groups **A)** Microtubule made in 70:30 ethanol: water solution and cooled at 1°C/20min **B)** Microtubule made in 60:40 ethanol: water solution and cooled at 1°C/40min.

## Release Profile Comparisons

A release profile was created comparing Batches A-D and a graph of the Total BSA release was compiled as displayed in Figure C6.

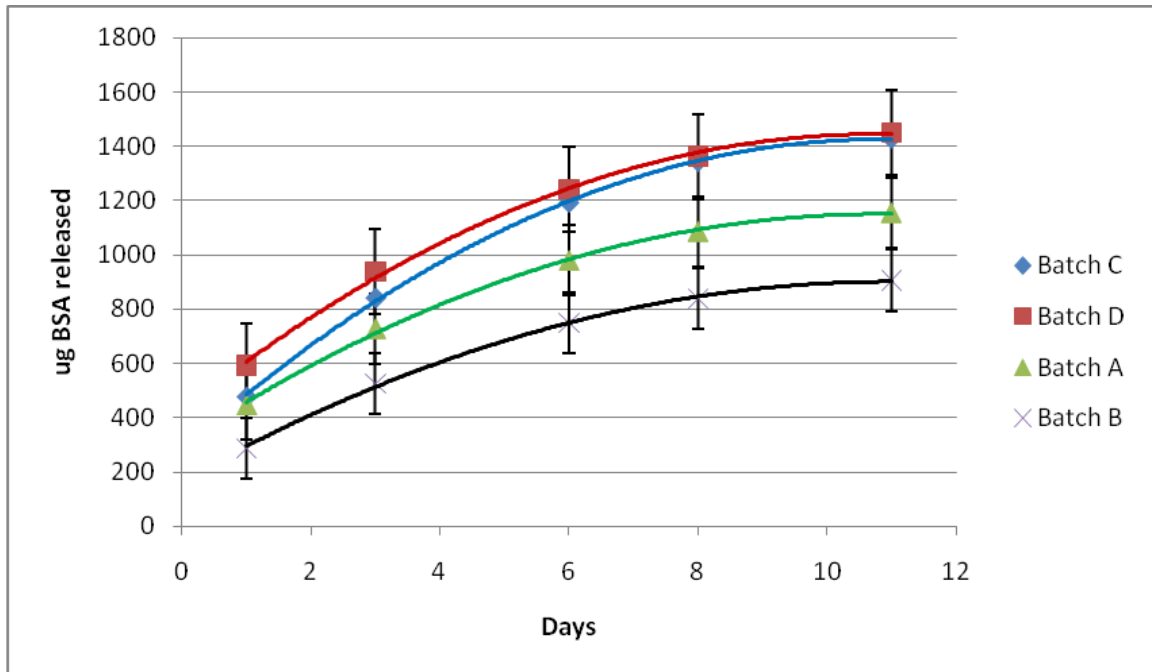


**Figure C-6: Average BSA release from lipid microtubules over two weeks.** Four batches of microtubules were load with BSA total quantity of protein released over two weeks was displayed. Batch A: cooled at 1°C/40 min and mixed in 70:30 ethanol: water. Batch B: cooled at 1°C/20 min and mixed in 70:30 ethanol: water. Batch C: cooled at 1°C/40 min and mixed in 60:40 ethanol: water. Batch D: cooled at 1°C/20 min and mixed in 60:40 ethanol: water. With a p-value of 1.43 ( $\alpha= 0.05$ ), no significant difference was found between any conditions.



## Discussion

From the results, we can determine that altering the standard protocol when creating lipid microtubules will affect the overall length. When microtubules were created in 70:30 ethanol/water solution and the cooling rate was decreased from the standard 1°C/40 min to 1°C/20 min, the resulting microtubules were significantly longer. This change resulted in ~90 µm microtubules as opposed to ~60 µm. This change may be due to the lipid forming in a more stable energy state. Other published articles acknowledge that the length can be changed by altering the cooling process; however, the exact change is not identified. [229]

Furthermore, a difference in length was observed when the ethanol/water ratio of the solution was altered. The microtubules used in this experiment were the relatively longer microtubules that were cooled at 1°C/20 min. Of the ratios tested, (50:50, 60:40, 70:30, 80:20), there was a statistically different length found between all groups except between 60:40 and 70:30. Once again, there are journal articles which use microtubules created in 60:40 and some that use 70:30; however, studies comparing the two ethanol ratios have not been looked into.[229]

From the needle study it was observed that the microtubules broke after passage through an 18 gauge needle; however, after passage through subsequently higher gauges the length did not significantly change between 18,23, and 27 gauges. Despite the original lengths being different (100 µm and 60 µm), once the microtubules passed through the needle, the length was reduced by ~20 µm in each batch resulting in 80 µm and 40 µm microtubules respectively.

Due to this insignificant change in length between 60:40 and 70:30, and the significant change found when altering the cooling rate (1°C/20 min and 1°C/40 min), these four conditions were tested to determine how the mass transfer of a protein from these microtubules is affected. Results were showed no significant difference in amount of protein between the Batches. However, the difference in protein released between each batch increased over two weeks. It is interesting to note that the microtubules formed in 60:40 solution and cooled at both cooling rates released relatively more protein than those formed in the 70:30 ethanol/water solution. Length analysis was unable to be completed on these microtubules due to time restraints. Images were taken of a few Batches; however, the lengths have yet to be analyzed. Therefore, definite conclusions can not be made as to how length affected the mass transfer. Further studies should be conducted which vary the concentration of protein loaded into the longer microtubules. These release profiles should be compared to each other as well as the release profiles produced from the standard microtubules. With this data, one can determine how much drug to initially administer for therapeutic use.

### **Conclusion**

This study demonstrates how lipid microtubule length can be affected by altering the rate at which the lipid mixed in an ethanol/water solution passes through its transition temperature. Length can also be significantly altered by changing the ethanol/water ratio. As the cooling rate is increased, the length increases. No significant difference in length was found when using solutions of 60:40 or 70:30 ethanol/water to mix the tubules into. Also, passage of the longer microtubules through an 18G needle showed a significant reduction in length. However, when comparing the resulting length when passed through

23G and 27 G to that resulting from 18G, no significant difference was found. Lastly, a release profile showed no significant difference in the release of BSA protein from four batches of microtubules created under various conditions of cooling at 1°C/20 min or 1°C/40 min, and created in solutions of 60:40 or 70:30 ethanol/water. Although no statistically significant difference was found, those microtubules created in 60:40 ethanol/water solution released relatively more protein over the course of two weeks as opposed to those created in 70:30. Lipid microtubules provide a promising future in drug delivery applications; however, more studies need to be conducted to obtain conclusive results.

## **APPENDIX D: NT-3 FOR PROMOTING SCHWANN CELL FUNCTION ACROSS LONG PERIPHERAL NERVE GAPS**

### **INTRODUCTION**

Traumatic peripheral nerve injuries pose a significant clinical challenge, affecting over 200,000 patients annually in the United States alone [203]. In the case of extended injury gaps, autologous segments of nerve are typically harvested and grafted across the injury site in order to promote spontaneous axonal regeneration across the defect. Autografting techniques, however, require the sacrifice of healthy nerve tissue and result in functional outcomes that are less than ideal [8, 231].

As alternative to autograft repair, peripheral nerve defects can be bridged with engineered nerve guidance channels, typically consisting of tubular conduits of synthetic or biological materials. A nerve guidance channel functions to bridge the two stumps of an injured nerve, constraining a pathway for an endogenous sequence of nerve repair [13]. Critical to this regenerative sequence is the migration through the channel of non-neuronal cell types such as Schwann cells and fibroblasts. Schwann cells in particular play a major role in contributing to axonal growth and maturation [15, 232].

One technique for enhancing cell migration and nerve regeneration through a guidance channel is to include topographically oriented surfaces or scaffolding within the channel interior [138, 142, 233, 234]. These aligned substrates provide topographic cues to adherent cells, stimulating alignment and directed migration. As an example, electrospun meshes of aligned sub-micron scale polymer fibers have been demonstrated as pro-regenerative scaffolding substrates, able to promote Schwann cell migration and nerve regeneration across critical sized nerve gaps [203] [163].

Another method for promoting cell migration and nerve regeneration through a guidance channel is to incorporate the delivery of chemical cues. Neurotrophic factors, for example, are able to influence axons and non-neuronal cells by stimulate intracellular pathways conducive to regeneration. NT-3 is a neurotrophin that has been demonstrated to stimulate a pro-regenerative phenotype within both axons and Schwann cells [89]. Neurotrophins control cellular responses via low affinity NGF receptors and high affinity Trk receptors [204]. Among them, Neurotrophin-3 is able to activate all three types of trk receptors and has shown to be vital in nerve regeneration. Schwann cell migration is significantly enhanced by NT-3 [85, 89, 90], whereas BDNF acts through the p75 receptor on the Schwann cells to promote the myelination of nerves [220]. Studies have also shown that NT-3 deficient Schwann cell impair nerve regeneration because they decrease Schwann cell survival and influence the myelination process [84].

Other than stimulating Schwann cell migration, NT-3 has also been shown to play a role in axonal growth. NT-3 has been shown to have chemotatic effects on embryonic neuron populations, and attractive effects on axonal growth by stimulating the polymerization and accumulation of F-actin. [235] NT-3 also increases the expression of microtubule associated protein 5 (MAP-5) which influences the organization of microtubules in regenerative neurons and axon growth cones and stimulates their growth. [236] Thus, NT-3 plays a vital role in axonal guidance and growth after injury and can be used to stimulate nerve growth.

Advanced approaches for enhancing nerve guidance scaffold function will possibly involve the use of both physical and chemical cues to stimulate cell migration and nerve regeneration. This type of combinational design will help to better simulate the

complex natural terrain of neural tissue in which topographic and chemical cues are intricately patterned. Furthermore achieving spatiotemporal control over the presentation of these cues will allow better simulation of natural tissue and control over regeneration. .

In this study, we explore the effects on Schwann cell migration of controlled NT-3 release, delivered in combination with aligned topographic cues provided by electrospun thin-films of aligned poly(acrylonitrile-co-methylacrylate) (PAN-MA) fibers. We hypothesize that local sustained release of NT-3 will stimulate endogenous SCs into the nerve gap from the proximal and distal stumps. Presence of NT-3 will also stimulate axonal guidance and growth and provide spacial and temporal cues to enhance nerve regeneration. Therefore, the presence of topographical (oriented polymer fibers) and chemotactic (NT-3) cues will stimulate Schwann cell migration induced regeneration. This approach allows examination of the effects sustained NT-3 delivery on Schwann cells already stimulated through topographic cues to migrate directionally.

A modified scratch assay and a dorsal root ganglia (DRG) migration assay were used to assess the effects of NT-3 on topographically directed Schwann cell migration *in vitro*. We also assessed the influence over Schwann cell migration and nerve regeneration of topographically patterned nerve guidance channels capable of delivering controlled NT-3 release. The channels contained a single aligned thin-film as well as agarose suspended loaded lipid microtubules, capable of delivering sustained release of NT-3. In these *in vivo* studies, critical length (15 mm) gaps in rat tibial nerve were repaired and short term (16 days) and long term (20 weeks) regeneration was examined.

## **MATERIALS AND METHODS**

### **Design of aligned fiber-based thin-film scaffolds**

### *Fabrication of aligned fiber thin-films*

Films consisting of aligned poly(acrylonitrile-co-methylacrylate, random copolymer, 4 mole percent methylacrylate) (PAN-MA) fibers were created through an electrospinning process. Briefly, a 7 % (w/v) PAN-MA solution was prepared by dissolving PAN-MA into the organic solvent N, N-Dimethyl Formamide (DMF, Acros Organics) at 60°C. This solution was loaded into a metered syringe and dispensed for 15 minutes at a constant flow-rate of 1ml/hr through a 19 gauge needle across a voltage field of 5-10kV. The ejected polymer fibers were collected 10 cm away on a 3.8 cm diameter metal drum, rotating at approximately 2500 rpm to produce aligned fiber thin-films, which were baked for 4 hours at 60°C to remove any residual DMF. Finally, 2.2 x 14mm sheets of aligned thin-films were manually cut with a razor blade and separated from the collected polymer mass with fine forceps for use in channel construction.

### ***In vitro testing with purified Schwann cell and DRG cultures***

#### *Effects of NT-3 on the migration of purified Schwann cells in culture*

Schwann cells were purified from the sciatic nerves of postnatal day 1 (P1) rat pups (Harlan) using a modified protocol from Brockes et. Al [170]. Briefly, sciatic nerves were dissected into 1 mm segments and dissociated in 1.33% collagenase solution for 30 mins. This was followed by treating the nerve segments with 0.25% Trypsin/EDTA for 30 mins. Cells were then mechanically dissociated using a pipette and incubated in culture media DMEM/F12 with 10% fetal bovine serum) with fibroblast growth factor (FGF) (50 ng/ml). After 24 hours, the culture media was replaced with similar media along with arbinoside (Ara-C) ( $10^{-5}$ ) for 48 hours to remove the more

quickly dividing fibroblasts. Purity of cells was assessed by immunostaining with S100. Cultures with purity of greater than 95% were used in migration assays.

To evaluate the effects of NT-3 on Schwann cell migration a scratch wound assay was used. Briefly, purified Schwann cells were seeded on 6-well plates and allowed to reach >95% confluence. One day prior to making the scratch, the cells were treated with 10 $\mu$ g/ml of Mitomycin-C in serum free media to block proliferation effects. The confluent layer of cells was then scratched with a pipette to create a 200  $\mu$ m gap, and conditioned media with and without NT-3 (50 ng/ml) was added to the cultures. Cells were imaged using ZEISS bright field microscope on the day of the scratch and on the following day under sterile conditions. Migration distance of Schwann cells within the gap was quantified using ImagePro. This distance was subtracted from the original gap width to evaluate how NT-3 is able to induce the migration of Schwann cells.

#### *Effects of NT-3 on DRG growth on aligned fibers*

Dorsal root ganglia (DRGs) were also harvested from P1 rat pups. The nerve roots were removed and the ganglia were seeded on aligned fiber based films with diameter of 600-800 nm. To encourage attachment to the films, the ganglia were first incubated for several hours with only a thin layer of medium. Afterwards, each experimental condition was fully covered with DMEM/F12 media with 10% FBS and 50 ng/ml nerve growth factor (NGF). To quantify the effects of NT-3 on axonal outgrowth and Schwann cell migration from DRG cultures, 50 ng/ml of NT-3 was added to half of the DRG cultures. DRGs were allowed to grow for one week and fixed for immunostaining with Histochoice . The substrates were stained for axons (NF160, 1:500 dilution, Sigma-Aldrich) and 2) Schwann cells, (S100, 1:250, Dako). Nuclei were



labeled with DAPI (Invitrogen) in PBS at a concentration of 10 $\mu$ M. The following secondary antibodies were used: Goat anti-rabbit IgG Alexa 488/594, goat anti-mouse IgG1 Alexa 488/594, and goat anti-chick IgG (Invitrogen). 15 of the longest NF160<sup>+</sup> axons and 15 furthest S100<sup>+</sup> Schwann cells were measured from the edge of the DRGs. ImagePro was used to quantify the migration distance of Schwann cells and the extent of neurite extension under the effects of NT-3.

### **Aligned fiber-based nerve guidance channels for sustained NT-3 delivery**

#### *Fabrication of aligned fiber-based nerve guidance scaffolds*

Aligned fiber-based nerve guidance channels were fabricated from polysulfone tubes (Koch Membrane Systems) and electrospun aligned thin-films of PAN-MA polymer fibers. The polysulfone tubing (inner diameter: 1.6 mm, outer diameter: 2.2 mm, molecular weight cutoff: 50kDa) was halved lengthwise using a custom machined aluminum template. One thin-film strip of aligned fibers was secured through the length of one of the tube sections, using a medical grade UV curing adhesive (1187-M-SV01, Dymax).

#### *Lipid-microtubes for NT-3 delivery*

Hollow and open-ended lipid microtubes were fabricated using 1,2-bis-(triscosa-10,12-diynoyl)-sn-glycero-3-phosphocholine (DC8,9PC, Avanti Polar Lipids, Alabaster, AL). These methods have been previously published our lab. [226]. Briefly, the lipid were dissolved in 70% ethanol at a concentration of 1 mg/ml. The solution was slowly cooled from 55 °C to 21 °C, heated to 33 °C and cooled again to 20 °C by a programmed water bath for 48 hours. During this cooling procedure, the microtubes self-assemble. After 2 weeks of incubation at room temperature, 50 mM of trehalose was

mixed gently and incubated overnight to stabilize the growth factor as shown previously [237] . The microtubes were then centrifuged, dried overnight and embedded with the NT-3 dissolved in PBS.

### ***In Vivo* Implantation of NT-3 releasing nerve guidance scaffolds**

#### *Experimental groups*

Nerve regeneration was evaluated at 16 days and 20 weeks post-implantation. The sixteen day time point (8 animals) was chosen, based on prior experience in our lab, to allow axons and Schwann cells to travel a significant distance through the guidance channels, without allowing Schwann cell derived from the proximal and distal nerve stumps to meet in the middle. In order to determine Schwann cell migration distances, it is important that these two Schwann cell populations remained distinct.) The 20 week time point (18 animals) was chosen to allow for functional muscular reinnervation.

#### *Implantation techniques*

Nerve guidance channels were implanted to bridge 15 mm gaps in the tibial branch of the sciatic nerve of Fischer 344 rats (250-300g), as described in [203]. Rats were anesthetized under inhaled isoflurane, and given a subcutaneous injection of Marcaine (0.25% w/v, Hospira, Inc.) for post-surgical pain relief. The thigh muscles in the right leg were exposed and delineated to expose the underlying sciatic nerve, which was freed from surrounding connective tissue. The tibial nerve branch was transected several several millimeters distal to the common peroneal - tibial bifurcation, and the nerve stumps were pulled 1 mm into each end of a 17 mm guidance channel and sutured into place (10-0 nylon suture, Ethilon) to create a 15 mm gap. The muscles were reapposed with 4-0 vicryl sutures (Ethicon Inc.), and wound clips (Braintree Scientific,

Inc.) were used to close the skin incision. The rats were placed under a warm light to recover from anesthesia, and then housed separately with access to food and water *ad libitum* in a colony room maintained at constant temperature (19-22°C) and humidity (40-50%) on a 12:12 h light/dark cycle. To prevent chewing of the toes, a mixture of New Skin (MedTech) and Metronidazole (ICN Biomedical Research Products) was used as described in [238]. Animals were maintained in facilities approved by the Institutional Animal Care and Use Committee (IACUC) at the Georgia Institute of Technology and in accordance with the current United States Department of Agriculture, Department of Health and Human Services, and National Institutes of Health regulations and standards.

### **Evaluation of Nerve Regeneration**

#### *Histological analysis of nerve regeneration*

At the end of the prescribed regeneration times, guidance channels were explanted for histological analysis of nerve regeneration. Guidance channels from the 16 day regeneration group were sectioned longitudinally at a thickness of 18µm and reacted with immunofluorescent markers to quantify the distance of axonal regeneration and Schwann cell migration into the channels. Rats were perfused intracardially with saline followed by 4% paraformaldehyde in PBS (Sigma-Aldrich), and explanted guidance channels were post-fixed, washed, and stored in 30% sucrose in PBS for 24 hours. Samples were embedded in O.C.T. gel (Tissue Tek) and frozen for cryosectioning (CM30505, Leica). Using techniques previously described (Young-tae), the sections were reacted for immunofluorescent demonstration of markers on 1) axons (NF160, 1:500 dilution, Sigma-Aldrich) and 2) Schwann cells, (S100, 1:250, Dako). Nuclei were labeled with DAPI (Invitrogen) in PBS at a concentration of 10µM. The following secondary

antibodies were used: Goat anti-rabbit IgG Alexa 488/594, goat anti-mouse IgG1 Alexa 488/594, and goat anti-chick IgG (Invitrogen).

Sections at 150 um interval were immunostained to capture the presence of unique Schwann cells. 20 longest processes from the edge of the conduit were measured using ImagePro for each sample. Both Schwann cell infiltration and axonal growth were quantified in order to observe the effects of NT-3 on short term regenerative events.

In the 20 week group, guidance channels were explanted and post-fixed following electrophysiological testing. A 2 mm long cross-section from the center of each guidance channel was cut with a fine razor and embedded in resin for fine sectioning, as previously described (Dodla, 2008). Briefly the samples were post-fixed over night in 1% osmium tetroxide in PBS, dehydrated in a graded ethanol series, and imbedded in LX112 resin (Ladd Research Industries, Inc.). The samples were then cut with a microtome into 1µm thick cross-sections, slide mounted, and stained with Toluidine blue (0.1%, Sigma) for imaging under a light microscope.

#### *Electrophysiological analysis*

In the 20 week groups, electrophysiological measurements were taken of nerve conduction velocity (NCV) through the regenerated nerves. NCV measurements are positively correlated with the size of myelinated axons and degree of myelination. Briefly, the site of nerve injury was exposed, and two pairs of stainless steel bipolar hook electrodes were positioned on the nerve. One pair of electrodes was placed on the sciatic nerve, 10 mm proximal to the implanted guidance channel, and the other pair was placed distal to the implanted guidance channel, 10 mm distal to the implanted guidance channel. A stimulator (Model S88, Grass Technologies) and stimulus isolation unit

(Model SIU5B, Grass) was used to apply supramaximal square voltage pulses of 100 $\mu$ s duration at a rate of 1Hz, through the distal pair of electrodes. The evoked compound nerve action potentials (CNAPs) were recorded upstream from the proximal pair of electrodes. The recorded signals were filtered and amplified (Model 1700, A-M Systems) and digitally sampled at 25kHz. (Multichannel Systems DAQ card.) The recordings were averaged, and the latency of the onset of the evoked CNAP was determined off-line. The distance between the stimulating and recording electrodes divided by this latency value to calculate the conduction velocity of the CNAPs through the regenerated nerves.

#### *2.5.4. Myelinated axons counts and quantification of axonal diameters and myelin thickness*

Two millimeter long sections of regenerated nerve were removed from the center of each scaffold. These explants were resin embedded, cut into 1 $\mu$ m thick slide mounted cross-sections, and stained with toluidine-blue. Images of regenerated nerve cross-sections were viewed under a Nikon Eclipse 80i light microscope (Japan), using a 100x oil-immersion objective lens. A 100x montage image was compiled for each nerve, using a NeuroLucida<sup>®</sup> system (MBF Bioscience, Williston, VT), coupled to a mechanized stage and MicroFire<sup>™</sup> camera (Optronics, Goleta, CA).

Myelinated axons were manually counted from these 100x montages, using Image-Pro<sup>®</sup> Plus software (Media Cybernetics, Inc., Bethesda, MD). Myelin thickness and axonal diameters were quantified by sampling subsets of the entire axonal population. A 25 $\times$ 25 grid was overlaid above each image, using Adobe<sup>®</sup> Photoshop<sup>®</sup> CS3 (San Jose, CA), and a cell in the upper left-hand portion of the image containing myelinated axons was selected, and grid cells spaced evenly apart from the initially

selected cell were chosen for analysis. Between 5-25% of the total myelinated axon population was analyzed from each nerve cross-section. Image-Pro<sup>®</sup> Plus software was used to measure myelin thickness and axonal diameter of myelinated axons. Axonal diameters were calculated using a circle-equivalent technique, in which the cross-sectional area of each axon was measured and then converted into an axonal diameter using a formula that assumes a circular cross-section.

#### *Muscle Fiber analysis*

The rats' gastrocnemius muscle was explanted, fixed with 4% paraformaldehyde for 1 hour, soaked in a 30% sucrose solution overnight, and then frozen in Tissue-Tek Optimal Cutting Temperature compound (Sakura Finetek USA Inc.; Torrance, CA) at -80 °C. Longitudinal 16 µm thick sections of the muscle were obtained by cryosectioning. The muscle sections were then stained with Masson's Trichrome stain. Muscle fibrosis was measured by

#### 2.6 Statistics

ANOVA, combined with Tukey post hoc tests, was used to calculate the significance of differences between mean values. A *p* value less than 0.05 was considered statistically significant.

## RESULTS

### Effects of NT-3 on the migration of purified Schwann cells in vitro

Scratch wound assay was used to evaluate the effects of NT-3 on Schwann cells. Purified Schwann cells were allowed to reach confluence and a  $681 \pm 20 \mu\text{m}$  gap was created using a micro pipette (Fig D1 A, B). Cells were allowed to migrate within the gap overnight and the bridging of the gap was evaluated by microscopy. Schwann cell migration was significantly higher ( $p < 0.05$ ) within the gap when NT-3 ( $566 \pm 42 \mu\text{m}$ ) was added to the cultures compared to control conditions ( $401 \pm 40 \mu\text{m}$ ).

### Effects of NT-3 on DRG growth on aligned fibers

To investigate if NT-3 can enhance the growth of peripheral nerve cells on fiber based topography, DRGs were seeded on aligned fiber films and the effects of NT-3 were evaluated. DRGs were seeded on the fiber films to quantify Schwann cell migration and neurite outgrowth under the influence of NT-3. Schwann cells migrated parallel to the direction of the fibers. The migration distance of S100 positive Schwann cells was significantly greater,  $2109 \pm 416 \mu\text{m}$ , on fibers with soluble NT-3 compared to control,  $956 \pm 307 \mu\text{m}$ , where Schwann cell migration was less ( $p < 0.05$ ) (Fig D2). Similar results for neurite outgrowth were also observed. NF160 positive axons extended along the fibers to significantly greater ( $p < 0.05$ ),  $1779 \pm 324 \mu\text{m}$  length than on smooth films,  $778 \pm 258 \mu\text{m}$ . These results demonstrate that NT-3 can enhance migration of neural cells on aligned fibers.

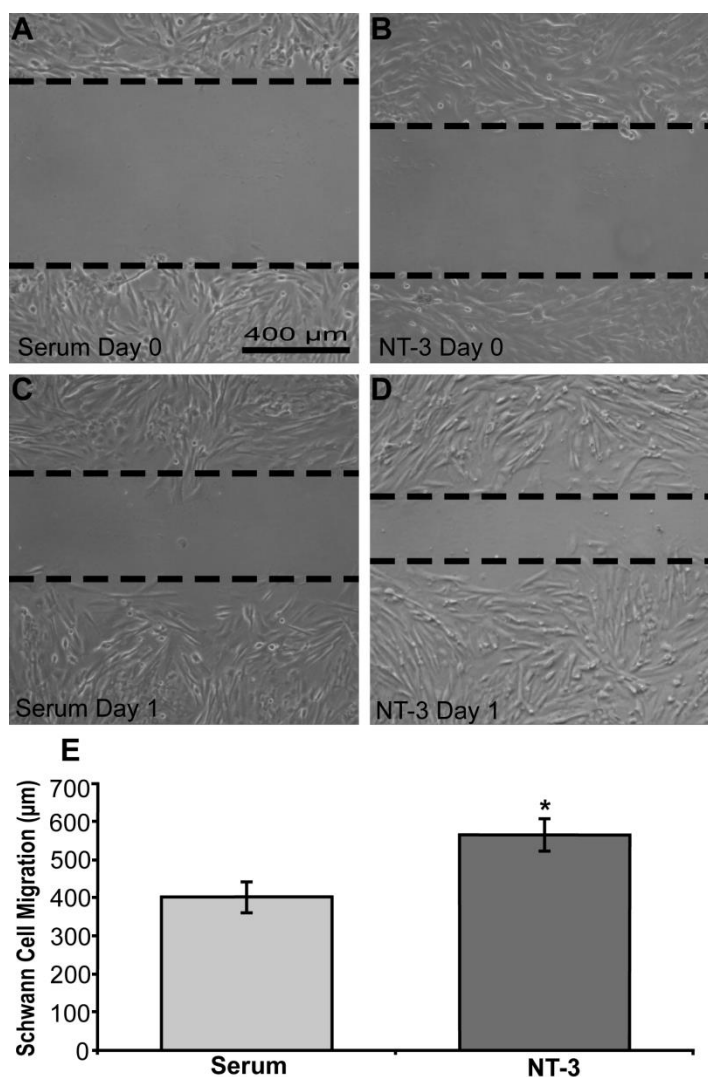


**Figure D-1: Scratch Wound Assay.** (A): Bright field micrograph of the scratch wound in a confluent Schwann cell culture without NT-3 on Day 0. (B): The scratch wound in a confluent Schwann cell culture with NT-3 on Day 0. (C): The scratch wound on Day 1 for the Schwann cell culture without NT-3. (D): The scratch wound on Day 1 for the Schwann cell culture with NT-3. (E): The Schwann cells in the culture with NT-3 added were able to migrate a significantly greater distance over the scratch wound. \* $P < 0.05$ ; the error bars represent standard error of the mean (SEM).



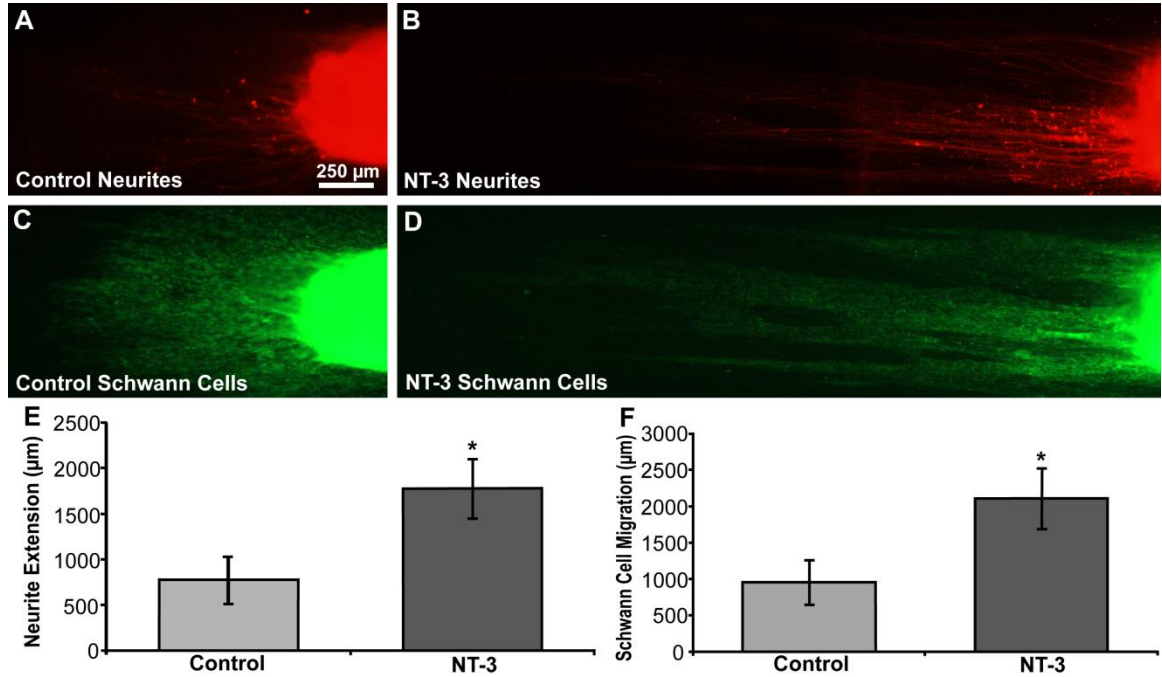


**Figure D-2: DRG Growth on Aligned Fibers After 1 Week.** (A): Neurite extension from DRG without NT-3; stained for NF-160. (B): Neurite extension from DRG with NT-3. (C): Schwann cell migration from DRG without NT-3; stained for S-100. (D): Schwann cell migration from DRG with NT-3. (E): The neurites in cultures with NT-3 added extended a significantly greater distance. (F): The Schwann cells in cultures with NT-3 added migrated a significantly greater distance. \*P < 0.05; the error bars represent SEM.

### **Effects of NT-3 on early nerve regeneration through nerve guidance channels**

To investigate the effects of NT-3 on peripheral nerve regeneration, we released NT-3 *in vivo* using lipid microtubes embedded in agarose within the fiber based conduit. Schwann cell migration and neurite outgrowth from the proximal end of the scaffold were quantified to evaluate the effects of NT-3. A higher density of Schwann cell infiltration was observed in conduits with NT-3 compared to scaffolds with just fiber present. Schwann cells migration was significantly higher in the presence of NT-3 ( $3965 \pm 106 \mu\text{m}$ ) compared to PBS control ( $1928 \pm 610 \mu\text{m}$ ). Neurite outgrowth from the proximal end was also quantified to observe how NT-3 stimulated axonal growth. Scaffold where NT-3 was present, axonal growth was significantly higher ( $3172 \pm 533 \mu\text{m}$ ) compared to PBS control ( $1511 \pm 701 \mu\text{m}$ ). Schwann cells and axons were observed to co-localize in the conduit. This data suggests that Schwann cell migration and neurite outgrowth were both enhanced in the presence of NT-3 in aligned fiber based conduits over 16 days *in vivo* (Figure D3).

### **Effects of NT-3 on long term nerve regeneration through nerve guidance channels**

The results from histology, Figure D4 A-C, and subsequent quantitative morphology analysis showed no significant difference in average myelin thickness between the three experimental groups ( $p=0.09$ ). As seen in Figure D4 D, the average myelin thickness was  $0.479 \pm 0.0236 \mu\text{m}$  for the fiber only group,  $0.572 \pm 0.0262 \mu\text{m}$  for the fiber with NT-3 group, and  $0.528 \pm 0.0274 \mu\text{m}$  for the autograft group. There was also found to be no significant difference between the experimental groups in terms of average circle-equivalent axon diameter ( $p=0.5$ ). However, when the circle-equivalent axon diameter values were divided into  $1 \mu\text{m}$  bins, as seen in Figure 4 E, it was noticed

that for the 0-1  $\mu\text{m}$  range there was a significantly smaller percentage of axons for the fiber only group ( $p=0.001$ ) compared to the other two groups and for the 2-3  $\mu\text{m}$  range the autograft group had a marginally significant fewer percentage of axons ( $p=0.06$ ) than the other two experimental groups. The majority of axons, 74-79%, for all three experimental groups had circle-equivalent diameters in the 1-3  $\mu\text{m}$  range.

As seen in Figure D5, the average compound action potential (CAP) conduction velocity was  $19.9 \pm 2.40$  m/s for the fiber only,  $19.9 \pm 2.30$  m/s for the fiber with NT-3 group, and  $29.1 \pm 2.18$  m/s for the autograft group. While the average CAP conduction velocity for the fiber groups with and without NT-3 were similar, it was significantly higher for the autograft group ( $p<0.05$ ).

It was observed in bright field micrographs of the Masson's trichrome stained gastrocnemius muscle that the autograft group had larger and more uniform muscle cells (Figure D6 C) than the fiber only (Figure D6 A) and fiber with NT-3 (Figure D6 B) groups. The autograft group also had fewer collagen fibers than the other two groups, but the fiber only group tended to have more collagen fibers than the fiber with NT-3 group.

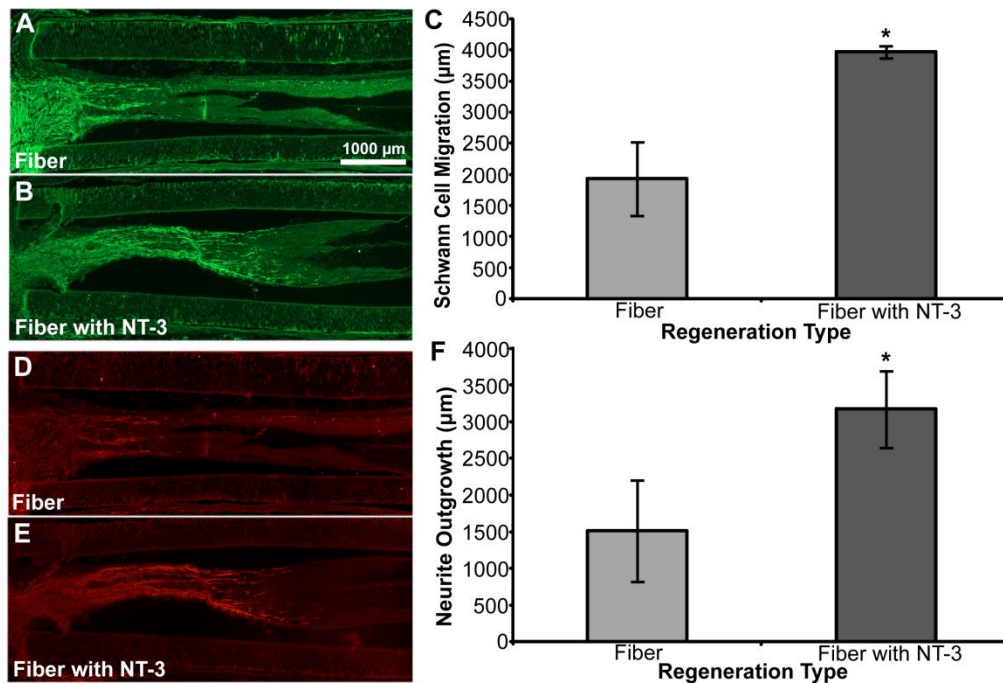


**Figure D-3: Effects of NT-3 after 16 Days In Vivo.** (A): Schwann cell migration along aligned fibers; stained for S-100. (B): Schwann cell migration along aligned fibers with NT-3. (C): Schwann cells migrated a significantly greater distance for the fibers with NT-3 compared to fibers without NT-3. (D): Axon extension along aligned fibers; stained for NF-160. (E): Axon extension along aligned fibers with NT-3. (F) Axons extended a significantly greater distance for the fibers with NT-3 compared to fibers without NT-3. \* $P < 0.05$ ; the error bars represent SEM.

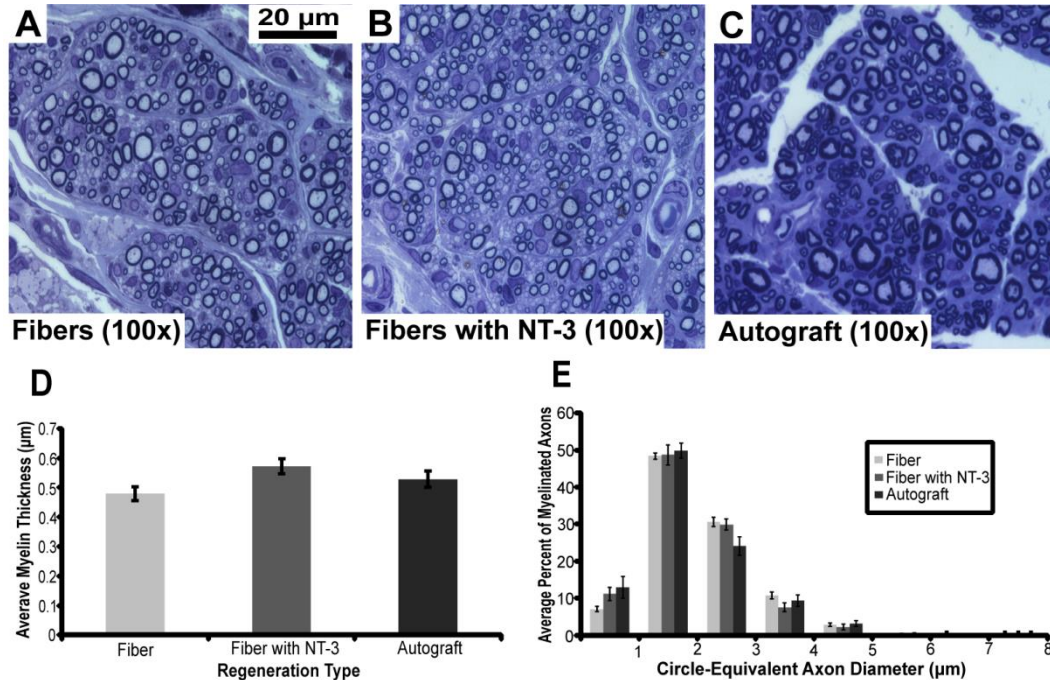


**Figure D-4: Quantitative 20 Week Nerve Morphology.** (A): Representative image at 100x of axons found in the regenerated nerve of the fibers with NT-3 experimental group. (B): Axons typical of the fibers only experimental group. (C): Axons typical of the autograft experimental group. (D): The average myelin thickness was not significantly different between the three experimental groups. (E): A distribution of the circle-equivalent axon diameter for each of the three experimental groups; bin size = 1 μm; error bars represent SEM.

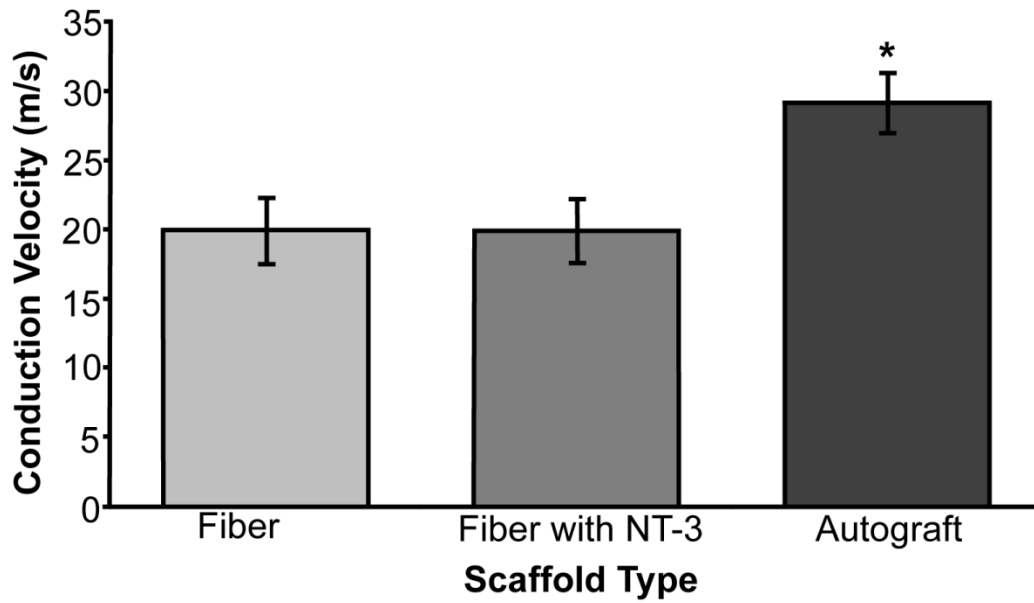


**Figure D-5: Compound Action Potential Conduction Velocity at 20 Weeks.** The fiber only and fiber with NT-3 groups had similar conduction velocities, but the conduction velocity for the autograft group was significantly higher. \* $P < 0.05$ ; error bars represent SEM.

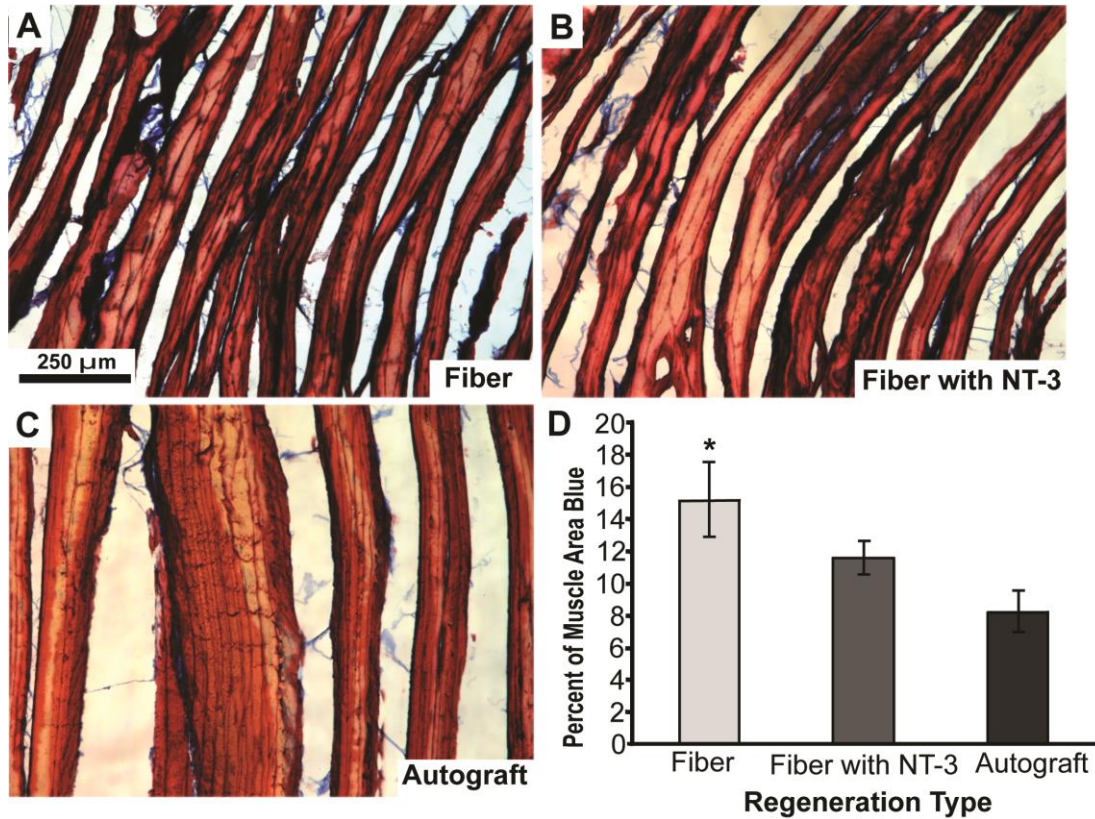


**Figure D-6: Gastrocnemius Muscle at 20 Weeks.** (A): Representative image at 10x of a longitudinal section stained with Masson's trichrome for the fibers only experimental group. (B): Fibers with NT-3. (C): Autograft. (D): The average percent of sampled muscle area that stained positive for collagen (blue). \* $P < 0.035$ ; error bars represent SEM.

## APPENDIX E: PROTOCOL FOR STAINING FIBRIN

1. Allow 2.5g iron alum to dissolve overnight at room temperature in 50 ml. distilled water: to this add 0.25 g of dye and boil for three minutes: filter when cool into a staining jar and add 7 ml. glycerol. Stain for five minutes and rinse in tap water; filter on Mayer's haemalum for five minutes and wash.
2. The yellow mordant is 80 % ethanol, saturated with picric acid 200 ml., orange G 0.4 g., and Lissamine Fast Yellow 2G,0.4 g. Apply yellow mordant for three to five minutes and then wash in tap water for one minute. If used for more than five minutes it may produce some reddening of the nuclear staining.
3. Stain with Acid fuchsin or acid magenta (acid violet 19) used as a 1 % solution in 1% aqueous acetic acid for five minutes and rinse.
4. The differentiator is 30 ml. of the yellow mordant (2 above) with 70 ml. of 80% ethanol. Differentiate for 10 to 15 seconds and rinse.
5. Stain with a 1% solution of phosphotungstic acid in water for five minutes. If the tissue contains hyaline collagen, prolong staining to 10 minutes and then treat with McFarlane's red differentiator.

### McFarlane's Stock Solution

Phosphotungstic acid ..... 25 g.

Picric acid ..... 2.5 g.

95 % ethanol ..... 100 ml.

### McFarlane's Red Differentiator

Stock solution ..... 40 ml.

95% ethanol ..... 40 ml.

Distilled water ..... 20 ml.

6. Stain with soluble blue (acid blue 22) at 1% or light green SF (acid green 5) at 2% in 1% aqueous acetic acid. This dye works slowly.

Mix 40 ml of dibutyl phthalate and 400 ml xylene to mount the slides.



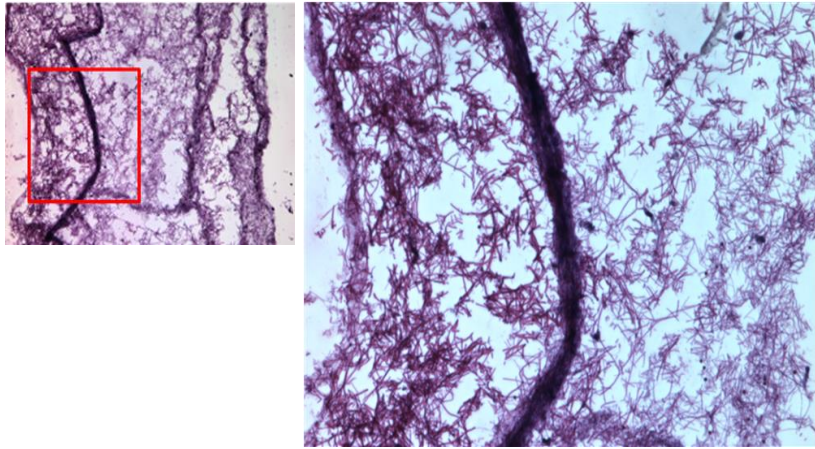


**Figure E-1: Picro-mallory fibrin staining.** A) Fibrin cable interacting with single film fiber scaffold 10x. B) 20x

## REFERENCES

1. *Dodla, M.C. and R.V. Bellamkonda, Differences between the effect of anisotropic and isotropic laminin and nerve growth factor presenting scaffolds on nerve regeneration across long peripheral nerve gaps. Biomaterials, 2008. 29(1): p. 33-46.*
2. *Noble, J., et al., Analysis of upper and lower extremity peripheral nerve injuries in a population of patients with multiple injuries. J Trauma, 1998. 45(1): p. 116-22.*
3. *Lee, S.K. and S.W. Wolfe, Peripheral nerve injury and repair. J Am Acad Orthop Surg, 2000. 8(4): p. 243-52.*
4. *Millesi, H., G. Meissl, and A. Berger, The interfascicular nerve-grafting of the median and ulnar nerves. J Bone Joint Surg Am, 1972. 54(4): p. 727-50.*
5. *Ansselin, A.D. and D.F. Davey, Axonal regeneration through peripheral nerve grafts: the effect of proximo-distal orientation. Microsurgery, 1988. 9(2): p. 103-13.*
6. *Zuo, J., Y.J. Hernandez, and D. Muir, Chondroitin sulfate proteoglycan with neurite-inhibiting activity is up-regulated following peripheral nerve injury. J Neurobiol, 1998. 34(1): p. 41-54.*
7. *Groves, M.L., et al., Axon regeneration in peripheral nerves is enhanced by proteoglycan degradation. Exp Neurol, 2005. 195(2): p. 278-92.*
8. *Nichols, C.M., et al., Effects of motor versus sensory nerve grafts on peripheral nerve regeneration. Exp Neurol, 2004. 190(2): p. 347-55.*
9. *Salzer, J.L. and R.P. Bunge, Studies of Schwann cell proliferation. I. An analysis in tissue culture of proliferation during development, Wallerian degeneration, and direct injury. J Cell Biol, 1980. 84(3): p. 739-52.*
10. *Salzer, J.L., R.P. Bunge, and L. Glaser, Studies of Schwann cell proliferation. III. Evidence for the surface localization of the neurite mitogen. J Cell Biol, 1980. 84(3): p. 767-78.*

11. Salzer, J.L., et al., *Studies of Schwann cell proliferation. II. Characterization of the stimulation and specificity of the response to a neurite membrane fraction. J Cell Biol*, 1980. **84**(3): p. 753-66.
12. Bunge, R.P., *Some observations on the role of the Schwann cells in peripheral nerve regeneration., in Nerve Repair and Regeneration: Its Clinical and Experimental Basis*, D.L. Jewett and H.R. McCarroll, Editors. 1980, C.V. Mosby Co.: St. Louis. p. 371.
13. Williams, L.R., et al., *Spatial-temporal progress of peripheral-nerve regeneration within a silicone chamber - parameters for a bioassay. Journal of Comparative Neurology*, 1983. **218**(4): p. 460-470.
14. Williams, L.R., et al., *Exogenous matrix precursors promote functional nerve regeneration across a 15-mm gap within a silicone chamber in the rat. Journal of Comparative Neurology*, 1987. **264**(2): p. 284-290.
15. Liu, H.M., *The role of extracellular-matrix in peripheral-nerve regeneration - a wound chamber study. Acta Neuropathologica*, 1992. **83**(5): p. 469-474.
16. Williams, L.R., et al., *Competence of nerve-tissue as distal insert promoting nerve regeneration in a silicone chamber. Brain Res*, 1984. **293**(2): p. 201-211.
17. Aebischer, P., V. Guenard, and R.F. Valentini, *The morphology of regenerating peripheral-nerves is modulated by the surface microgeometry of polymeric guidance channels. Brain Res*, 1990. **531**(1-2): p. 211-218.
18. Williams, L.R. and S. Varon, *MODIFICATION OF FIBRIN MATRIX FORMATION INSITU ENHANCES NERVE REGENERATION IN SILICONE CHAMBERS. Journal of Comparative Neurology*, 1985. **231**(2): p. 209-220.

19. Zhao, Q., et al., *Repair of the transected rat sciatic-nerve - matrix formation within implanted silicone tubes. Restorative Neurology and Neuroscience, 1993. 5(3): p. 197-204.*
20. Aebischer, P., et al., *Blind-ended semipermeable guidance channels support peripheral-nerve regeneration in the absence of a distal nerve stump. Brain Res, 1988. 454(1-2): p. 179-187.*
21. Arai, T., G. Lundborg, and L.B. Dahlin, *Bioartificial nerve graft for bridging extended nerve defects in rat sciatic nerve based on resorbable guiding filaments. Scandinavian Journal of Plastic and Reconstructive Surgery and Hand Surgery, 2000. 34(2): p. 101-108.*
22. Ngo, T.T.B., et al., *Poly(L-lactide) microfilaments enhance peripheral nerve regeneration across extended nerve lesions. Journal of Neuroscience Research, 2003. 72(2): p. 227-238.*
23. Anselin, A.D., T. Fink, and D.F. Davey, *Peripheral nerve regeneration through nerve guides seeded with adult Schwann cells. Neuropathol Appl Neurobiol, 1997. 23(5): p. 387-98.*
24. Koshimune, M., et al., *Creating bioabsorbable Schwann cell coated conduits through tissue engineering. Biomed Mater Eng, 2003. 13(3): p. 223-9.*
25. Midha, R., *Emerging techniques for nerve repair: nerve transfers and nerve guidance tubes. Clin Neurosurg, 2006. 53: p. 185-90.*
26. Narakas, A.O., *Thoughts on neurotization or nerve transfers in irreparable nerve lesions. Clin Plast Surg, 1984. 11: p. 153-159.*
27. Tuttle, H.K., *Exposure of the brachial plexus with nerve transplantation. JAMA, 1913. 61: p. 15-17.*

28. Weiss, P., *Scientific apparatus and laboratory methods: Reunion of stumps of small nerves by tubulation instead of suture. Science, 1940. 93(2403): p. 67-67.*
29. Foidart-Dessalle, M., et al., *Sciatic nerve regeneration through venous or nervous grafts in the rat. Exp Neurol, 1997. 148(1): p. 236-46.*
30. Risitano, C., G. Cavallero, and M. Lentini, *Autogenous vein and nerve grafts: A comparative study of nerve regeneration in the rat. J Hand Surg (British Vol) 1989. 14B: p. 102-104.*
31. Kosaka, M., *Enhancement of rat peripheral nerve regeneration through artery-including silicone tubing. Exp Neurol, 1990. 107(1): p. 69-77.*
32. Tseng, C.Y., et al., *Histologic analysis of Schwann cell migration and peripheral nerve regeneration in the autogenous venous nerve conduit (AVNC). J Reconstr Microsurg, 2003. 19(5): p. 331-40.*
33. Kim, Y.T., et al., *The role of aligned polymer fiber-based constructs in the bridging of long peripheral nerve gaps. Biomaterials, 2008.*
34. Belkas, J.S., et al., *Peripheral nerve regeneration through a synthetic hydrogel nerve tube. Restor Neurol Neurosci, 2005. 23(1): p. 19-29.*
35. Nicoli Aldini, N., et al., *Effectiveness of a bioabsorbable conduit in the repair of peripheral nerves. Biomaterials, 1996. 17(10): p. 959-62.*
36. Nicoli Aldini, N., et al., *Guided regeneration with resorbable conduits in experimental peripheral nerve injuries. Int Orthop, 2000. 24(3): p. 121-5.*
37. Lundborg, G., L.B. Dahlin, and N. Danielsen, *Ulnar nerve repair by the silicone chamber technique. Case report. Scand J Plast Reconstr Surg Hand Surg, 1991. 25(1): p. 79-82.*
38. Merle, M., et al., *Complications from silicon-polymer intubulation of nerves. Microsurgery, 1989. 10(2): p. 130-3.*

39. *Lundborg, G., et al., Tubular repair of the median or ulnar nerve in the human forearm: a 5-year follow-up. J Hand Surg [Br], 2004. 29(2): p. 100-7.*
40. *Braga-Silva, J., The use of silicone tubing in the late repair of the median and ulnar nerves in the forearm. J Hand Surg [Br], 1999. 24(6): p. 703-6.*
41. *Belkas, J.S., M.S. Shoichet, and R. Midha, Peripheral nerve regeneration through guidance tubes. Neurol Res, 2004. 26(2): p. 151-60.*
42. *Hudson, T.W., G.R. Evans, and C.E. Schmidt, Engineering strategies for peripheral nerve repair. Clin Plast Surg, 1999. 26(4): p. 617-28, ix.*
43. *Doolabh, V.B., M.C. Hertl, and S.E. Mackinnon, The role of conduits in nerve repair: a review. Rev Neurosci, 1996. 7(1): p. 47-84.*
44. *Hadlock, T., et al., A tissue-engineered conduit for peripheral nerve repair. Arch Otolaryngol Head Neck Surg, 1998. 124(10): p. 1081-6.*
45. *Molander, H., et al., Regeneration of peripheral nerve through a polyglactin tube. Muscle Nerve, 1982. 5(1): p. 54-7.*
46. *Den Dunnen, W.F., et al., Long-term evaluation of nerve regeneration in a biodegradable nerve guide. Microsurgery, 1993. 14(8): p. 508-15.*
47. *Evans, G.R., et al., In vivo evaluation of poly(L-lactic acid) porous conduits for peripheral nerve regeneration. Biomaterials, 1999. 20(12): p. 1109-15.*
48. *Bryan, D.J., et al., Enhanced peripheral nerve regeneration elicited by cell-mediated events delivered via a bioresorbable PLGA guide. J Reconstr Microsurg, 2003. 19(2): p. 125-34.*
49. *Valero-Cabre, A., et al., Superior muscle reinnervation after autologous nerve graft or poly-L-lactide-epsilon-caprolactone (PLC) tube implantation in comparison to silicone tube repair. J Neurosci Res, 2001. 63(2): p. 214-23.*

50. Pankajakshan, D., et al., Development of a fibrin composite-coated poly(epsilon-caprolactone) scaffold for potential vascular tissue engineering applications. *J Biomed Mater Res B Appl Biomater*, 2008. **87**(2): p. 570-9.
51. Atzet, S., et al., Degradable Poly(2-hydroxyethyl methacrylate)-co-polycaprolactone Hydrogels for Tissue Engineering Scaffolds. *Biomacromolecules*, 2008. **9**(12): p. 3370-7.
52. Kim, B.S. and D.J. Mooney, Development of biocompatible synthetic extracellular matrices for tissue engineering. *Trends Biotechnol*, 1998. **16**(5): p. 224-30.
53. Mohanna, P.N., et al., A composite poly-hydroxybutyrate-glia growth factor conduit for long nerve gap repairs. *J Anat*, 2003. **203**(6): p. 553-65.
54. Young, R.C., M. Wiberg, and G. Terenghi, Poly-3-hydroxybutyrate (PHB): a resorbable conduit for long-gap repair in peripheral nerves. *Br J Plast Surg*, 2002. **55**(3): p. 235-40.
55. Doyle, C., E.T. Tanner, and W. Bonfield, In vitro and in vivo evaluation of polyhydroxybutyrate and of polyhydroxybutyrate reinforced with hydroxyapatite. *Biomaterials*, 1991. **12**(9): p. 841-7.
56. Hazari, A., et al., A new resorbable wrap-around implant as an alternative nerve repair technique. *J Hand Surg [Br]*, 1999. **24**(3): p. 291-5.
57. Hazari, A., et al., A resorbable nerve conduit as an alternative to nerve autograft in nerve gap repair. *Br J Plast Surg*, 1999. **52**(8): p. 653-7.
58. Babensee, J.E., et al., Host response to tissue engineered devices. *Adv Drug Deliv Rev*, 1998. **33**(1-2): p. 111-139.
59. Sung, H.J., et al., The effect of scaffold degradation rate on three-dimensional cell growth and angiogenesis. *Biomaterials*, 2004. **25**(26): p. 5735-42.
60. Kweon, H., et al., A novel degradable polycaprolactone networks for tissue engineering. *Biomaterials*, 2003. **24**(5): p. 801-8.

61. Midha, R., et al., Growth factor enhancement of peripheral nerve regeneration through a novel synthetic hydrogel tube. *J Neurosurg*, 2003. **99**(3): p. 555-65.
62. Jenq, C.B. and R.E. Coggeshall, Nerve regeneration through holey silicone tubes. *Brain Res*, 1985. **361**(1-2): p. 233-41.
63. Zhang, N., C. Zhang, and X. Wen, Fabrication of semipermeable hollow fiber membranes with highly aligned texture for nerve guidance. *J Biomed Mater Res A*, 2005. **75**(4): p. 941-9.
64. Valentini, R.F., Nerve guidance channels, in *The Biochemical engineering Handbook*, J. D.Bronzino, Editor 2000, CRC Press LLC: Boca Raton.
65. Ghasemi-Mobarakeh, L., et al., Electrospun poly(epsilon-caprolactone)/gelatin nanofibrous scaffolds for nerve tissue engineering. *Biomaterials*, 2008. **29**(34): p. 4532-9.
66. Valmikinathan, C.M., et al., Novel nanofibrous spiral scaffolds for neural tissue engineering. *J Neural Eng*, 2008. **5**(4): p. 422-32.
67. Ekaputra, A.K., et al., Combining electrospun scaffolds with electrosprayed hydrogels leads to three-dimensional cellularization of hybrid constructs. *Biomacromolecules*, 2008. **9**(8): p. 2097-103.
68. Panseri, S., et al., Electrospun micro- and nanofiber tubes for functional nervous regeneration in sciatic nerve transections. *BMC Biotechnol*, 2008. **8**: p. 39.
69. Prabhakaran, M.P., et al., Electrospun biocomposite nanofibrous scaffolds for neural tissue engineering. *Tissue Eng Part A*, 2008. **14**(11): p. 1787-97.
70. Healy, J.M., et al., Pharmacokinetics and biodistribution of novel aptamer compositions. *Pharm Res*, 2004. **21**(12): p. 2234-46.
71. Weddell, G., Axonal regeneration in cutaneous nerve plexuses. *J Anat*, 1942. **77**(Pt 1): p. 49-62 3.



72. Holmes, D.F., et al., *STEM/TEM studies of collagen fibril assembly. Micron*, 2001. **32**(3): p. 273-85.
73. Birk, D.E. and F.H. Silver, *Collagen fibrillogenesis in vitro: comparison of types I, II, and III. Arch Biochem Biophys*, 1984. **235**(1): p. 178-85.
74. Archibald, S.J., et al., *A collagen-based nerve guide conduit for peripheral nerve repair: an electrophysiological study of nerve regeneration in rodents and nonhuman primates. J Comp Neurol*, 1991. **306**(4): p. 685-96.
75. Archibald, S.J., et al., *Monkey median nerve repaired by nerve graft or collagen nerve guide tube. J Neurosci*, 1995. **15**(5 Pt 2): p. 4109-23.
76. Kemp, S.W., et al., *Collagen Nerve Conduits Promote Enhanced Axonal Regeneration, Schwann Cell Association, and Neovascularization Compared to Silicone Conduits. Tissue Eng Part A*, 2009.
77. Kalbermatten, D.F., et al., *New fibrin conduit for peripheral nerve repair. J Reconstr Microsurg*, 2009. **25**(1): p. 27-33.
78. Zeugolis, D.I., et al., *Electro-spinning of pure collagen nano-fibres - just an expensive way to make gelatin? Biomaterials*, 2008. **29**(15): p. 2293-305.
79. Cao, X. and M.S. Shoichet, *Defining the concentration gradient of nerve growth factor for guided neurite outgrowth. Neuroscience*, 2001. **103**(3): p. 831-40.
80. Piotrowicz, A. and M.S. Shoichet, *Nerve guidance channels as drug delivery vehicles. Biomaterials*, 2006. **27**(9): p. 2018-27.
81. Chew, S.Y., et al., *Sustained release of proteins from electrospun biodegradable fibers. Biomacromolecules*, 2005. **6**(4): p. 2017-24.

82. Xu, X., et al., *Peripheral nerve regeneration with sustained release of poly(phosphoester) microencapsulated nerve growth factor within nerve guide conduits. Biomaterials, 2003. 24(13): p. 2405-12.*
83. Tabata, Y., *Tissue regeneration based on growth factor release. Tissue Eng, 2003. 9 Suppl 1: p. S5-15.*
84. Sahenk, Z., J. Seharaseyon, and J.R. Mendell, *CNTF potentiates peripheral nerve regeneration. Brain Res, 1994. 655(1-2): p. 246-50.*
85. Yamauchi, J., J.R. Chan, and E.M. Shooter, *Neurotrophins regulate Schwann cell migration by activating divergent signaling pathways dependent on Rho GTPases. Proc Natl Acad Sci U S A, 2004. 101(23): p. 8774-9.*
86. Vogelin, E., et al., *Effects of local continuous release of brain derived neurotrophic factor (BDNF) on peripheral nerve regeneration in a rat model. Exp Neurol, 2006. 199(2): p. 348-53.*
87. Utley, D.S., et al., *Brain-derived neurotrophic factor and collagen tubulization enhance functional recovery after peripheral nerve transection and repair. Arch Otolaryngol Head Neck Surg, 1996. 122(4): p. 407-13.*
88. Yang, Y., et al., *Development and evaluation of silk fibroin-based nerve grafts used for peripheral nerve regeneration. Biomaterials, 2007. 28(36): p. 5526-35.*
89. Yamauchi, J., et al., *The neurotrophin-3 receptor TrkC directly phosphorylates and activates the nucleotide exchange factor Dbs to enhance Schwann cell migration. Proc Natl Acad Sci U S A, 2005. 102(14): p. 5198-203.*
90. Yamauchi, J., J.R. Chan, and E.M. Shooter, *Neurotrophin 3 activation of TrkC induces Schwann cell migration through the c-Jun N-terminal kinase pathway. Proc Natl Acad Sci U S A, 2003. 100(24): p. 14421-6.*

91. Fukaya, K., et al., *Oxidized galectin-1 stimulates the migration of Schwann cells from both proximal and distal stumps of transected nerves and promotes axonal regeneration after peripheral nerve injury. J Neuropathol Exp Neurol*, 2003. **62**(2): p. 162-72.
92. Thompson, D.M. and H.M. Buettner, *Schwann cell response to micropatterned laminin surfaces. Tissue Eng*, 2001. **7**(3): p. 247-65.
93. Yu, X. and R.V. Bellamkonda, *Tissue-engineered scaffolds are effective alternatives to autografts for bridging peripheral nerve gaps. Tissue Eng*, 2003. **9**(3): p. 421-30.
94. Zhang, Z., et al., *Neurite outgrowth on well-characterized surfaces: preparation and characterization of chemically and spatially controlled fibronectin and RGD substrates with good bioactivity. Biomaterials*, 2005. **26**(1): p. 47-61.
95. Ahmed, Z., S. Underwood, and R.A. Brown, *Nerve guide material made from fibronectin: assessment of in vitro properties. Tissue Eng*, 2003. **9**(2): p. 219-31.
96. Deister, C., S. Aljabari, and C.E. Schmidt, *Effects of collagen 1, fibronectin, laminin and hyaluronic acid concentration in multi-component gels on neurite extension. J Biomater Sci Polym Ed*, 2007. **18**(8): p. 983-97.
97. Tonge, D.A., et al., *Effects of extracellular matrix components on axonal outgrowth from peripheral nerves of adult animals in vitro. Exp Neurol*, 1997. **146**(1): p. 81-90.
98. Silva, G.A., et al., *Selective differentiation of neural progenitor cells by high-epitope density nanofibers. Science*, 2004. **303**(5662): p. 1352-5.
99. Kiyotani, T., et al., *Nerve regeneration across a 25-mm gap bridged by a polyglycolic acid-collagen tube: a histological and electrophysiological evaluation of regenerated nerves. Brain Res*, 1996. **740**(1-2): p. 66-74.

100. Lohmeyer, J.A., et al., Bridging extended nerve defects with an artificial nerve graft containing Schwann cells pre-seeded on polyglactin filaments. *Int J Artif Organs*, 2007. **30**(1): p. 64-74.
101. Hadlock, T.A., et al., A new artificial nerve graft containing rolled Schwann cell monolayers. *Microsurgery*, 2001. **21**(3): p. 96-101.
102. Mosahebi, A., et al., Effect of allogeneic Schwann cell transplantation on peripheral nerve regeneration. *Exp Neurol*, 2002. **173**(2): p. 213-23.
103. Tsuda, Y., et al., Cellular control of tissue architectures using a three-dimensional tissue fabrication technique. *Biomaterials*, 2007. **28**(33): p. 4939-46.
104. Haastert, K., et al., Differentially promoted peripheral nerve regeneration by grafted Schwann cells over-expressing different FGF-2 isoforms. *Neurobiol Dis*, 2006. **21**(1): p. 138-53.
105. Marchesi, C., et al., Skin-derived stem cells transplanted into resorbable guides provide functional nerve regeneration after sciatic nerve resection. *Glia*, 2007. **55**(4): p. 425-38.
106. Nie, X., et al., Improvement of peripheral nerve regeneration by a tissue-engineered nerve filled with ectomesenchymal stem cells. *Int J Oral Maxillofac Surg*, 2007. **36**(1): p. 32-8.
107. Keilhoff, G., et al., Transdifferentiation of mesenchymal stem cells into Schwann cell-like myelinating cells. *Eur J Cell Biol*, 2006. **85**(1): p. 11-24.
108. Mimura, T., et al., Peripheral nerve regeneration by transplantation of bone marrow stromal cell-derived Schwann cells in adult rats. *J Neurosurg*, 2004. **101**(5): p. 806-12.
109. Takahashi, K. and S. Yamanaka, Induction of pluripotent stem cells from mouse embryonic and adult fibroblast cultures by defined factors. *Cell*, 2006. **126**(4): p. 663-76.

110. Dimos, J.T., et al., *Induced pluripotent stem cells generated from patients with ALS can be differentiated into motor neurons. Science, 2008. 321(5893): p. 1218-21.*
111. Nix, W.A. and H.C. Hopf, *Electrical stimulation of regenerating nerve and its effect on motor recovery. Brain Res, 1983. 272(1): p. 21-5.*
112. Geremia, N.M., et al., *Electrical stimulation promotes sensory neuron regeneration and growth-associated gene expression. Exp Neurol, 2007. 205(2): p. 347-59.*
113. Al-Majed, A.A., et al., *Brief electrical stimulation promotes the speed and accuracy of motor axonal regeneration. J Neurosci, 2000. 20(7): p. 2602-8.*
114. English, A.W., et al., *Electrical stimulation promotes peripheral axon regeneration by enhanced neuronal neurotrophin signaling. Dev Neurobiol, 2007. 67(2): p. 158-72.*
115. Fine, E.G., et al., *Improved nerve regeneration through piezoelectric vinylidene fluoride-trifluoroethylene copolymer guidance channels. Biomaterials, 1991. 12(8): p. 775-780.*
116. Lee, J.Y., J.W. Lee, and C.E. Schmidt, *Neuroactive conducting scaffolds: nerve growth factor conjugation on active ester-functionalized polypyrrole. J R Soc Interface, 2008.*
117. Dubin, R.A., et al., *Carbon nanotube fibers are compatible with Mammalian cells and neurons. IEEE Trans Nanobioscience, 2008. 7(1): p. 11-4.*
118. Malarkey, E.B. and V. Parpura, *Applications of carbon nanotubes in neurobiology. Neurodegener Dis, 2007. 4(4): p. 292-9.*
119. Cellot, G., et al., *Carbon nanotubes might improve neuronal performance by favouring electrical shortcuts. Nat Nanotechnol, 2009. 4(2): p. 126-33.*
120. Li, N. and A. Folch, *Integration of topographical and biochemical cues by axons during growth on microfabricated 3-D substrates. Exp Cell Res, 2005. 311(2): p. 307-16.*
121. Johansson, F., et al., *Axonal outgrowth on nano-imprinted patterns. Biomaterials, 2006. 27(8): p. 1251-8.*

122. Britland S., P.C., Denyer M., Morgan H., Curtis A., and Wilkinson C., Morphogenetic guidance cues can interact synergistically and hierarchically in steering nerve cell growth. *Experimental Biology Online*, 1996. **1**(2): p. 1-15.
123. Ressler, L., et al., Fabrication of planar cobalt electrodes separated by a sub-10nm gap using high resolution electron beam lithography with negative PMMA. *Ultramicroscopy*, 2007. **107**(10-11): p. 985-8.
124. Wilkinson, C.D., Making structures for cell engineering. *Eur Cell Mater*, 2004. **8**: p. 21-5; discussion 25-6.
125. Wilson, D.L., et al., Surface organization and nanopatterning of collagen by dip-pen nanolithography. *Proc Natl Acad Sci U S A*, 2001. **98**(24): p. 13660-4.
126. Murugan, R. and S. Ramakrishna, Design strategies of tissue engineering scaffolds with controlled fiber orientation. *Tissue Eng*, 2007. **13**(8): p. 1845-66.
127. Silva, G.A., Nanotechnology approaches for the regeneration and neuroprotection of the central nervous system. *Surg Neurol*, 2005. **63**(4): p. 301-6.
128. Hung, A.M. and S.I. Stupp, Simultaneous self-assembly, orientation, and patterning of peptide-amphiphile nanofibers by soft lithography. *Nano Lett*, 2007. **7**(5): p. 1165-71.
129. Yang, Y., et al., Biocompatibility evaluation of silk fibroin with peripheral nerve tissues and cells in vitro. *Biomaterials*, 2007. **28**(9): p. 1643-52.
130. Allmeling, C., et al., Use of spider silk fibres as an innovative material in a biocompatible artificial nerve conduit. *J Cell Mol Med*, 2006. **10**(3): p. 770-7.
131. Dubey, N., P.C. Letourneau, and R.T. Tranquillo, Guided neurite elongation and schwann cell invasion into magnetically aligned collagen in simulated peripheral nerve regeneration. *Exp Neurol*, 1999. **158**(2): p. 338-50.

132. Li, M., et al., *Electrospinning polyaniline-contained gelatin nanofibers for tissue engineering applications. Biomaterials*, 2006. **27**(13): p. 2705-15.
133. Li, W.J., et al., *Electrospun nanofibrous structure: a novel scaffold for tissue engineering. J Biomed Mater Res*, 2002. **60**(4): p. 613-21.
134. Recknor, J.B., D.S. Sakaguchi, and S.K. Mallapragada, *Directed growth and selective differentiation of neural progenitor cells on micropatterned polymer substrates. Biomaterials*, 2006. **27**(22): p. 4098-108.
135. Bidez, P.R., 3rd, et al., *Polyaniline, an electroactive polymer, supports adhesion and proliferation of cardiac myoblasts. J Biomater Sci Polym Ed*, 2006. **17**(1-2): p. 199-212.
136. Schnell, E., et al., *Guidance of glial cell migration and axonal growth on electrospun nanofibers of poly-epsilon-caprolactone and a collagen/poly-epsilon-caprolactone blend. Biomaterials*, 2007. **28**(19): p. 3012-25.
137. Hsu, S.H., et al., *Fabrication and evaluation of microgrooved polymers as peripheral nerve conduits. Biomed Microdevices*, 2007. **9**(5): p. 665-74.
138. Thompson, D.M. and H.M. Buettner, *Oriented Schwann cell monolayers for directed neurite outgrowth. Ann Biomed Eng*, 2004. **32**(8): p. 1120-30.
139. Hadlock, T., et al., *A polymer foam conduit seeded with Schwann cells promotes guided peripheral nerve regeneration. Tissue Eng*, 2000. **6**(2): p. 119-27.
140. Glass-Brudzinski, J., D. Perizzolo, and D.M. Brunette, *Effects of substratum surface topography on the organization of cells and collagen fibers in collagen gel cultures. J Biomed Mater Res*, 2002. **61**(4): p. 608-18.
141. Charest, J.L., A.J. Garcia, and W.P. King, *Myoblast alignment and differentiation on cell culture substrates with microscale topography and model chemistries. Biomaterials*, 2007. **28**(13): p. 2202-10.

142. Manwaring, M.E., J.F. Walsh, and P.A. Tresco, Contact guidance induced organization of extracellular matrix. *Biomaterials*, 2004. **25**(17): p. 3631-8.
143. Luthen, F., et al., The influence of surface roughness of titanium on beta1- and beta3-integrin adhesion and the organization of fibronectin in human osteoblastic cells. *Biomaterials*, 2005. **26**(15): p. 2423-40.
144. Chamberlain, L.J., et al., Collagen-GAG substrate enhances the quality of nerve regeneration through collagen tubes up to level of autograft. *Exp Neurol*, 1998. **154**(2): p. 315-329.
145. Yoshii, S. and M. Oka, Collagen filaments as a scaffold for nerve regeneration. *J Biomed Mater Res A*, 2001. **56**(3): p. 400-405.
146. Ceballos, D., et al., Magnetically aligned collagen gel filling a collagen nerve guide improves peripheral nerve regeneration. *Exp Neurol*, 1999. **158**(2): p. 290-300.
147. Yoshii, S., et al., 30 mm regeneration of rat sciatic nerve along collagen filaments. *Brain Res*, 2002. **949**(1-2): p. 202-208.
148. Matsusaki, M., et al., Fabrication of cellular multilayers with nanometer-sized extracellular matrix films. *Angew Chem Int Ed Engl*, 2007. **46**(25): p. 4689-92.
149. Cai, J., et al., Permeable guidance channels containing microfilament scaffolds enhance axon growth and maturation. *J Biomed Mater Res A*, 2005. **75**(2): p. 374-86.
150. Lundborg, G., et al., Nerve regeneration in silicone chambers: influence of gap length and of distal stump components. *Exp Neurol*, 1982. **76**(2): p. 361-75.
151. Rutkowski, G.E., et al., Synergistic effects of micropatterned biodegradable conduits and Schwann cells on sciatic nerve regeneration. *J Neural Eng*, 2004. **1**(3): p. 151-7.



152. Bini, T.B., et al., *Electrospun poly(L-lactide-co-glycolide) biodegradable polymer nanofibre tubes for peripheral nerve regeneration*. *Nanotechnology*, 2004. **15**(11): p. 1459-1464.
153. Chen, M.B., F. Zhang, and W.C. Lineaweaver, *Luminal fillers in nerve conduits for peripheral nerve repair*. *Ann Plast Surg*, 2006. **57**(4): p. 462-71.
154. Schlosshauer, B., et al., *Synthetic nerve guide implants in humans: a comprehensive survey*. *Neurosurgery*, 2006. **59**(4): p. 740-7; discussion 747-8.
155. Hoke, A. and T. Brushart, *Introduction to special issue: Challenges and opportunities for regeneration in the peripheral nervous system*. *Exp Neurol*, 2010. **223**(1): p. 1-4.
156. Ribeiro-Resende, V.T., et al., *Strategies for inducing the formation of bands of Bungner in peripheral nerve regeneration*. *Biomaterials*, 2009. **30**(29): p. 5251-9.
157. Shin, R.H., et al., *Treatment of a segmental nerve defect in the rat with use of bioabsorbable synthetic nerve conduits: a comparison of commercially available conduits*. *J Bone Joint Surg Am*, 2009. **91**(9): p. 2194-204.
158. Evans, G.R., *Challenges to nerve regeneration*. *Semin Surg Oncol*, 2000. **19**(3): p. 312-8.
159. Dillon, G.P., et al., *The influence of physical structure and charge on neurite extension in a 3D hydrogel scaffold*. *J Biomater Sci Polym Ed*, 1998. **9**(10): p. 1049-69.
160. Koh, H.S., et al., *In vivo study of novel nanofibrous intra-luminal guidance channels to promote nerve regeneration*. *J Neural Eng*, 2010. **7**(4): p. 046003.
161. Nisbet, D.R., et al., *Review paper: a review of the cellular response on electrospun nanofibers for tissue engineering*. *J Biomater Appl*, 2009. **24**(1): p. 7-29.
162. Venugopal, J., et al., *Nanotechnology for nanomedicine and delivery of drugs*. *Curr Pharm Des*, 2008. **14**(22): p. 2184-200.

163. Clements, I.P., et al., *Thin-film enhanced nerve guidance channels for peripheral nerve repair. Biomaterials*, 2009. **30**(23-24): p. 3834-3846.
164. Hoffman-Kim, D., J.A. Mitchel, and R.V. Bellamkonda, *Topography, cell response, and nerve regeneration. Annu Rev Biomed Eng*, 2010. **12**: p. 203-31.
165. Yang, Y. and K.W. Leong, *Nanoscale surfacing for regenerative medicine. Wiley Interdiscip Rev Nanomed Nanobiotechnol*, 2010. **2**(5): p. 478-95.
166. Badami, A.S., et al., *Effect of fiber diameter on spreading, proliferation, and differentiation of osteoblastic cells on electrospun poly(lactic acid) substrates. Biomaterials*, 2006. **27**(4): p. 596-606.
167. Chew, S.Y., et al., *The effect of the alignment of electrospun fibrous scaffolds on Schwann cell maturation. Biomaterials*, 2008. **29**(6): p. 653-61.
168. Shih, Y.R., et al., *Growth of mesenchymal stem cells on electrospun type I collagen nanofibers. Stem Cells*, 2006. **24**(11): p. 2391-7.
169. Smeal, R.M., et al., *Substrate curvature influences the direction of nerve outgrowth. Ann Biomed Eng*, 2005. **33**(3): p. 376-82.
170. Brockes, J.P., K.L. Fields, and M.C. Raff, *Studies on cultured rat Schwann cells. I. Establishment of purified populations from cultures of peripheral nerve. Brain Res*, 1979. **165**(1): p. 105-18.
171. Mukhatyar, V., et al., *Tissue Engineering Strategies Designed to Realize the Endogenous Regenerative Potential of Peripheral Nerves. Advanced Materials*, 2009. **21**(46): p. 4670-4679.
172. Xu, X.M., et al., *Axonal regeneration into Schwann cell-seeded guidance channels grafted into transected adult rat spinal cord. J Comp Neurol*, 1995. **351**(1): p. 145-60.

173. Cornbrooks, C.J., et al., *In vivo and in vitro observations on laminin production by Schwann cells. Proc Natl Acad Sci U S A*, 1983. **80**(12): p. 3850-4.
174. McGarvey, M.L., et al., *Synthesis and effects of basement membrane components in cultured rat Schwann cells. Dev Biol*, 1984. **105**(1): p. 18-28.
175. Gupta, D., et al., *Aligned and random nanofibrous substrate for the in vitro culture of Schwann cells for neural tissue engineering. Acta Biomater*, 2009. **5**(7): p. 2560-9.
176. Wang, W., et al., *Effects of Schwann cell alignment along the oriented electrospun chitosan nanofibers on nerve regeneration. J Biomed Mater Res A*, 2009. **91**(4): p. 994-1005.
177. Torigoe, K., K. Hashimoto, and G. Lundborg, *A role of migratory Schwann cells in a conditioning effect of peripheral nerve regeneration. Exp Neurol*, 1999. **160**(1): p. 99-108.
178. Torigoe, K., *The role of migratory Schwann cells in nerve regeneration as studied by the film model. J Peripher Nerv Syst*, 1997. **2**(3): p. 227-31.
179. Bettinger, C.J., R. Langer, and J.T. Borenstein, *Engineering substrate topography at the micro- and nanoscale to control cell function. Angew Chem Int Ed Engl*, 2009. **48**(30): p. 5406-15.
180. Baron-Van Evercooren, A., et al., *Fibronectin promotes rat Schwann cell growth and motility. J Cell Biol*, 1982. **93**(1): p. 211-6.
181. Bailey, S.B., et al., *The influence of fibronectin and laminin during Schwann cell migration and peripheral nerve regeneration through silicon chambers. J Neurocytol*, 1993. **22**(3): p. 176-84.
182. Brown, R.A. and J.B. Phillips, *Cell responses to biomimetic protein scaffolds used in tissue repair and engineering. Int Rev Cytol*, 2007. **262**: p. 75-150.

183. Sell, S., et al., *Extracellular matrix regenerated: tissue engineering via electrospun biomimetic nanofibers*. *Polymer International*, 2007. **56**(11): p. 1349-1360.
184. Woo, K.M., V.J. Chen, and P.X. Ma, *Nano-fibrous scaffolding architecture selectively enhances protein adsorption contributing to cell attachment*. *J Biomed Mater Res A*, 2003. **67A**(2): p. 531-537.
185. Previtali, S.C., et al., *The extracellular matrix affects axonal regeneration in peripheral neuropathies*. *Neurology*, 2008. **71**(5): p. 322-31.
186. Milner, R., et al., *Division of labor of Schwann cell integrins during migration on peripheral nerve extracellular matrix ligands*. *Dev Biol*, 1997. **185**(2): p. 215-28.
187. Ahmed, Z. and R.A. Brown, *Adhesion, alignment, and migration of cultured Schwann cells on ultrathin fibronectin fibres*. *Cell Motil Cytoskeleton*, 1999. **42**(4): p. 331-43.
188. Ruoslahti, E. and M.D. Pierschbacher, *New perspectives in cell adhesion: RGD and integrins*. *Science*, 1987. **238**(4826): p. 491-7.
189. Gonzalez-Garcia, C., et al., *Effect of nanoscale topography on fibronectin adsorption, focal adhesion size and matrix organisation*. *Colloids Surf B Biointerfaces*, 2010. **77**(2): p. 181-90.
190. Rico, P., et al., *Substrate-induced assembly of fibronectin into networks: influence of surface chemistry and effect on osteoblast adhesion*. *Tissue Eng Part A*, 2009. **15**(11): p. 3271-81.
191. Diener, A., et al., *Control of focal adhesion dynamics by material surface characteristics*. *Biomaterials*, 2005. **26**(4): p. 383-92.
192. Keselowsky, B.G., D.M. Collard, and A.J. Garcia, *Surface chemistry modulates focal adhesion composition and signaling through changes in integrin binding*. *Biomaterials*, 2004. **25**(28): p. 5947-54.

193. Gugutkov, D., et al., *Biological activity of the substrate-induced fibronectin network: insight into the third dimension through electrospun fibers*. *Langmuir*, 2009. **25**(18): p. 10893-900.
194. Luis, A.L., et al., *Evaluation of two biodegradable nerve guides for the reconstruction of the rat sciatic nerve*. *Biomed Mater Eng*, 2007. **17**(1): p. 39-52.
195. Li, W.J., et al., *Fabrication and characterization of six electrospun poly(alpha-hydroxy ester)-based fibrous scaffolds for tissue engineering applications*. *Acta Biomater*, 2006. **2**(4): p. 377-85.
196. Zhang, C., et al., *Early spatiotemporal progress of myelinated nerve fiber regenerating through biological chitin conduit after injury*. *Artif Cells Blood Substit Immobil Biotechnol*, 2010. **38**(2): p. 103-8.
197. Arai, T., G. Lundborg, and L.B. Dahlin, *Bioartificial nerve graft for bridging extended nerve defects in rat sciatic nerve based on resorbable guiding filaments*. *Scand J Plast Reconstr Surg Hand Surg*, 2000. **34**(2): p. 101-8.
198. Kim, S.M., S.K. Lee, and J.H. Lee, *Peripheral nerve regeneration using a three dimensionally cultured schwann cell conduit*. *J Craniofac Surg*, 2007. **18**(3): p. 475-88.
199. Li, Q., et al., *Nerve conduit filled with GDNF gene-modified Schwann cells enhances regeneration of the peripheral nerve*. *Microsurgery*, 2006. **26**(2): p. 116-21.
200. Tansey, K.E., et al., *Peripheral nerve repair through multi-luminal biosynthetic implants*. *Ann Biomed Eng*, 2011. **39**(6): p. 1815-28.
201. Lynam, D., et al., *Precision microchannel scaffolds for central and peripheral nervous system repair*. *J Mater Sci Mater Med*, 2011. **22**(9): p. 2119-30.
202. Yoshii, S. and M. Oka, *Peripheral nerve regeneration along collagen filaments*. *Brain Res*, 2001. **888**(1): p. 158-162.

203. Kim, Y.T., et al., *The role of aligned polymer fiber-based constructs in the bridging of long peripheral nerve gaps. Biomaterials*, 2008. **29**(21): p. 3117-27.
204. Sterne, G.D., et al., *Neurotrophin-3 delivered locally via fibronectin mats enhances peripheral nerve regeneration. Eur J Neurosci*, 1997. **9**(7): p. 1388-96.
205. Mukhatyar, V.J., et al., *Role of fibronectin in topographical guidance of neurite extension on electrospun fibers. Biomaterials*, 2011. **32**(16): p. 3958-68.
206. Steed, M.B., et al., *Advances in bioengineered conduits for peripheral nerve regeneration. Atlas Oral Maxillofac Surg Clin North Am*, 2011. **19**(1): p. 119-30.
207. Krick, K., et al., *Signaling cue presentation and cell delivery to promote nerve regeneration. Curr Opin Biotechnol*, 2011. **22**(5): p. 741-6.
208. Sarig-Nadir, O. and D. Seliktar, *Compositional alterations of fibrin-based materials for regulating in vitro neural outgrowth. Tissue engineering. Part A*, 2008. **14**(3): p. 401-11.
209. Pittier, R., et al., *Neurite extension and in vitro myelination within three-dimensional modified fibrin matrices. Journal of neurobiology*, 2005. **63**(1): p. 1-14.
210. Akassoglou, K., et al., *Fibrin is a regulator of Schwann cell migration after sciatic nerve injury in mice. Neuroscience letters*, 2003. **338**(3): p. 185-8.
211. Cotter, L., et al., *Dlg1-PTEN interaction regulates myelin thickness to prevent damaging peripheral nerve overmyelination. Science*, 2010. **328**(5984): p. 1415-8.
212. Martini, R., et al., *Interactions between Schwann cells and macrophages in injury and inherited demyelinating disease. Glia*, 2008. **56**(14): p. 1566-77.
213. Rotshenker, S., *Wallerian degeneration: the innate-immune response to traumatic nerve injury. J Neuroinflammation*, 2011. **8**: p. 109.
214. Taskinen, H.S., et al., *Peripheral nerve injury induces endoneurial expression of IFN-gamma, IL-10 and TNF-alpha mRNA. J Neuroimmunol*, 2000. **102**(1): p. 17-25.

215. Saino, E., et al., *Effect of electrospun fiber diameter and alignment on macrophage activation and secretion of proinflammatory cytokines and chemokines. Biomacromolecules*, 2011. **12**(5): p. 1900-11.
216. Gaudet, A.D., P.G. Popovich, and M.S. Ramer, *Wallerian degeneration: gaining perspective on inflammatory events after peripheral nerve injury. J Neuroinflammation*, 2011. **8**: p. 110.
217. Scholz, J. and C.J. Woolf, *The neuropathic pain triad: neurons, immune cells and glia. Nat Neurosci*, 2007. **10**(11): p. 1361-8.
218. Anton, E.S., et al., *Nerve growth factor and its low-affinity receptor promote Schwann cell migration. Proc Natl Acad Sci U S A*, 1994. **91**(7): p. 2795-9.
219. Cragnolini, A.B. and W.J. Friedman, *The function of p75NTR in glia. Trends Neurosci*, 2008. **31**(2): p. 99-104.
220. Hempstead, B.L., *Coupling neurotrophins to cell migration through selective guanine nucleotide exchange factor activation. Proc Natl Acad Sci U S A*, 2005. **102**(16): p. 5645-6.
221. Carroll, S.L., et al., *Expression of neuregulins and their putative receptors, ErbB2 and ErbB3, is induced during Wallerian degeneration. J Neurosci*, 1997. **17**(5): p. 1642-59.
222. Thanos, P.K., S. Okajima, and J.K. Terzis, *Ultrastructure and cellular biology of nerve regeneration. J Reconstr Microsurg*, 1998. **14**(6): p. 423-36.
223. Terzis, J.K., D.D. Sun, and P.K. Thanos, *Historical and basic science review: past, present, and future of nerve repair. J Reconstr Microsurg*, 1997. **13**(3): p. 215-25.
224. Kolachala, V.L., et al., *The use of lipid microtubes as a novel slow-release delivery system for laryngeal injection. Laryngoscope*, 2011. **121**(6): p. 1237-43.

225. Meilander, N.J., et al., Sustained release of plasmid DNA using lipid microtubules and agarose hydrogel. *Journal of controlled release : official journal of the Controlled Release Society*, 2003. **88**(2): p. 321-31.
226. Meilander, N.J., et al., Lipid-based microtubular drug delivery vehicles. *Journal of controlled release : official journal of the Controlled Release Society*, 2001. **71**(1): p. 141-52.
227. Nakayama, K., et al., Enhancement of peripheral nerve regeneration using bioabsorbable polymer tubes packed with fibrin gel. *Artificial Organs*, 2007. **31**(7): p. 500-508.
228. Schnur, J.M., et al., Diacetylenic lipid tubules: experimental evidence for a chiral molecular architecture. *Science*, 1994. **264**(5161): p. 945-7.
229. Schnur, J.M., Lipid tubules: a paradigm for molecularly engineered structures. *Science*, 1993. **262**(5140): p. 1669-76.
230. Kaushik, J.K. and R. Bhat, Why is trehalose an exceptional protein stabilizer? An analysis of the thermal stability of proteins in the presence of the compatible osmolyte trehalose. *J Biol Chem*, 2003. **278**(29): p. 26458-65.
231. Sulaiman, O.A., et al., Chronic Schwann cell denervation and the presence of a sensory nerve reduce motor axonal regeneration. *Exp Neurol*, 2002. **176**(2): p. 342-54.
232. Williams, L.R., Exogenous fibrin matrix precursors stimulate the temporal progress of nerve regeneration within a silicone chamber. *Neurochemical Research*, 1987. **12**(10): p. 851-860.
233. Miller, C., S. Jeftinija, and S. Mallapragada, Synergistic effects of physical and chemical guidance cues on neurite alignment and outgrowth on biodegradable polymer substrates. *Tissue Eng*, 2002. **8**(3): p. 367-78.



234. Curtis, A. and C. Wilkinson, *Topographical control of cells. Biomaterials*, 1997. **18**(24): p. 1573-1583.
235. Paves, H. and M. Saarma, *Neurotrophins as in vitro growth cone guidance molecules for embryonic sensory neurons. Cell Tissue Res*, 1997. **290**(2): p. 285-97.
236. San Jose, I., et al., *Expression of the cytoskeletal protein MAP5 and its regulation by neurotrophin 3 (NT3) in the inner ear sensory neurons. Anat Embryol (Berl)*, 1997. **195**(3): p. 299-310.
237. Lee, H., R.J. McKeon, and R.V. Bellamkonda, *Sustained delivery of thermostabilized chABC enhances axonal sprouting and functional recovery after spinal cord injury. Proceedings of the National Academy of Sciences of the United States of America*, 2010. **107**(8): p. 3340-5.
238. Zhang, Y.P., et al., *A topical mixture for preventing, abolishing, and treating autophagia and self-mutilation in laboratory rats. Contemporary Topics in Laboratory Animal Science*, 2001. **40**(2): p. 35-36.